AD-A210 365

(2)

AEFA Project No. 83-01

VERIFICATION OF U-21 CLOUD PARAMETER MEASUREMENT EQUIPMENT AND COMPARISON OF NATURAL AND ARTIFICIAL ICE ACCRETION CHARACTERISTICS ON ROTOR BLADE AIRFOIL SECTIONS

Daumants Belte
Project Officer/Engineer

Robert D. Robbins
Project Pilot

DTIC
ELECTE
JUL 18 1989
S D
E

May 1987

Final Report

AEFA

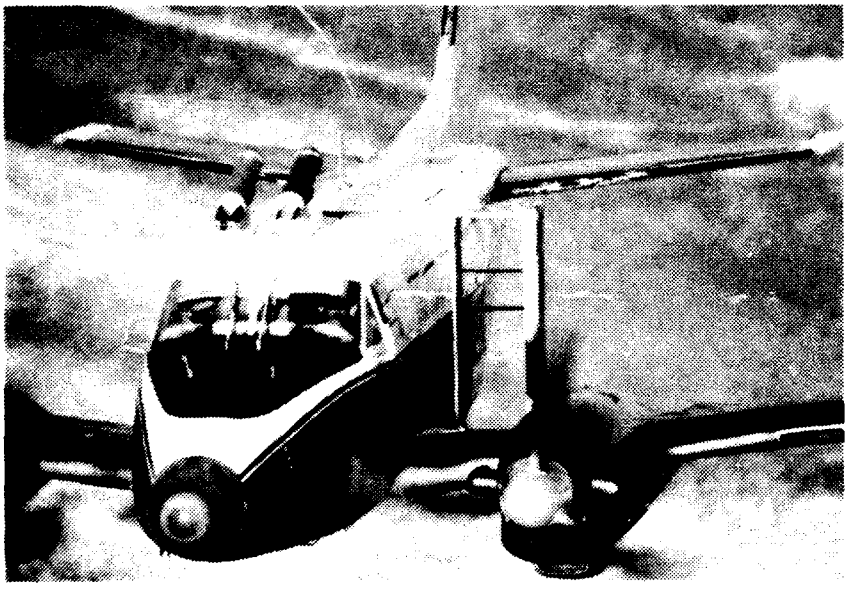

Approved for public release, distribution unlimited.

AVIATION ENGINEERING FLIGHT ACTIVITY
Edwards Air Force Base, California 93523-5000

DISCLAIMER NOTICE

The findings of this report are not to be construed as an official Department of the Army position unless so designated by other authorized documents.

DISPOSITION INSTRUCTIONS

Destroy this report when it is no longer needed. Do not return it to the originator.

TRADE NAMES

The use of trade names in this report does not constitute an official endorsement or approval of the use of the commercial hardware and software.

REPORT DOCUMENTATION PAGE

Form Approved OMB No. 0704-0188

1a. REPORT SECURITY CLASSIFICATION UNCLASSIFIED	1b. RESTRICTIVE MARKINGS
2a. SECURITY CLASSIFICATION AUTHORITY U.S. ARMY AVIATION SYSTEMS COMMAND	3. DISTRIBUTION/AVAILABILITY OF REPORT
2b. DECLASSIFICATION/DOWNGRADING SCHEDULE	
4. PERFORMING ORGANIZATION REPORT NUMBER(S) AEFA PROJECT NO. 83-01	5. MONITORING ORGANIZATION REPORT NUMBER(S)
6a. NAME OF PERFORMING ORGANIZATION U.S. ARMY AVIATION ENGINEERING FLIGHT ACTIVITY 6b. OFFICE SYMBOL (If applicable)	7a. NAME OF MONITORING ORGANIZATION
6c. ADDRESS (City, State, and ZIP Code) EDWARDS AIR FORCE BASE, CALIFORNIA 93523-5000	7b. ADDRESS (City, State, and ZIP Code)
8a. NAME OF FUNDING/SPONSORING ORGANIZATION U.S. ARMY AVIATION SYSTEMS COMMAND 8b. OFFICE SYMBOL (If applicable)	9. PROCUREMENT INSTRUMENT IDENTIFICATION NUMBER
8c. ADDRESS (City, State, and ZIP Code) 4300 GOODFELLOW BLVD. ST. LOUIS, MO 63120-1798	10. SOURCE OF FUNDING NUMBERS PROGRAM ELEMENT NO. E7-8ET024-01 / PROJECT NO. -E7-E7 / TASK NO. / WORK UNIT ACCESSION NO.

11. TITLE (Include Security Classification)
Verification of U-21 Cloud Parameter Measurement Equipment and Comparison of Natural and Artificial Ice Accretion Characteristics on Rotor Blade Airfoil Sections. Unclassified

12. PERSONAL AUTHOR(S)
Daumants Belte, Robert D. Robbins

13a. TYPE OF REPORT	13b. TIME COVERED	14. DATE OF REPORT (Year, Month, Day)	15. PAGE COUNT
FINAL	FROM 07/03/83 TO 29/03/85	May 1987	136

16. SUPPLEMENTARY NOTATION

17. COSATI CODES			18. SUBJECT TERMS (Continue on reverse if necessary and identify by block number)
FIELD	GROUP	SUB-GROUP	Airfoil Icing, Artificial Icing, Droplet Impingement, Helicopter Blade Section, Helicopter Icing Spray System, Ice Accretion, Icing Cloud, Icing Similitude, Liquid Water Content, Particle Measurement.

19. ABSTRACT (Continue on reverse if necessary and identify by block number)

The U.S. Army Aviation Engineering Flight Activity icing research and qualification facilities include an instrumented JU-21A aircraft to measure icing cloud parameters, and a JCH-47C equipped with the Helicopter Icing Spray System (HISS) to provide an artificial icing capability. An in-flight comparison of cloud measurements made between the JU-21A and the University of Wyoming Super King Air atmospheric research aircraft in natural icing conditions showed reasonable agreement. A subsequent phase of this program investigated ice accretion characteristics on airfoil sections representing UH-1H and UH-60A helicopter rotor blades in three scale sizes in both natural icing conditions and the artificial cloud produced by HISS. Two airfoil sections of 18-inch span were mounted on a structural framework over the left wing of the JU-21A and progressive stages of ice accretion were documented with sequence photography. Airfoil icing immersions, which typically lasted from 10 to 20 minutes each, were conducted at incidence angle from 0 to 9°. Ice profile tracings made from the photographs allowed comparison of ice accretions between natural and artificial cloud types, different temperatures, incidence angles, airfoil section types, and airfoil scale sizes. Limitations of the ice shape test rig included an airspeed gradient along and normal to the blade span, boundary layer effects against the outboard wall, observation angle parallax, and perspective view distortion along the leading edge. Analysis of the ice shape results indicated a lower than expected accretion rate for artificial icing conditions, and showed that artificial ice formations begin to assume streamlined profile characteristics similar to rime ice formations at temperatures 3° to 4°C warmer than for natural ice.

20. DISTRIBUTION/AVAILABILITY OF ABSTRACT	21. ABSTRACT SECURITY CLASSIFICATION
☐ UNCLASSIFIED/UNLIMITED ☒ SAME AS RPT. ☐ DTIC USERS	UNCLASSIFIED

22a. NAME OF RESPONSIBLE INDIVIDUAL	22b. TELEPHONE (Include Area Code)	22c. OFFICE SYMBOL
SHEILA R. LEWIS	(805) 277-2115	SAVTE-PR

DD Form 1473, JUN 86 *Previous editions are obsolete.*

TABLE OF CONTENTS

Accession For
NTIS GRA&I
DTIC TAB
Unannounced
Justification
By
Distribution/
Availability Codes
Dist Special
A-1

INTRODUCTION

BACKGROUND

1. The US Army Aviation Systems Command (AVSCOM) periodically tasks the US Army Aviation Engineering Flight Activity (AEFA) to conduct in-flight icing tests of aircraft, mission equipment, and ice protection systems in support of various research, development, and qualification efforts. To support these tests, AEFA operates two aircraft: (1) a JU-21A fixed wing aircraft equipped with instrumentation to measure icing cloud parameters, and (2) a JCH-47C helicopter equipped with the Helicopter Icing Spray System (HISS) to provide artificial icing. Continued use of this equipment has led to interagency agreements with the Federal Aviation Administration to provide input to a data base that defines the natural icing environment and seeks to improve in-flight artificial icing simulation capabilites.

2. The US Army's approach to icing qualification flight testing consists of a two-phase effort that combines flight in the artificial icing spray cloud produced by HISS with subsequent verification flight in natural icing conditions. Results of such tests during previous years on UH-1H and UH-60A helicopters raised some questions with respect to types of ice accretion formed on rotor blades and their relative performance penalties. Comparison of results between helicopter types (different rotor systems) and between natural and artificial icing environments suggested trends that required further investigation. AVSCOM addressed these issues in a test request (ref 1, app A) for a 3-phase program to gather comparative natural cloud measurement data for sensor verification (Phase I), and to compare ice accretion characteristics at different airfoils during natural (Phase II) and artificial (Phase III) icing conditions. AEFA prepared separate test plans (refs 2 and 3) for the cloud measurement and icing phases. Additional test plans (refs 4 and 5) were prepared for airworthiness evaluation of the JU-21A modifications.

TEST OBJECTIVES

3. The objectives of this program were:

a. Obtain comparative measurements of natural cloud parameters determined by AEFA JU-21A and the University of Wyoming Beech Aircraft Corporation (BAC) Super King Air to verify icing sensor performance (Phase I).

b. Design, fabricate, install and flight test full and partial scale airfoil sections mounted on the AFFA JU-21A to determine their ice accretion characteristics in natural (Phase II) and artificial (Phase III) icing conditions.

DESCRIPTION

4. A US Army JU-21A aircraft (S/N 66-18008) made by the RAC and fitted with cloud measuring equipment served as the project test bed. Shown in figure 1, it is an unpressurized, low-wing, all metal, twin turboprop airplane with tricycle landing gear with a maximum takeoff gross weight of 9650 lb. The aircraft incorporates various ice protection systems and is certified for flight into moderate icing conditions.

5. Onboard instrumentation included two Particle Measuring Systems, Inc. laser spectrometers (Models FSSP-100 and OAP 200X) a Cloud Technology Inc. hot wire liquid water content (LWC) sensor; a Rosemount total air temperature probe; and an EG&G International, Inc. hygrometer to measure dew point. A visual ice accretion indicator fabricated from an OH-6A tail rotor blade section (NACA 0012) was mounted on the right side of the aircraft near the cockpit window. A 1 1/4-inch diameter hole was cut in the fuselage skin forward of the left front cabin window and a threaded plug was installed to allow extending hand-held probes and ice removal devices during flight.

6. The Airfoil Section Array (ASA) assembly was designed and built under contract by Task Research, Inc. The ASA assembly, shown in figure 2, consisted of a structural framework mounted above the left wing of the JU-21A inboard of the engine nacelle. The design allowed routine removal from the aircraft to restore the JU-21A to the normal utility airplane configuration. Two types of test airfoil sections were fabricated by Task Research, Inc.: NACA 0012 and SC1094 R8. These correspond to the main rotor blade crosssections of the UH-1H and UH-60A helicopters, respectively. Each airfoil had an 18 inch span and was available in three sizes: full scale (21-inch chord), 3/4 scale (15.75 in. chord), and 6-inch chord. Two airfoil sections were placed one above the other in the ASA framework, with a vertical separation of 9-1/2 inches. For ice shape documentation, two 35mm cameras with motor drives and automatic sequencing were installed immediately inside the forward cabin window and aligned with the airfoil leading edges. The incidence angle of each airfoil was adjustable in flight by a motor drive, and the leading edges had imbedded electrical heater elements imbedded to allow in-flight deicing. An end plate attached to each airfoil was marked with a half-inch grid to provide a background for viewing the ice formations.

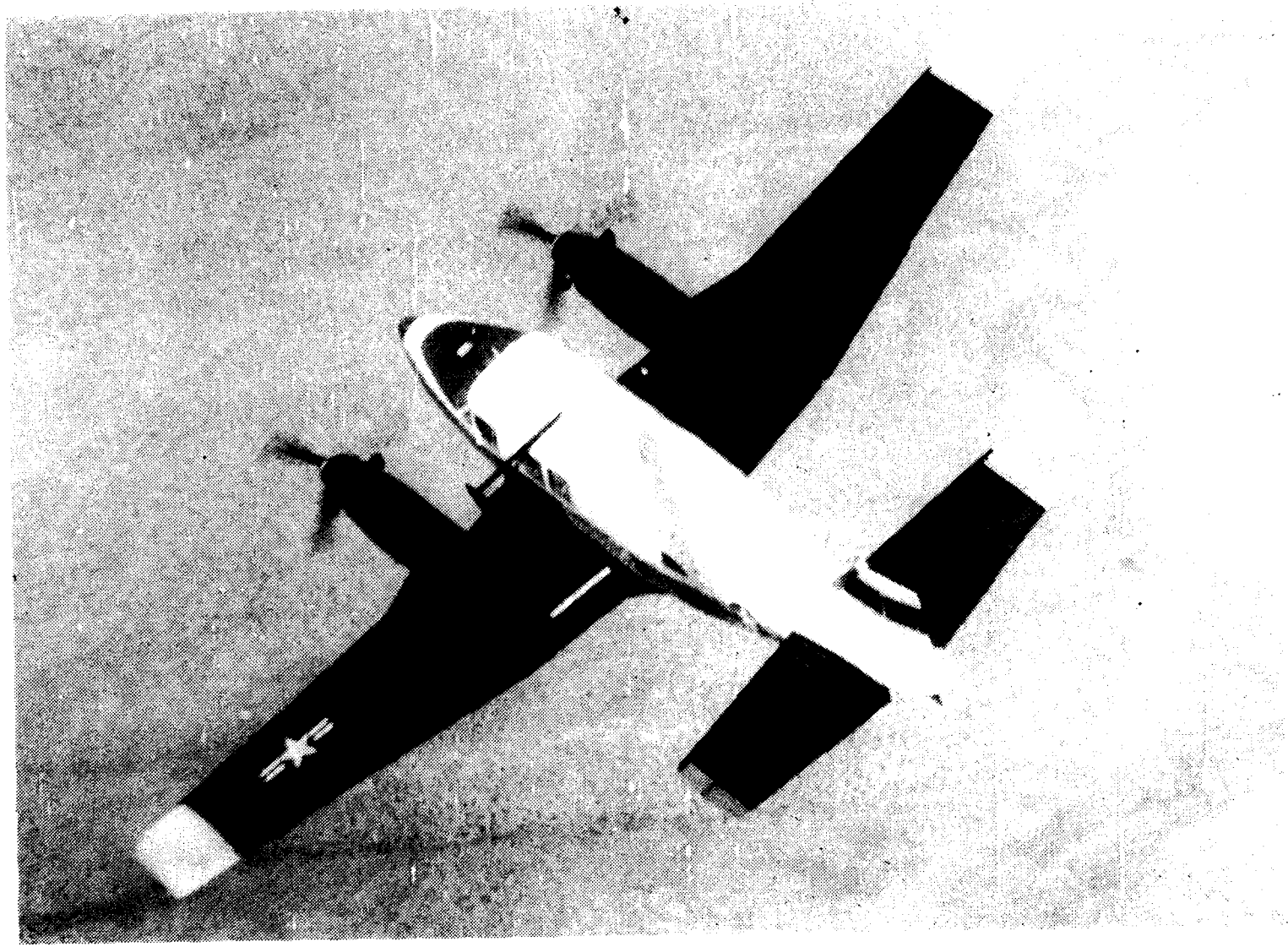

Figure 1. JU-21A Aircraft S/N 66-18008

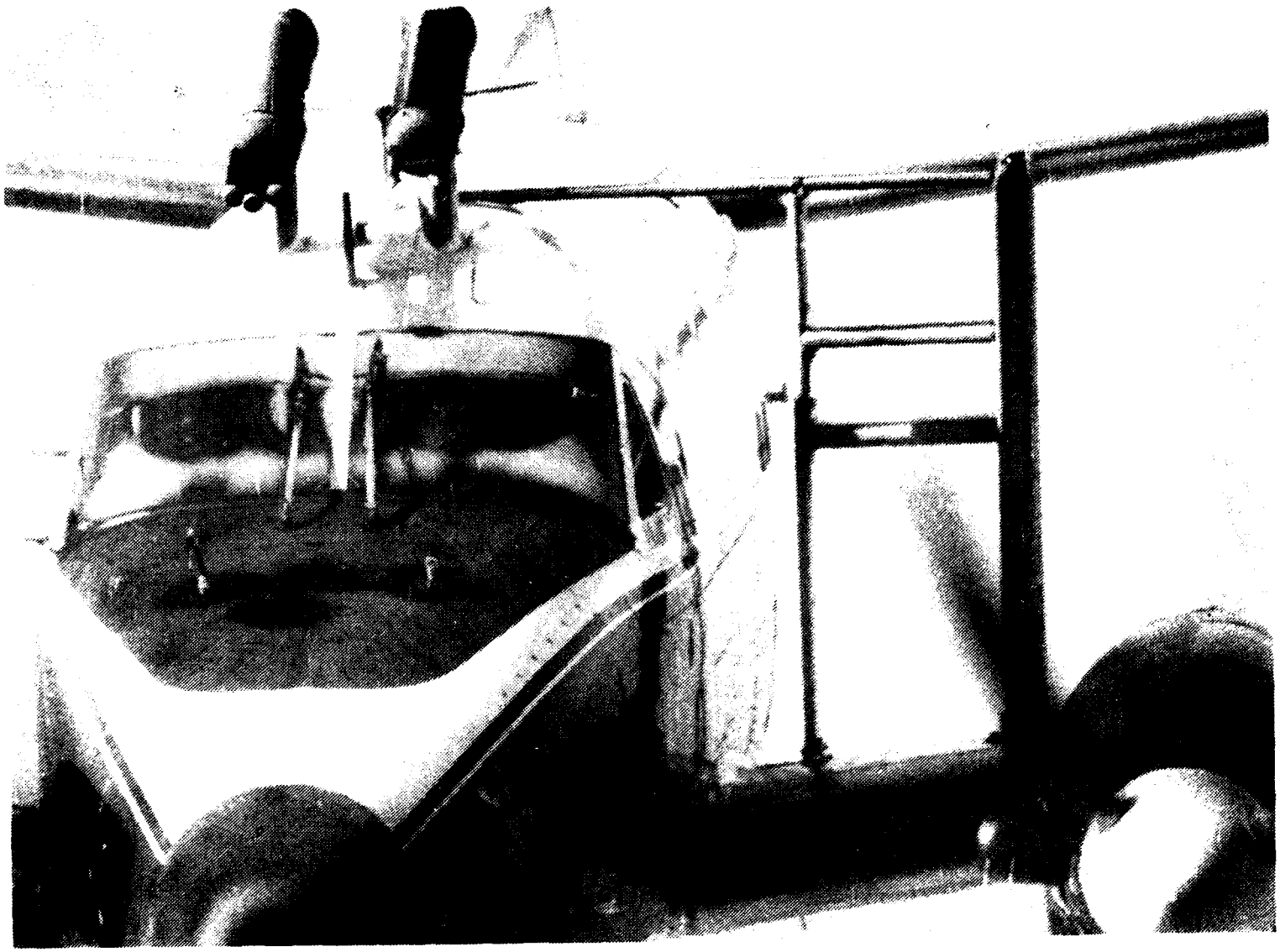

Figure 2. ASA Assembly Installed on JU-21A

The outboard support pylon was equipped with a leading edge pneumatic boot deicer.

7. Additional aircraft and systems involved in this evaluation included the University of Wyoming operated BAC Super King Air A200(T) (Civil Registration N2UW) with installed cloud measuring instrumentation, and the AEFA operated Boeing Vertol JCH-47C (US Army S/N 68-15814) equipped with the HISS. Detailed descriptions of these aircraft and systems are contained in appendixes B and C.

TEST SCOPE

8. In-flight cloud measurement comparisons (Phase I) were flown in the vicinity of McClellan Air Force Base, California (field elevation 76 ft) from 7 through 18 March 1983. The AEFA JU-21A made four natural icing cloud measurement flights totalling 5.7 hours. These were flown in proximity with the University of Wyoming Super King Air to obtain concurrent cloud measurement data.

9. Airworthiness qualification flights of the ASA assembly on the JU-21A were conducted at Edwards Air Force Base, California (field elevation 2302 ft) from 14 December 1984 through 4 January 1985 in visual meteorological conditions. Aircraft handling qualities were evaluated with various airfoil section and incidence combinations installed on the ASA during five flights totalling 8.2 hours.

10. Natural and artificial icing tests of the ASA (Phases II and III) were flown in the vicinity of Duluth, Minnesota (field elevation 1429 ft) from 16 January through 29 March 1985. A total of 54 icing encounters (30 natural and 24 artificial) were documented during 20 flights. Total cloud immersion times for ASA ice accretion were 8.0 hours of natural and 5.4 hours of artificial icing. For these tests, pressure altitude varied from 2980 to 13,620 ft and temperature varied from -6.5° to -24.5°C for natural and -5.5° to -19.5°C for artificial icing. Engine start gross weight was between 8220 and 9520 lb at longitudinal center of gravity (cg) locations from fuselage station 151.9 to 155.2 (mid). Flight limitations contained in the operator's manual (ref 6, app A) and in the airworthiness release (ref 7) were observed during testing.

TEST METHODOLOGY

11. Comparative natural cloud measurements between the JU-21A and the University of Wyoming Super King Air were obtained in cumuliform clouds of one to four miles horizontal extent at airspeeds ranging from 160 to 200 knots true airspeed (KTAS). The Super King Air was lead aircraft for the cloud penetrations with the JU-21A following in trail formation approximately three miles to the rear. The Super King Air pilot transmitted heading, altitude and airspeed at cloud entry while the JU-21A followed on the same path several knots slower to avoid closure.

12. A flight loads and stress analysis of the ASA structure was performed before the first flight to calculate operating limits and safety margins. Airworthiness of the ASA installed on the JU-21A was verified before icing by using established flight test techniques (ref 8, app A) as described in appendix D. Performance and handling qualities were evaluated for all phases of a flight profile, including stalls and simulated engine failures. Data were hand recorded using standard aircraft instrumentation and cockpit indicators. An instrumented JT-28B pace aircraft provided airspeed calibration and allowed observation of tufts attached to various portions of the JU-21A airframe during test maneuvers. Before flight, the aircraft was weighed with the ASA installed to determine longitudinal, lateral, and vertical cg.

13. The natural icing tests of the ASA blade sections were generally flown in stratiform clouds in instrument meteorological conditions under instrument flight rules. Coordination with air traffic control to find and stay in the icing environment was accomplished using a combination of radar vectoring, navigational aid holding, and block airspace assignment. Icing immersion was initiated by descending into the cloud tops. By remaining within the upper 200 ft of the layer, the aircraft was exposed to the highest ambient LWC available. Average airspeed was generally maintained between 150 and 155 KTAS. Immersion was terminated by climbing above the cloud.

14. Artificial icing tests were performed by flying in the spray cloud produced by the HISS (fig. 3). The cloud was entered from beneath, and standoff distance was maintained approximately 180 ft behind the spray booms by using the HISS radar altimeter and positioning light system. For all artificial icing flights, airspeed was 120 KTAS and a water flow rate of 13 gal/min was set to produce a nominal LWC of 0.5 gm/m^3.

15. Two test airfoils were placed one above the other in the ASA assembly on the JU-21A. Airfoil ice accretions were photographed

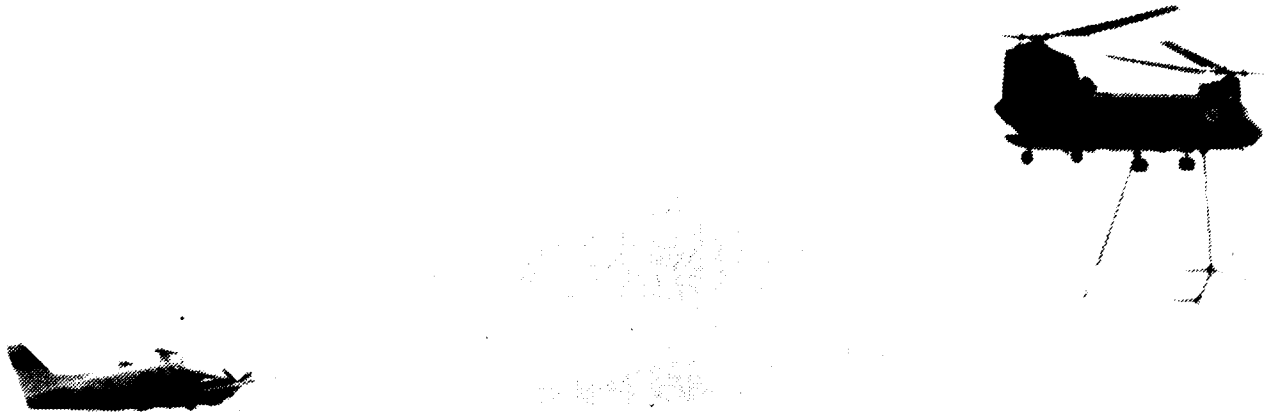

Figure 3. JCH-47C HISS and JU-21A in
Artificial Icing Test Formation

using two 35mm cameras sighted along the airfoil leading edges. The cameras were started simultaneously on cloud entry, and automatically took a sequence of photographs throughout the immersion. Duration of cloud exposure was predicated on providing a sufficient ice thickness to allow an adequate indication of shape and accretion characteristics. Three icing immersions were generally accomplished per flight at test airfoil incidence angles of 0°, +6° and +9°.

16. Ice protection systems on the JU-21A were activated as required during the icing flights. Test conditions and icing cloud characteristics were measured by the onboard instrumentation system. Test techniques and data analysis methods are described in appendix D.

RESULTS AND DISCUSSION

GENERAL

17. The mission of the AEFA JU-21A as a chase, scout, and calibration platform in support of icing test programs provides frequent exposure of this aircraft to both natural and artificial icing environments. This program addressed two mission related areas of interest: verification of the accuracy of the installed cloud measuring equipment, and comparison of the ice accretion characteristics between natural and artificial icing conditions.

18. In-flight comparison of the JU-21A cloud measurement system against similar equipment installed on another aircraft showed reasonable agreement between measured natural cloud parameters. Airworthiness test flights of the Airfoil Section Array (ASA) icing assembly demonstrated satisfactory operation with no adverse effects on JU-21A flying qualities. Ice accretion characteristics were evaluated in natural and artificial icing conditions using UH-1H and UH-60A rotor blade airfoil profiles in three scale sizes. The ice formations produced were correlated with type of icing condition and temperature, type of airfoil section, airfoil scale size, and airfoil incidence angle. Subsequent sections of this report separately discuss the cloud measurement comparison, the ASA airworthiness qualification, and the ASA icing test results.

CLOUD MEASUREMENT COMPARISON

General

19. The cloud measurement instrumentation on the JU-21A is routinely used in support of icing qualification flights to document natural icing conditions encountered by the test aircraft. Such measurements are also useful as input to a database to characterize statistically the natural icing environment. Comparison of the JU-21A measurements against a separate sensor system provides a common basis to establish confidence in the accuracy of the cloud data. The University of Wyoming Super King Air (described in app B) with instrumentation for cloud physics research (app C) was used for this in-flight data comparison. As described in appendix D, the aircraft flew in trail formation through cumuliform clouds to obtain near concurrent measurements (after proper correlation of time scales). Time history data from representative cloud penetrations are presented in figures E-1 through E-5, which compare the LWC and median volumetric diameter (MVD) drop size measurements from both aircraft.

Drop Size Measurements

20. The drop size measurements obtained from both FSSP-100 probes measurements are presented figures 1 through 5 in terms of MVD. The MVD is the diameter such that half of the total water volume is contained in drops larger and half in drops smaller than this median diameter. Agreement between both probes was generally close (usually within 2 μm). Three sample cloud spectra from each probe are shown in figure F-6, selected from the sequences presented in figures F- 1, F-4 and F-5. Some differences can be expected because these are one-second samples obtained more than a minute apart. Agreement of drop size measurements made by the JU-21A and those made by the Super King Air FSSP-100 are satisfactory.

Liquid Water Content

21. The general trends of LWC fluctuations with time in figures F-1 through F-5 show consistently good agreement among all sensors, considering the 70-second time interval between aircraft and the cumuliform nature of the sampled clouds. Comparison of measured LWC values among sensors, however, show some differences. Neglecting irregular fluctuations that produced varying degrees of data scatter throughout, some overall trends can be distinguished using the JU-21A FSSP-100 laser spectrometer data as a baseline for comparison.

22. LWC values from the Super King Air Commonwealth Scientific and Industrial Research Organization (CSIRO) probe essentially agreed with the JU-21A values of LWC (within 10% and without bias). Data from Johnson-Williams probe (described in app C) gave average LWC readings about 15% lower than the CSIRO and JU-21A measurements. The Super King Air FSSP-100 consistently measured 20 to 50% higher values for LWC than the JU-21A FSSP-100. The least agreement among all probes is shown in figure F-5. The Super King Air FSSP-100 measurement of LWC was over twice as great as that of the JU-21A FSSP-100, and agreement between hot-wire probes showed major variations with time. The discrepancies in this case may be attributed to particular characteristics of the individual cloud sampled and a possible malfunction of the Super King Air FSSP-100 (para 25).

23. The differences in LWC of 20 to 50% between FSSP-100 probes were larger than expected. Several factors contribute to this. The laser spectrometers are designed primarily as particle sizing devices, and are not intended to serve as accurate LWC sensors. However, LWC is readily computed by summing volumes of the water drops counted and factoring against total sample volume (a function of airspeed and sample area, related to laser beam width

and depth of field). The FSSP-100 resolves drop diameters into 15 3- μm increments. The LWC computation uses the center diameter of each increment to calculate water volume, which is a function of the cube of the drop diameter. Small shifts in drop diameter become magnified as large changes in volume. LWC accuracy ranges of 20% are generally quoted for this method, but better results are often obtained depending on the particular spectrometer.

24. Various investigations (e.g., refs 9 and 10, app A) have been performed to identify and compare sources of error and calibration uncertainties for the particle sizing spectrometers. Close tolerances are required for several factors that determine size and count accuracy, such as the sample area, velocity reject, delay time, total strobe rate and activity counter functions. Actual values for specific probes have been found to differ from those quoted by the manufacturer, sometimes by a significant percentage, causing systematic errors in LWC potentially as large as 70%. Other aspects that can introduce bias and affect quality of the data include airspeed-related sizing errors, uniformity of sample area illumination, count efficiency dependency on particle size and position within the laser beam, and scattered light collection angle variation. These parameters can vary from one probe to another. Comparison of several spectrometers in the NASA-Lewis Icing Research Tunnel (ref 11) revealed that a given probe produced repeatable measurements, but different probes showed significant variability of LWC indications between instruments and from the calibrated tunnel setting (as large as 68%).

25. While individual adjustments to software calibration algorithms can improve accuracy for a particular spectrometer, sustained use of the probes in an operational environment has tended to introduce intermittent and gradual malfunctions in the electronics and optical alignment that are often subtle and difficult to identify. Short of complete instrument failure, the probes often continue to produce degraded data values that may appear reasonable with progressive discrepancies in accuracy during operation not becoming apparent for some time. Such a situation appeared to be the case in that the Super King Air FSSP-100 data produced higher values for LWC than actual. The magnitude of shift in the data (20 to 50%) was within an error range that could typically occur from an intermittent malfunction. This emphasizes the desirability of having available a second device specifically designed for LWC (such as the CSIRO or Johnson-Williams probes) to serve as a cross-check of the spectrometer data. Potential unreliability of using drop sizing devices for LWC estimation is recognized in current FAA guidelines for rotorcraft icing certification (ref 12) which states that "other calibrated devices for measurement of LWC should be used".

26. Comparison between the JU-21A FSSP-100 data from these tests and the Super King Air hot wire probe data indicated that the JU-21A instrumentation showed reasonable agreement. Despite this encouraging result from the first phase of this program, various problems subsequently arose with the JU-21A instrumentation in later phases, as described in reference 13. Both the FSSP-100 and OAP-200X spectrometers experienced difficulties during the icing program, including malfunctions of the lasers, power supplies, interface electronics to the recording system, optical alignment and beam distortion. These problems degraded overall quality of the laser spectrometer particle size and LWC data to the extent that the measurements were not considered reliable and estimated LWC and MVD values for cloud composition were used (para 52).

ASA AIRWORTHINESS EVALUATION

27. Installation of the ASA icing assembly onto the JU-21A constituted an experimental modification of the aircraft configuration. Airworthiness was established by a combination of engineering analysis and flight tests. Flight loads calculations and stress analyses of the ASA structure were performed to determine operating limits and safety margins.

28. The airworthiness evaluation flights investigated performance and handling qualities for all phases of an icing flight profile, including emergency situations and procedures. The aircraft configurations flown, the maneuvers evaluated, and the specific test procedures used are discussed in appendix D.

29. The airworthiness evaluation flights established satisfactory test airfoil operation from incidence angles of -5° to +10°, absence of flutter or excessive vibration in the ASA structure, and satisfactory aircraft handling qualities throughout the flight envelope. No adverse airflow effects were noted behind the ASA on either the empennage or near the left fuselage static port.

30. The aerodynamic effects of the ASA installation had minimal effect on aircraft handling qualities. A few minor differences were noted when compared to the baseline (no ASA) aircraft configuration. To maintain wings level for cruise, 50% of available left aileron trim was required. In trimmed level flight with the largest test airfoils installed, an ASA incidence angle change from 0° to +9° produced a gradual climb rate of approximately 100 ft per minute. Stall speed and single engine minimum control speeds were either unchanged or lowered (improved) by up

to 3 knots in some configurations. A previously known effect of mounting the laser spectrometer probes over the cabin roof was a perceptible yaw oscillation in trimmed flight above 170 KTAS which was attributed to airflow effects on the vertical stabilizer. Addition of the ASA assembly eliminated this undesirable characteristic. The ASA produced no adverse effects on aircraft flight characteristics within the envelope evaluated.

ASA ICING TESTS

General

31. Results of natural and artificial icing tests from previous years on the UH-1H and UH-60A raised some issues when general trends were compared. While performance assessment in the artificial cloud is hindered by formation flight techniques and the disturbed flow field behind the HISS, relative performance penalties caused by rotor icing appeared to vary considerably both between helicopter types and between the natural and artificial icing environments. Table 1 summarizes the maximum performance penalties encountered from some previous icing programs (refs 14 through 21, app A). In general, percentage of torque rise (increased power required) between shedding cycles in natural icing conditions appeared greater for the UH-60A than for the UH-1H. Performance penalties for the UH-60A were more severe in the natural clouds than behind the HISS; performance penalties for the UH-1H, however, were more severe behind the HISS than in natural clouds.

32. Since rotor drag characteristics are associated with the types of ice shapes produced, such observations suggested differences in accretion characteristics between airfoil types and natural versus artificial environments. The approach taken in this program was to compare directly ice shape characteristics in the icing environments used for qualification testing by flying various airfoil sections on the JU-21A. The ASA was not instrumented to measure aerodynamic performance changes. Several other flight test and wind tunnel investigations have studied ice accretion characteristics on rotorcraft airfoils in recent years, and are discussed in paragraph 21, appendix D. A general engineering summary of technical data related to ice accretion characteristics is given in reference 22, which discusses effects of airspeed, temperature, pressure, drop size, LWC, body size and geometry. More recent analyses have quantified ice accretion properties using various thermodynamic and nondimensional parameters to correlate icing characteristics with free stream conditions and airfoil geometry characteristics (chord length, incidence angle, leading edge

Table 1. Maximum Increase in Power Required (Percent)

Aircraft	Project Number	Natural Icing	Project Number	Artificial Icing
UH-60A	79-19	23	81-18	13
	80-14	30		
	81-18	28		
UH-1H	74-31	21	78-21-2	14
	79-02	<10	80-13	25
	80-13	<5	83-23	13

radius, thickness ratio, and camber). These parameters and relationships are discussed in more detail in paragraphs 22 through 27, appendix D.

33. Before comparing the different ice shapes available (para 50), some discussion is appropriate regarding ASA icing operations, relevant observations during the test flights, and factors to be considered when interpreting the data. The following paragraphs address these aspects of the ASA icing tests.

Limitations

34. Icing of rotor segments on the JU-21A provides some insight regarding comparative ice accretion characteristics for different airfoil sections. However, a number of limitations apply and various factors affect applicability of such two dimensional steady-state results to actual helicopter rotors. As a helicopter blade segment revolves in forward flight, it experiences periodic changes in angle of attack and relative airspeed. An angle of attack of about 6° represents an approximate mid-span average over the azimuth. Centrifugal forces, airspeed and total air temperature rise increase radially along the span. By comparison, the ASA airfoils at a given setting had a fixed incidence angle and a constant airspeed, and were not subject to centrifugal force. The constant airspeeds flown during this evaluation (120 and 155 KTAS) correspond to hover conditions at spanwise locations of 6.0 and 7.7 ft from the hub for the UH-1H, and 7.5 and 9.7 ft for the UH-60A. In forward flight at any airspeed, the airspeed component would be alternately added to and subtracted from these values once per revolution (5.4 times per second for the UH-1H and 4.3 times per second for the UH-60A).

35. To validate the two-dimensional blade profile approach, uniform airflow over the ASA test section was desired. The selection of ASA mounting location was based on practical considerations. The test section was placed 10 inches from the side of the aircraft and 9 ft, 9 in. aft of the left propeller near the inboard edge of the propeller disk (7 ft, 9 in. diameter). A tufted rod airflow survey had indicated a relatively smooth flow field beyond 7 inches from the fuselage side, but the extent of propwash influence was not known. A hand-held probe with total and static pressure ports (para 8, app C) was extended ahead of the test airfoils from the cabin to obtain local airspeed measurements just ahead of the test section. In flight at 109 KCAS, airspeed in front of the ASA between inboard and outboard edges changed from 123 to 132 KCAS. The transition occurred about midspan over a distance of about 3 inches. With the left engine shut down and the propeller stopped (not a configuration used for

icing), the gradient disappeared and airspeed became constant (at 117 KCAS) across the entire span. It is apparent (figs. F-1 and F-2) that the presence of a 9 knot airspeed gradient across the test airfoils affected the flow field and drop trajectories and resulted in changes of ice accretion profile along the blade span. These effects were most pronounced on the large airfoils in clear icing conditions.

36. The sequence photographs show the ice shapes seen at the outboard end of the span against a background grid. This edge of the airfoil rested flush against the flat surface of the support pylon, which acted as an end plate for the blade sections. Boundary layer effects along this wall became apparent from the ice accretion characteristics. Ice did not form on the test section within 1/2 to 3/4 inches of the wall (fig. F-3). The water drops contained in the airflow streamlines were apparently deflected this distance away from the surface. The deflected water impacted the airfoil immediately beyond this area, resulting in a thicker ice accretion on the zone photographed than on the rest of the airfoil. In rime conditions with streamlined ice shapes, the added accretion was consistently near 30%. However, more complex flow behavior was indicated in clear icing conditions with "double horned" ice formations (para 51). The additional LWC affected ice shape profile by exaggerating the protruding "horns" (as shown in fig. F-4) and a straightforward LWC correction factor cannot be assumed.

37. An additional factor affecting the boundary layer involved ice accretions on the support pylon leading edge ahead of the test airfoils (6.2 in. forward of the 6 in. chord airfoil leading edges and 2.6 in. for the 21 in. chord). Without ice, tufts along the outboard pylon surface indicated uniform airflow. When pylon ice accretions approached 1/2 inch thickness (the minimum for effective pneumatic boot deicing), the tufts were disturbed to include gyrations such as spinning in full circles against the surface wall. This flow disruption was more pronounced in clear icing conditions than in rime conditions. Most immersions experienced some periods of flow disruption along the end wall between pylon deicing cycles. Additionally, the tips of the sheet metal end plates attached to the airfoils that held the reference grid were sometimes bent outward slightly from the pylon surface by air pressure and would vibrate. Both the elevated LWC conditions (about 30%) near the end wall and mixed airflow patterns of the boundary layer along this surface were factors that influenced the ice cross-sections photographed and should be noted when interpreting the ice shape results.

38. The existence of an ice-free gap between the ice shapes and the end wall reference grid introduced parallax in the photographs. This was considered negligible for the larger airfoils since the cameras could be sighted along the airfoil leading edges. In practice, the lens was centered one to two inches ahead of the leading edge to allow a clear field-of-view without blockage by spanwise ice closer to the camera. The 6 inch chord sections pivoted on the same mounting points but their small size set their leading edges further aft, masking them behind the inboard pylon. The camera sighting axes could not be positioned less than 7 inches ahead of their leading edges, producing an offset angle of 11° for a perpendicular distance of 35-3/4 inches between the grid and camera film plane. With a 1/2 to 3/4 inch space between the ice formations and grid, the 6-inch chord airfoils had to accumulate 0.10 to 0.15 inches of ice before a silhouette could be seen against the grid. The ice profiles shown for the 6-inch airfoils show an ice thickness undersized by approximately this amount. This measurement error decreases slightly as the ice becomes thicker and offset angle decreases. Considering the magnitude of other effects on the ice profiles (para 35 through 37), the size of the parallax error was not considered significant and no corrections were applied.

39. Viewing the ice shapes at the far end of the blade span also introduced some perspective effects. The field-of-view was focused on the outboard edge against the grid, but also included the inboard edge (18 inches closer) and all spanwise locations. Other than at the leading edge, the actual airfoil contour at the far end was masked by blade surfaces closer to the camera. Additional masking occurred as ice accreted on these surfaces. As a result, only the forward portions of the ice contour were visible at the far end, and the limits of ice impingement further aft were not available for the ice shape tracings (para 20, app D).

40. The sequence photographs were taken in pairs (e.g., figs. F-5 and F-6) with the upper and lower cameras aligned to show part of the other corresponding airfoil (upper surface of the bottom blade and lower surface of the top blade). The larger blades projected ahead of the inboard support pylon and provided a clear view of the airfoil contours and ice cross-section along their inboard surface. These profiles were also photographed occasionally between the normal sequence exposures by adjusting the lenses for closer focus. Such inboard surface views (not possible for the 6 in. blades) showed ice shapes directly (fig. F-7) with no parallax or perspective distortion. The inboard blade surface was always exposed to provide direct scaling.

The span edge flow effects on ice accretions here were less pronounced than the boundary layer effects along the outboard end wall. This type of approach suggests an alternative technique that could be used to improve photographic ice shape documentation. Future programs of this sort should use a test arrangement that allows direct viewing of the airfoil and ice shapes cross-sections along their inboard surfaces.

41. An index line marked on the outboard support pylon parallel to the aircraft waterline provided airfoil incidence angle data. As measured with an inclinometer, in-flight deck angles were approximately 2° nose-up for the two configurations and airspeeds flown (120 KTAS with 35% flaps and 155 KTAS with zero flaps). At zero incidence angle, tufts on the support pylon aligned closely with the horizontal reference line. As angle setting increased, the tufts were deflected downward by airflow around the blade sections. A direct correlation between incidence angle and airfoil angle of attack was not made; however, the incidence angle settings represent consistent changes in relative airfoil attitude between conditions.

42. Between icing immersions, the blade sections were deiced using built-in electrical heater mats. As power was applied, the ice bond visibly changed appearance while a water layer formed along the blade surface beneath the ice. When this had occurred over the entire 18-inch span, the ice was free to shed. In instances when air pressure kept the debonded ice in place over the leading edge, incidence angle changes were made from -5° to +10° until the ice was shed. This procedure usually took noticeably more effort for the SC1094 R8 airfoils than for the NACA 0012, since the "droop snoot" profile provided a contour that tended to keep the ice sections balanced over a wider incidence angle range. In the absence of centrifugal forces, ice shedding was more difficult to induce for the SC1094 R8 airfoils than for the NACA 0012 blade sections.

43. When shedding was delayed while the heaters were in operation, occasional streams of water tended to run back over the airfoil from beneath the ice. This water froze and remained on the airfoils, since the aft blade sections were not heated beyond 10% chord on the upper and 15% on the lower surfaces. The resulting edge roughness at the heater boundary formed surface irregularities that became ice collection surfaces for subsequent immersions, as shown in figures F-8 and F-9. While this characteristic affected overall airfoil ice accretion, it was not considered a significant influence on the leading edge ice shapes that were photographed (para 39).

44. The largest airfoil sections had heaters with a lower power density than the others (para 9, app B) and were usually more difficult to deice. A cold region on one span retained ice formations (fig. F-10) that were removed by scraping with a bent metal tube extended from the cabin. This removal method was also applied occasionally to the outboard support pylon. A leading edge pneumatic boot connected to the aircraft bleed air supply (para 6, app B) was installed on this pylon at the test site, but debonded ice segments several inches long would sometimes remain balanced after boot cycling. Ice on the pylon leading edge caused disrupted airflow over the inboard surface boundary layer and affected ice accretion on the airfoils (para 37). The inboard pylon had no deicing provision other than the manual technique. Since the larger airfoil sections extended forward of the inboard pylon leading edge, pylon ice accretions tended to overlap against the inboard surface of the airfoils. Thicker accretions caused physical interference with airfoil angle adjustment, and at colder temperatures resulted in stalling of the angle drive motor.

45. The ASA was usually not deiced after the last immersion on a flight to allow closer inspection of the ice upon landing. However, ice shapes were generally not retained very well on the airfoils after landing. This was primarily attributable to engine exhaust gas impingement during various taxi operations before shutdown. Fine details of ice structure such as rime feathers and individual ice spicules on the airfoil bottom surfaces were normally lost in this process.

46. Hot turbine exhaust impingement on the ASA in flight was indicated by presence of an ice-free zone formed on the outboard pylon. This clear area extended from 6 inches above the pylon base to 10 inches below the lower airfoil (fig. F-11). The location and tapered appearance of ice at the upper edge indicated that exhaust gases did not impinge on the test airfoils in flight.

47. During operation of the ASA assembly some problems were encountered. The incidence angle drive motors become sluggish at cold temperatures (near -20°C), and would stall when the airfoil edges encountered significant inboard pylon ice accretions (para 44). The end plate reference grid decals became detached inflight and came off on two occasions, but application of tape and sealant along the forward edges resolved this problem. One end plate was bent outward and folded over by the airflow during a support (nonicing) flight at higher airspeeds. The end plate edges were subsequently trimmed to a smaller size and the problem did not recur. One leading edge heater temperature controller failed during the program and was replaced. Overall operation of the ASA assembly during the icing tests was satisfactory.

48. JU-21A propeller ice shedding is a common occurrence in the icing environment, and ice impact damage to the aircraft nose in the plane of prop disk has required skin repairs after every icing season. Ice shed from the propeller also struck the ASA and test blade sections occasionally, producing minor dents on the assembly. The most notable damage of this type was to the 6-inch chord airfoils, which incurred various degrees of surface denting and paint chipping by the end of the program. At one point, the small NACA 0012 section was returned to Task Research Inc. to repair a dent near the outboard edge that deformed the contour significantly. This outer span location suggests that some of the airfoil strikes may also have resulted from ice shed from the outboard ASA support pylon.

49. Close inspection of the ASA structure after the program ended revealed additional items that require repair before future use. These included pylon skin cracks around the airfoil mounting (pivot) locations, various elongated fastener holes, a weld bead crack on the plate that attaches inboard mast to the top cross-brace, and engine exhaust carbon deposits (potential source of corrosion) trapped between the outboard pylon skin surface and spar reinforcement straps. Both the test airfoils and the ASA structure sustained some damage during the program and should be reconditioned before further flight use.

Airfoil Section Ice Accretions

50. As described in appendix D, JU-21A icing immersions were flown with two airfoils mounted on the ASA simultaneously. Sequence photographs were taken along the airfoil leading edges against a background grid to view progressive stages of ice accretion with time. The ice shape data consist of tracings made from the photographs, and show incremental build-up of the ice profile cross-sections near the outboard edge of the airfoils. The following section discusses the available ice shape data with regard to correlation between natural and artificial conditions, temperatures, incidence angle, type of airfoil section, and airfoil scale size.

51. Temperature is a major factor influencing the type of ice formations produced by supercooled liquid drops. Rime ice conditions occur at temperatures cold enough for the cloud drops to freeze instantaneously on impact. At warmer temperatures, clear ice conditions result when some water flow occurs over the airfoil or ice surface before freezing. Characteristically, rime ice shapes on airfoils have a streamlined appearance, but clear ice conditions can produce nonstreamlined profiles such as "double-horned" ice formations. Intermediate conditions can produce a

combination of icing characteristics, such as a clear ice center section surrounded by rime ice feathers along the edges.

52. The lack of reliable spectrometer measurements for LWC and MVD (para 26) precludes availability of these two key icing parameters in the data. Some assumptions based on previous icing experience (ref 13, app A) were made to estimate their values, as discussed in paragraphs 16 through 18, appendix D. Based on these assumptions, the natural icing clouds were estimated to have an LWC of 0.2 gm/m^3 and an MVD of 20 μm. The artificial clouds were estimated to have an LWC of 0.5 gm/m^3 and an MVD of 35 μm.

53. The natural clouds were assumed to have an LWC only 40% as great as the LWC of the artificial clouds (0.2 versus 0.5 gm/m^3) but were flown at a 30% higher airspeed (155 versus 120 KTAS). The overall mass flux of LWC and potential ice thickness in the natural clouds for equal exposure times was, therefore, approximately 50% that of the artificial clouds. That is, the accumulation parameter or potential ice thickness for immersions of a particular size airfoil behind the HISS was about twice that of natural encounters for comparable elapsed times.

54. The test conditions and airfoil configurations are listed in tables 2 and 3. A parameter cross reference to correlate test conditions with the corresponding ice shape figures is presented in table E-1, and the ice shape data for each immersion are shown in figures F-7 through F-17 (natural) and F-18 through F-25 (artificial). These figures present data for the top and bottom airfoil pairs as mounted on the ASA for any given flight, and present each incidence angle selected.

55. Ice accretion rates on the test airfoils can be estimated from the profile tracings. Some variation is evident between consecutive layers in a number of cases, both between immersions and during a given immersion. Such differences can be attributed to LWC changes with time in natural clouds, and effects of direct sunlight in artificial clouds (para 50). Neglecting such individual variations, the accretion rates were approximately 1/2 inch for a ten minute immersion for both natural and artificial clouds over the entire temperature range. Since the mass flux of LWC and expected potential accumulation for artificial clouds was twice that of natural clouds (para 53), the observed rates in flight indicate a reduction of the actual accretion rate of the HISS spray below that anticipated. (For the conditions assumed, a 10 minute immersion produced a calculated 0.47 inch potential thickness for natural and 0.97 inch for artificial if ice density is assumed to be 0.8 gm/cm^3). This icing program was the first

Table 2. Artificial Icing Test Conditions

Flight Number	Average Conditions					ASA Airfoils		App E Figure Number
	Press Alt (ft)	Airspeed (KTAS)	Ambient Temperature (KTAS)	Relative Humidity (%)	Icing Duration (min.)	Angle (deg)	Chord Size and Section	
6	8320	121	-13.5	75	9	0	6 in. SC1094 R8 and 6 in. NACA 0012	23
	8020	120			9	6		
8	6700	121	-19.5	70	12	0	6 in. and NACA 0012 15.75 in.	25
	6860	120			10	6		
	6740	121			7	9		
12	5940	122	-16.5	60	12	0	6 in. and NACA 0012 21 in.	24
	6100	123	-16.0		12	3		
	6060	122	-16.5		11	6		
	5800	121			11	9		
14	7250	120	-7.0	55	20	0		21
					19	6		
	7500				20	9		
15	7300	120	-6.5	60	15	0		19
	7320	118			15	6		
	7060		-7.5		15	9		
16	9600	119	-11.0	50	16	0	21 in. SC1094 R8 and 21 in. NACA 0012	22
	10200				15	6		
	10400				15	9		
17	8800	119	-5.5	60	15	0		18
	8860	120			15	6		
	8900				15	9		
18	8040	121	-5.5	60	12	0	6 in. and SC1094 R8 21 in.	20
	8440	122	-6.5		10	6		
	8460	121			11	9		

Table 3. Natural Icing Test Conditions

Flight Number	Average Conditions				NASA Airfoils		App I Figure Number
	Press Alt (ft)	Airspeed (KTAS)	Ambient Temperature (KTAS)	Icing Duration (min.)	Angle (deg)	Chord Size and Section	
7	3960	146	-11.5	25	0	6 in. NACA 0012 and 6 in. SC1094 R8	14
	4040	148	-12.0	18	6		
7A	8800	159	-21.0	11	0		16
9	4240	151	-8.5	9	0	6 in. and 15.75 in. NACA 0012	13
	5000	153	-9.0	9	3		
	4120	149		8	6		
	4880	151	-10.5	11	9		
10A	11340	154	-12.0	13	0	15.75 NACA 0012 and 15.75 SC1094 R8	15
	11540	153		15	6		
	11160	163		22	9		
11	13220	158	-24.0	18	0	6 in. and 15.75 in. SC 1094 R8	17
	13040	159	-23.5	19	3		
	13160	158	-24.0	24	6		
	13620	160	-24.5	25	9		
13	5060	154	-7.0	16	0	6 in. and 21 in. NACA 0012	10
	5000	155		17	6		
	5060	154		16	9		
19	3300	149	-8.0	17	6	6 in. and 21 in. SC1094 R8	11
	3080	147	-6.5	12	0		
20	3220	154	-7.0	10	0	21 in. NACA 0012 and 21 in. SC1094 R8	9
	3040			17	6		
	2980	153		13	9		
21	3960	154		15	6		8
22	4000	153		20	0		
23	3400	154	-7.5	13	0	6 in. NACA 0012 and 6 in. SC1094 R8	7
	3460	156	-6.0	15	6		
	3700	153	-7.0	14	9		
24	4460	157	-8.5	21	0	15.75 in. NACA 0012 and 15.75 in. SC1094 R8	12
	4600	156	-9.0	19	6		
	4140	153		15	9		

to compare systematically HISS ice accretions with natural conditions and to identify quantitatively this apparent discrepancy. Spray cloud accretion rates should be evaluated in-flight to provide data for future modifications of the HISS configuration.

56. Differences in drop size distribution furnish a partial explanation for the discrepancy described in paragraph 55. In addition to smaller drops, the HISS cloud also contains drop diameters in the 40 to 200 μm range that are larger than normally assumed to occur in natural clouds (para 18, app D). Flow field and drop trajectory considerations (para 25, app D) indicate that impingement coverage of these larger drops will occur over a broader chordwise surface area. Although the aft impingement limits are not visible on the tracings, they can be seen on the inboard edge views as described in paragraph 40. Broader chordwise ice coverage with the HISS is apparent by comparing figures F-12 and F-13 (natural icing at -7°C for incidence angles of 0° and 6°) with figures F-14 through F-16 (artificial icing at -5.5°C for angles of 0°, 6°, and 9°). Total ice quantities on the airfoils for an incidence angle of 0° can be compared in figure F-7 (natural ice at -7°C for 20 minutes and photo F-14 (artificial ice at -5.5° for 15 minutes). By compensating for the immersion time difference with an estimated adjustment to thickness, the total quantity of accreted ice is roughly twice as large for artificial as natural. This result is consistent with the expected difference in water mass flux.

57. These observations indicate that stagnation line ice thicknesses for equivalent values of LWC are lower for the HISS than for natural clouds (by as much as 50% on the test airfoils), and the artificial ice accretions are formed over a larger surface area. Such effects are primarily dependent on drop sizes contained in the cloud and the surface contours and flow field around the particular object exposed. Both large and small drop diameters are normally expected to impinge in the stagnation area, and size distribution differences alone do not entirely explain the reduced ice thicknesses seen with the HISS. Additional factors that may affect accretion with the larger drop sizes include partial supercooling, runback, or impact erosion. Greater turbulence in the HISS spray may affect trajectories of the smaller drops. Analytical studies of artificial cloud drop size distributions should include these factors.

58. In both natural and artifical icing environments, the colder range of test temperatures (conducive to rime icing) resulted in streamlined ice accretions with rounded leading edges. Artificial and natural rime ice contours were generally similar to each other. Spray from the HISS was capable of producing rime feathers

that would form on various surface discontinuities such as those shown on the inboard support pylon in figure F-17.

59. At warmer temperatures conducive to glaze ice and nonstreamlined "double horned" formations, several effects were observed. With direct sunlight shining on the test airfoils during immersions behind the HISS, small ice protrusions broke off after a few seconds of accretion. This prevented the formation of any prominent horn shapes in the artificial icing environment. No similar shedding process occurred in the natural environment since direct sunlight was precluded.

60. In both natural and artificial glaze ice conditions, the 6-inch chord airfoils exhibited a vertical vibration after some ice had been accreted. No vibrations were seen for the larger scale airfoils with proportionately greater chord and thickness. As a result, vertical cracks frequently appeared in the ice formations along the span (fig. F-18) and ice sections would occasionally be lost, exposing portions of the blade surface underneath (fig. F-19). In rime icing conditions, such vibrations were not as pronounced and no cracks occurred. The elevated airfoil vibration levels of clear ice compared to rime ice are attributed to greater aerodynamic loads resulting from the clear formations.

61. Clear ice formations in natural clouds had more pronounced "double horned" shape than those behind the HISS, as demonstrated by comparing figures F-10 and F-19. The tendency to form nonstreamlined ice shapes persisted at temperatures as low as -10°C in natural clouds (figs. F-12 through F-15), whereas HISS ice started to assume a conformal contour below -7°C (fig. F-21) and became streamlined at -11°C (fig. F-22). This indicates that artificial ice began to exhibit rime-like conformal shape characteristics at temperatures 3 to 4°C warmer than natural ice. The HISS was capable of producing "double-horned" glaze formations on actual helicopter rotors, as documented during artificial icing of the AH-64A rotor system at -5°C during a concurrent program (ref 13, app A).

62. Increasing airfoil incidence tended to result in ice formation further toward the lower surface of the leading edge contour. The geometry of the SC1094 R8 "droop snoot" profile resulted in slightly different orientation of the ice formations than for the symmetrical NACA 0012 airfoils, as seen in figure F-15. Ice accretions in the shape of spicule formations reached as far aft as the trailing edge of the lower airfoil surfaces, commonly at 9° incidence and occasionally for 6° (fig. F-21). Such lower

surface formations were evident behind the HISS but not in natural conditions, and were attributed to the presence of larger drop sizes. Similar artificial formations were also seen on actual rotors, such as those of the SH-60B Seahawk shown in figure F-21.

63. Comparison between the two airfoil types reveals that shape orientation is the only major difference in the ice accretions photographed. For immersions where direct comparison was possible, accretion thicknesses were generally similar. Airfoil geometry effects (para 25, app D) on impingement limits could not be photographically documented with the existing test arrangement.

64. Comparison of scaling effects for the different size airfoils introduces similitude considerations, discussed in the following section.

Icing Similitude

65. Icing similitude implies that proportionally scaled ice formations of similar shape will be produced on different-sized airfoils if the appropriate nondimensional parameters are held constant, as described in reference 23, appendix A. These parameters are defined and discussed in paragraphs 26 and 27, appendix D.

66. The values of the nondimensional parameters for each airfoil and immersion flown were calculated using the SIMICE computer routine (ref 23) and are compiled in tables E-2 through E-5. Two values for LWC and MVD were selected as input estimates and used throughout: 0.2 gm/m^3 at 20 μm for natural clouds and 0.5 gm/m^3 at 35 μm for artificial clouds. The scaling calculations used the MVD value for drop diameter, excluding other sizes from the distribution spectrum. While all specific test conditions are listed for each encounter, the computer routine did not use incidence angle in its calculations, and distinguished between airfoil types only by differences in leading edge diameter (3.16% chord for the NACA 0012 and an effective 3.50% for the SC1094 R8). Calculations for the accumulation parameter (Ac) used a value of 0.913 gm/cm^3 for ice density.

67. In addition to computing the scaling parameters, equivalent conditions were calculated for each case (while preserving similitude) that would represent an alternative airfoil scale at a different airspeed. The alternative values selected were 6- and 21-inch scale chords and airspeeds of 120 and 155 KTAS, whichever represented the configuration opposite of the one actually flown. The results were a new set of values for temperature, altitude, LWC, MVD, and icing duration with the same similitude parameters.

These equivalent conditions for the alternative airfoil scales and airspeeds are included in tables 2 through 5.

68. Comparison of such equivalent conditions indicates what sort of scaled ice formations are simulated by a given configuration. In natural clouds, the ice shapes produced on the full-scale sections simulated ice that would appear on 6-inch chord sections at 23% lower airspeed with drop sizes half as large (10 versus 20 μm), approximately twice the LWC, and one fifth the immersion time, at a much lower altitude. Conversely, the 6-inch chord sections simulated full-scale ice for drop sizes over twice as large (50 versus 20 μm), 75% of the LWC and five times the immersion time. In artificial conditions, ice formations on the full-scale sections would represent 6-inch chord airfoils at 30% higher airspeeds, less than half the drop size (15 versus 35 μm), 50% greater LWC, one-sixth the immersion time, at a somewhat higher altitude. Ice on the 6-inch chord airfoils would correspond to full size rotors for nearly twice the drop size (65 versus 35 μm) and half the LWC for immersion times six times as long.

69. Immersion times and LWC values can be adjusted as desired to affect directly the resulting ice thickness (accumulation parameter). Within the ASA operating constraints, the scaling relationships indicate that full size airfoils behind the HISS should be roughly comparable to 6-inch chord airfoils in natural conditions. A sample check of this relationship is provided by figure E-19 (full scale NACA 0012 behind the HISS) and figures E-7 and E-10 (6-inch chord blade sections in natural clouds). Ice on the small airfoils should be comparably scaled for much shorter immersion times. Comparison of the full-size shapes at 15 minutes with the 6-inch chord shapes at 5 minutes indicates that such a ratio of immersion times is not unreasonable.

70. Comparison of the accumulation parameters calculated for natural and artificial clouds generally confirms the ice thickness discrepancy described in paragraph 55. There is reasonable agreement between calculated and actual ice thickness in natural clouds but for artificial clouds, actual accretions are considerably lower than those calculated. Drop size does not affect calculation of the accumulation parameter, but it influences the actual accretions. With the broad size spectra of the HISS cloud (para 18, app D), use of a single value for drop size (MVD of 35 μm) may not provide an adequate representation of the thermodynamic effects on accretion since it neglects the effects of larger drops.

71. The relative magnitudes of some scaling parameters for actual helicopter rotors are indicated in figures E-26 and E-27. Mid-span

locations are shown for the UH-1H and UH-60A over a temperature range from -5 to -20°C at two values of LWC (0.2 and 0.5 gm/m^3) and MVD (20 and 35 μm). Blade airspeeds correspond to hover conditions, and a pressure altitude of 5000 ft was used for a 15 minute immersion time. One difference evident between rotor systems is the higher freezing fraction for the UH-60A at mid-span, which at -10°C is approximately twice that for the UH-1H. General comparison of these scaling values with those of the ASA sections reveals that modified inertia parameter and collection efficiencies are very similar to those for the 3/4 scale test airfoils. These parameters are lower for the full scale blades and higher for the 6-inch chord sections. This suggests that the ASA ice shapes most representative of those on actual rotors (at mid-span) are the accretions shown for the 3/4 scale (15.75-inch chord) blade sections.

CONCLUSIONS

72. This program successfully performed an in-flight natural cloud measurement comparison and gained some useful insights concerning natural and artificial (HISS) ice accretion on rotor blade sections by using an Airfoil Section Array (ASA) test assembly mounted on a JU-21A aircraft. The following conclusions were reached upon completion of this evaluation.

a. The JU-21A cloud measurement instrumentation showed reasonable agreement when compared in natural clouds to a second instrumented cloud measurement aircraft (para 26).

b. Installation of the ASA assembly on the JU-21A did not produce any adverse affects on aircraft flight characteristics (para 30).

c. Limitations to the ASA ice shapes technique included an airspeed gradient across the blade section span (para 35), boundary layer effects along the outboard wall (para 37), reference grid observation angle parallax (para 38), and perspective view distortion along the airfoil leading edge (para 39).

d. In the absence of centrifugal forces, ice shedding was more difficult to induce for the SC1094 R8 airfoils than for the NACA 0012 blade sections (para 42).

e. Overall operation of the ASA assembly during the icing tests was satisfactory (para 47).

f. Compared to natural icing, the HISS spray cloud produced ice accretion rates lower than expected (para 57).

g. Artificial and natural rime ice contours were generally similar to each other (para 58).

h. Clear ice formations produced by the HISS did not have as pronounced a "double-horned" shape as those in natural clouds, and the accretions tended to exhibit rime-like conformal shape characteristics at temperatures 3 to 4°C warmer than in natural conditions (para 61).

RECOMMENDATIONS

73. The following recommendations are made:

a. Future programs of this sort should use a test arrangement that allows direct viewing of the airfoil and ice shape cross-sections along their inboard surfaces (para 40).

b. The test airfoils and the ASA structure should be reconditioned before further flight use (para 49).

c. Spray cloud accretion rates should be evaluated in-flight to provide data for future modifications of the HISS configuration (para 55).

d. Analytical studies of artificial cloud drop size distribution should include the influence of turbulence, supercooling, runback, and impact erosion (para 57).

APPENDIX A. REFERENCES

1. Letter, AVRADCOM, DRDAV-DI, 25 January 1983, subject: Verification of U-21A Cloud Parameter Measurement Equipment and Comparison of Natural and Artificial Ice Accretion Characteristics on Rotor Blade Airfoil Sections. (Test Request)

2. Letter, USAAEFA, DAVTE-TA, 16 February 1983, subject: Test Plan, Verification of U-21A Cloud Parameter Measurement Equipment and Comparison of Natural and Artificial Ice Accretion Characteristics on Rotor Blade Airfoil Sections, USAAEFA Project No. 83-01 (Phase I).

3. Letter, USAAEFA, SAVTE-M, 6 January 1984, subject: Test Plan, Verification of U-21A Cloud Parameter Measurement Equipment and Comparison of Natural and Artificial Ice Accretion Characteristics on Rotor Blade Airfoil Sections (Phases II and III), USAAEFA Project No. 83-01.

4. Disposition Form, USAAEFA, SAVTE-M, 14 May 1984, subject: Project 83-01 Test Plan, U-21A Ice Accretion Chracteristics on Airfoil Section Array, High Speed Taxi Tests.

5. Disposition Form, USAAEFA, SAVTE-M, 26 November 1984, subject: Project 83-01 Test Plan, U-21A Ice Accretion Characteristics on Airfoil Sections Array, Handling Qualities Flight Test.

6. Technical Manual, Headquarters, Department of the Army, *U-21A Operator's Manual, TM 55-1510-209-10,* 29 October 1982.

7. Letter, AVSCOM, AMSAV-E, 10 December 1984, subject: Experimental Airworthiness Release, JU-21A, S/N 66-18008, Installation of Airfoil Section Array (ASA) for Ice Accretion Characteristics of Airfoil Sections, USAAEFA Project No. 83-01 (Phases II and III), with Revision 1, 14 December 1984

8. Technical Manual, Naval Air Test Center, USNTPS-FTM-No. 103, *Fixed Wing Stability and Control, Theory and Flight Test Techniques,* August 1969.

9. Scientific Report, Air Force Geophysics Laboratory, AFGL-TR-79-0251, (University of Wyoming Department of Atmospheric Science Scientific Report No. 1), *Conduct of Cloud Spectra Measurements,* October 1979.

10. Technical Report, University of Wyoming Department of Atmospheric Science, Report No. AS 138, *Determination of the Size and Concentration of Cloud Drops with an FSSP,* July 1982.

11. Technical Memorandum, NASA TM-83340/AIAA-83-0026, *Experimental Comparison of Icing Cloud Instruments*, January 1983.

12. Advisory Circular, Federal Aviation Administration, AC No. 29-2, Change 2, *Certification of Transport Category Rotorcraft*, May 1985.

13. Final Report, USAAEFA Project No. 82-05-3, *Helicopter Icing Spray System (HISS) Evaluation and Improvements*, February 1986.

14. Final Report, USAAEFA Project No. 74-31, *Natural Icing Tests, UH-1H Helicopter*, June 1974.

15. Final Report, USAAEFA Project No. 78-21-2, *Microphysical Properties of Artificial and Natural Clouds and Their Effects on UH-1H Helicopter Icing*, August 1979.

16. Final Report, USAAEFA Project No. 79-02, *JUH-1H Ice Phobic Coating Icing Tests*, July 1980.

17. Final Report, USAAEFA Project NO. 79-19, *Artificial and Natural Icing Tests, Production UH-60A Helicopter*, June 1980.

18. Final Report, USAAEFA Project No. 80-13, *HISS Calibration, Ice Phobics, and FAA R&D Evaluations*, August 1981.

19. Final Report, USAAEFA Project No. 80-14, *Limited Artificial and Natural Icing Tests, Production UH-60A Helicopter (Re-evaluation)*, August 1981.

20. Final Report, USAAEFA Project No. 81-18, *UH-60A Light Icing Envelope Evaluation with Blade Deicing Kit Installed but Inoperative*, June 1982.

21. Final Report, USAAEFA Project No. 83-23, *Evaluation of UH-1H Level Flight Performance Degradation Caused by Rotor Icing*, July 1984.

22. Technical Report, Federal Aviation Administration, Technical Report ADS-4, *Engineering Summary of Airframe Icing Technical Data*, March 1964 (AD608 865).

23. Technical Report, Arnold Engineering Development Center, AEDC-TR-85-30 Vol 1 (Revised), *Analysis and Verification of the Icing Scaling Equations*, March 1986.

24. Technical Report, AVRADCOM, TR 80-805/NASA TP-1701, *Aerodynamic Characteristics of Three Helicopter Rotor Airfoil Sections at Reynolds Numbers from Model Scale to Full Scale at Mach Numbers from 0.35 to 0.90*, September 1980.

25. Technical Report, Meteorology Research Inc, No. MRI 82 FR-1858, *US Army Small Intelligent Icing Data System (Army SIIDS)*, 3 February 1982.

26. Paper, American Institute of Aeronautics and Astronautics, Aircraft Systems and Technology Conference, AIAA-81-1646, *Measurements of Natural Aircraft Icing Conditions*, August 1981.

27. Technical Report, University of Wyoming Department of Atmospheric Science, *Guide for Users of the Wyoming Data Listings (SCCP-1982)*, Contract 7-07-83-V0001, Submitted to Division of Atmospheric Water Resources Research, US Bureau of Reclamation, Department of the Interior, 1982.

28. Final Report, USAAEFA Project No. 82-12, *Evaluation of UH-1H Hover Performance Degradation Caused by Rotor Icing*, August 1983.

29. Paper, American Helicopter Society, 41st Annual Forum, *The Aerodynamics of Rotor Blades with Ice Shapes Accreted in Hover and in Level Flight*, May 1985.

30. Technical Report, NASA CR-175089, *Wind Tunnel Tests of Rotor Blade Sections with Replications of Ice Formations Accreted in Hover*, March 1986.

31. Technical Memorandum, NASA TM-83556, *Ice Shapes and the Resulting Drag Increase for a NACA 0012 Airfoil*, January 1984.

32. Paper, American Helicopter Society, 39th Annual Forum, Preprint No. A-83-39-04-0000, *High Speed Ice Accretion on Rotorcraft Airfoils*, May 1983.

33. Paper, American Institute of Aeronautics and Astronautics, 22nd Aerospace Sciences Meeting, AIAA-84-0183, *Experimental Investigation of Ice Accretion on Rotorcraft Airfoils at High Speeds*, January 1984.

34. Paper, American Helicopter Society, 41st Annual Forum, *The Performance Characteristics of Simulated Ice on Rotorcraft Airfoils*, May 1985.

35. Technical Report, NASA CR-3910, *High Speed Ice Accretion on Rotorcraft Airfoils*, August 1985.

36. Paper, American Institute of Aeronautics and Astronautics, 19th Aerospace Sciences Meeting, AIAA-81-0403, *An Analytical Approach to Airfoil Icing*, January 1981.

37. Paper, American Institute of Aeronautics and Astronautics, 21st Aerospace Sciences Meeting, AIAA-83-0109, *An Analytic Evaluation of the Icing Properties of Several Low and Medium Speed Airfoils*, January 1983.

38. Article, American Institute of Aeronautics and Astronautics, Journal of Aircraft, Vol 21 No. 7, *Effect of Geometry on Airfoil Icing Characteristics*, July 1984.

APPENDIX B. DESCRIPTION

JU-21A

1. The aircraft used for the Airfoil Section Array (ASA) icing evaluation was a JU-21A, US Army Serial No. 66-18008, manufactured by Beech Aircraft Corporation. A dimensioned three-view drawing is shown in figure B-1. It is an unpressurized, low-wing, all metal, twin engine airplane with retractable tricycle landing gear and a maximum takeoff gross weight of 9650 lb. Power is provided by two T74-CP-700 (commercial designation PT6A-20) turboprop engines manufactured by Pratt and Whitney Aircraft/United Aircraft of Canada, Ltd. Each engine has an installed power rating of 550 shaft horsepower at standard day sea level conditions. The aircraft is certified for flight into moderate icing conditions, and incorporates electrothermal anti-icing systems for the windshield, pitot tube, stall warning vane, engine air inlet lip, fuel vents, heater air inlet, and for deicing the propeller blades. Pneumatic boots are incorporated for deicing the wing leading edges between the engine nacelles and a point 30 inches from the wing tips, and the vertical and horizontal stabilizers. The engines are equipped with extendable ice vanes ahead of the compressor inlet for particle deflection, and an autoignition system to reignite combustion in case of flameout due to water ingestion or icing. The instrumentation and data systems installed on the aircraft for these tests are described in appendix C.

AIRFOIL SECTION ARRAY (ASA)

2. The ASA was designed and built under contract by Task Research Inc. of Santa Paula, California specifically for this program. The assembly consists of a structural framework for mounting two test airfoil sections of 18 inch span over the left wing of the JU-21A inboard of the engine nacelle (figs. B-2 through B-4). The airfoils are horizontally supported at each end by two 53 in. vertical pylons. The entire assembly was designed for easy installation and removal for aircraft conversion between test and utility configurations.

3. The bottom of the outboard pylon is fastened to a bridging base plate that bolts flush to the aircraft wing at buttline (BL) 56.5. The front of the bridge attaches to the left wing hoisting hard point, and the rear is bolted to a reinforcing doubler plate within the wing. The inboard pylon fastens to a base plate secured on the wing at BL 38.5. The pylons are connected across the top by a cross bracing strut. This top strut extends past the inboard pylon over the aircraft fuselage and is bolted through the cabin roof to a reinforced channel fastened between ceiling stringers.

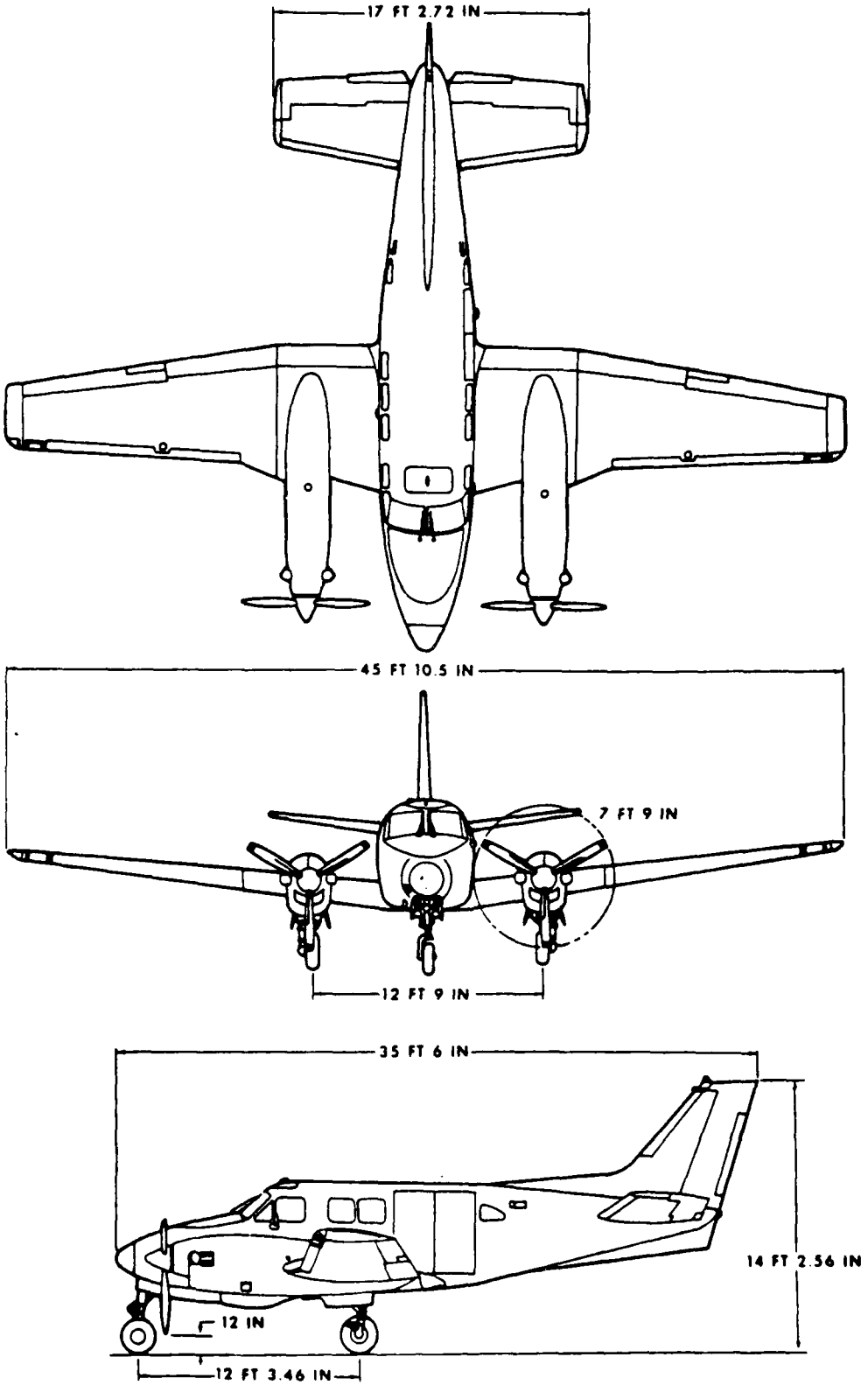

Figure B-1. U-21A 3-View Drawing

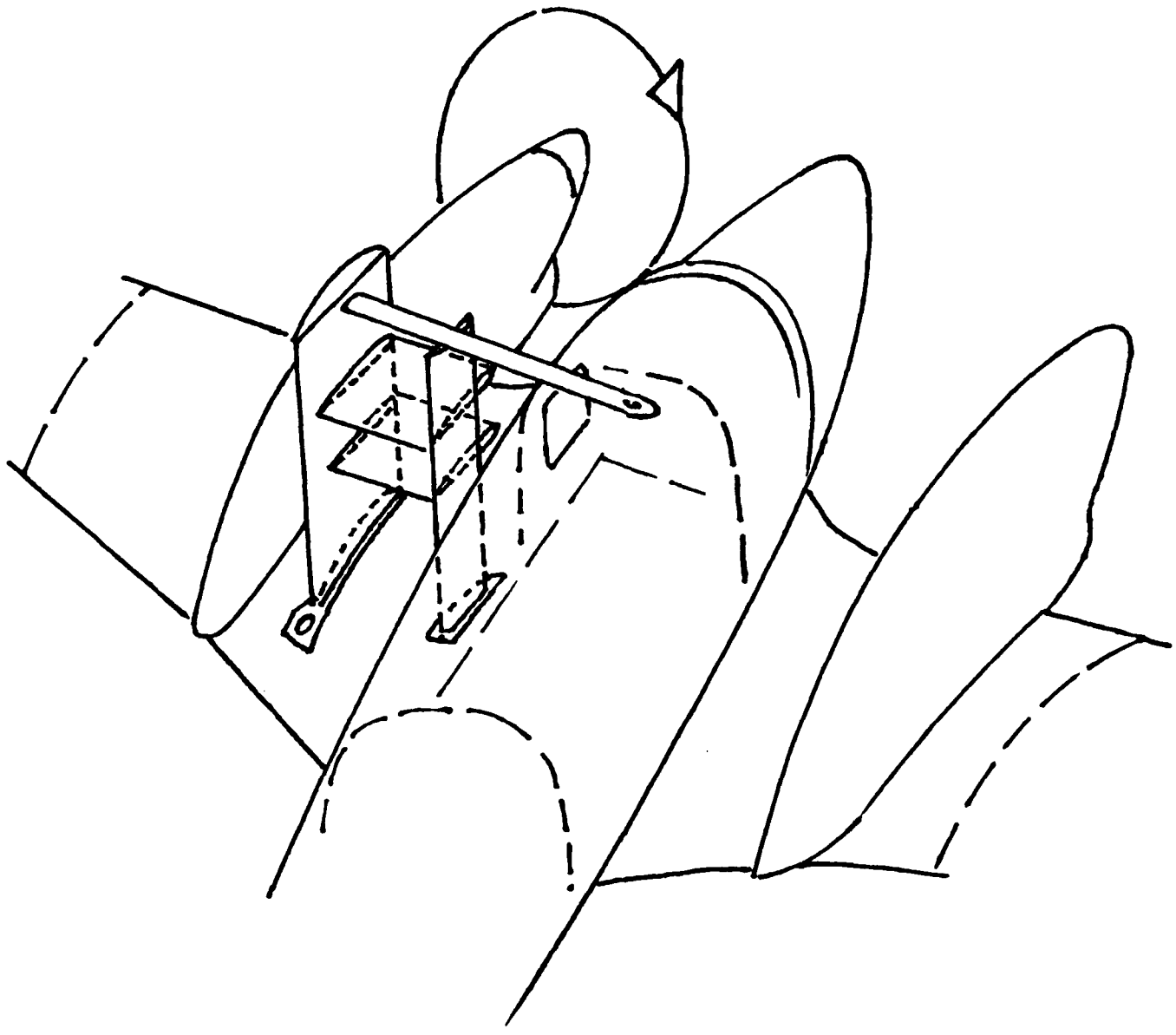

Figure B-2. ASA Installation on JU-21A

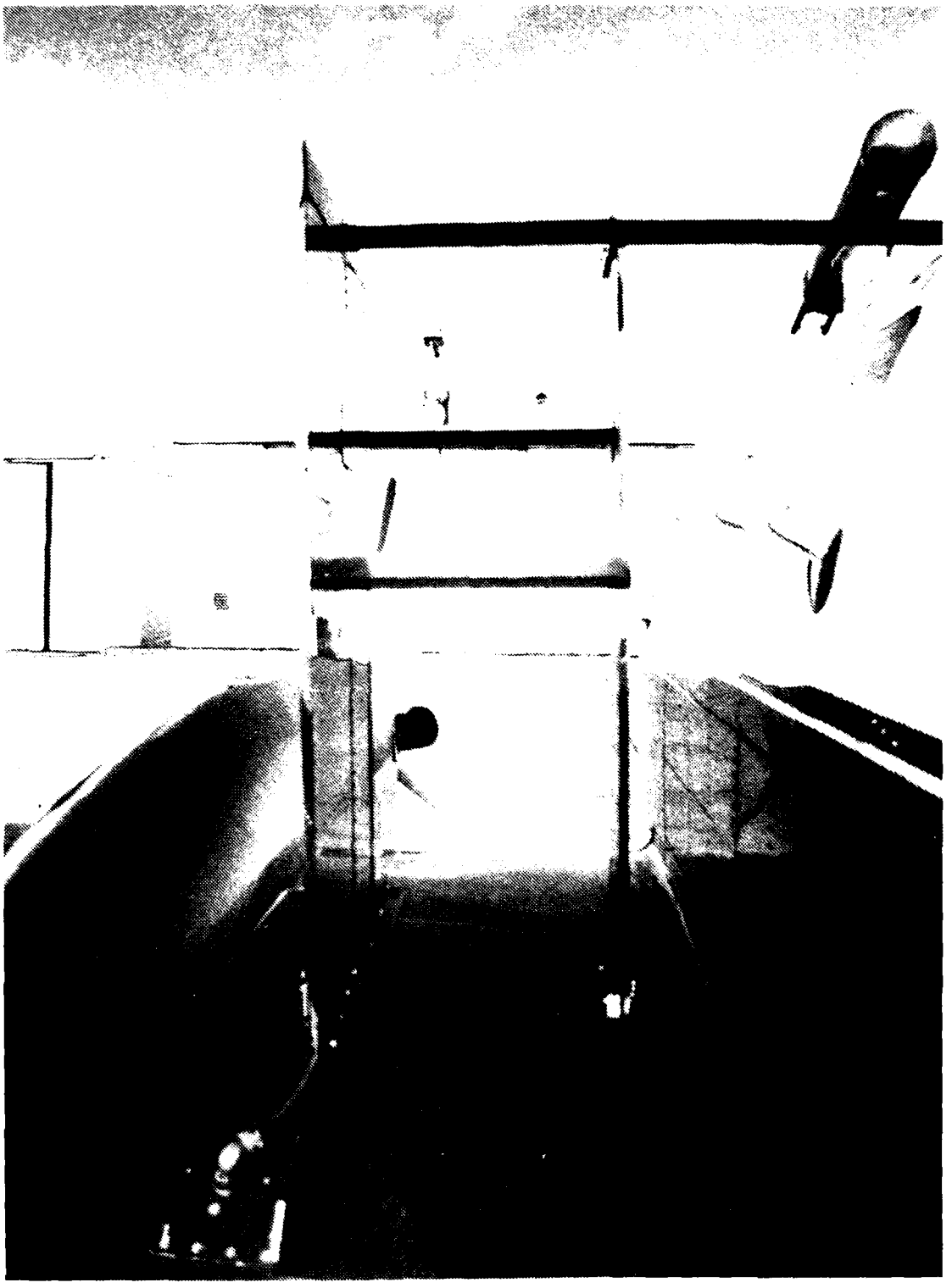

Figure B-3. ASA Assembly, Rear View

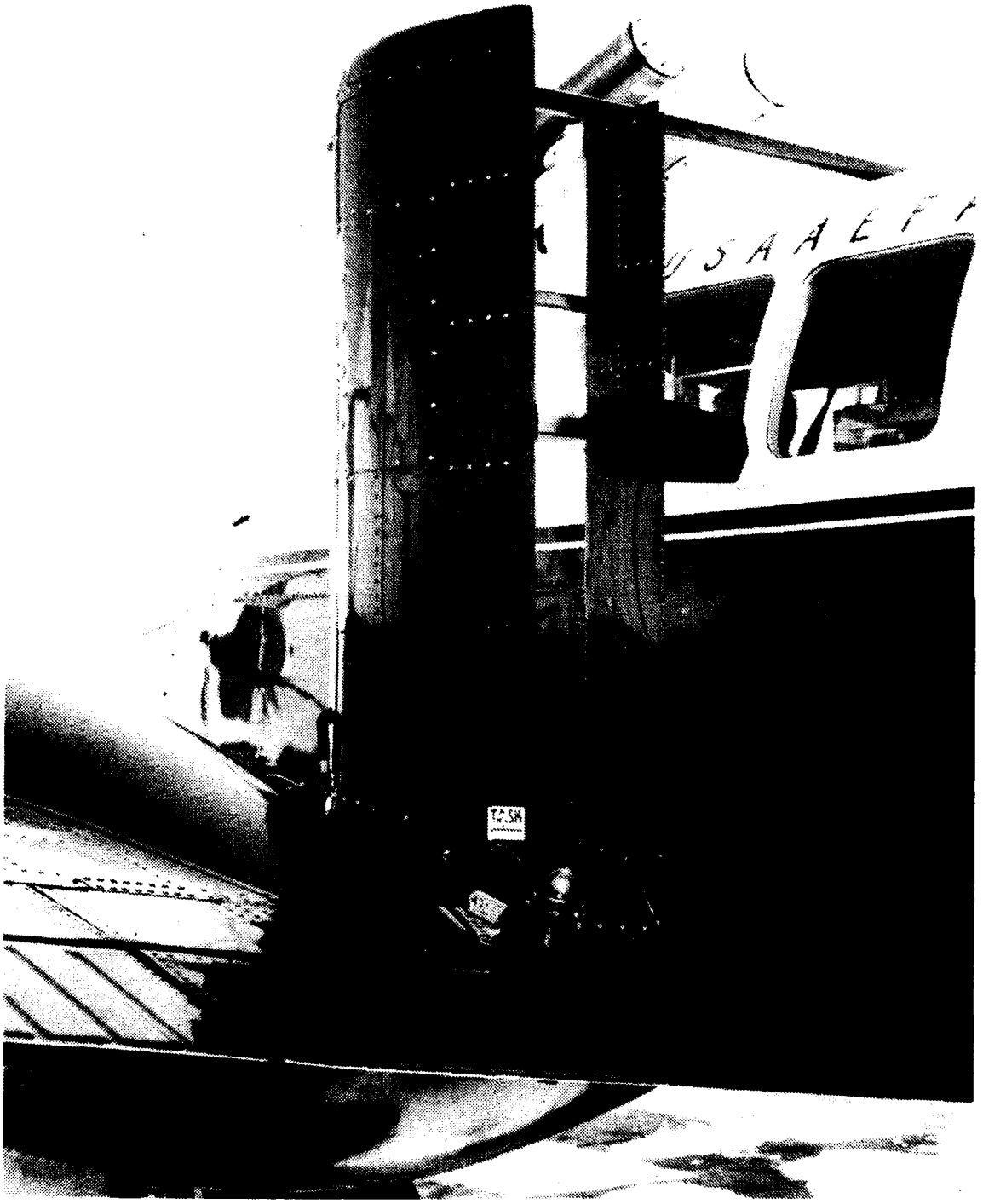

Figure B-4. ASA Assembly, Quartering View

4. The vertical pylons have airfoil-shaped cross sections with flat inner surfaces 18 inches apart so the ends of the test rotor blades sit flush against them. The outer pylon has a 23-inch chord with a maximum 13.7% thickness at 41.5% chord; the inboard pylon has a 9 inch chord with 14.4% thickness at 29.8%. Each pylon has two built-in pivot points for supporting the test airfoils. These pivots consist of Delrin™ bearing blocks vertically spaced 9 1/2 inches apart, with the lower pivot located 29 1/4 inches above the aircraft wing surface near fuselage station (FS) 170 (10 inches aft of the main wing spar).

5. The test airfoils bolt to steel inserts that rotate within the pivot blocks behind access panels on each pylon. Worm drive motors for changing airfoil incidence angle are installed in the outboard pylon. Microswitches limit the angle range from -5° to +20°. The outer pylon also contains the electric relays and heat sensing controllers for airfoil deicing. The electrical power and control wiring bundles are contained within the outer pylon. The aileron cable access panel has been modified to accept a cannon plug from the outboard pylon structure. A control panel in the cabin (fig. B-5) has switches to independently adjust each airfoil incidence angle and provide power to the leading edge heaters.

6. A pneumatic deicer boot for the outboard pylon leading edge was designed and fabricated by B.F. Goodrich. A pneumatic connection to the standard wing deicer bleed air supply was installed through the wing forward of the pylon. The pylon deicer activates whenever the wing boot is operated. Figure B-6 shows the base of the outboard pylon with the pneumatic connection at the leading edge and electrical connector (para 5) at the rear.

7. The airfoils chosen for the ASA evaluation were the main rotor blade sections of the UH-1H and UH-60A helicopters. The two-bladed UH-1H rotor has a normal operating speed of 324 rpm and a diameter of 48 ft; the blades have a NACA 0012 airfoil section with a 21-inch chord and a -10° twist. The four-bladed UH-60A rotor has a normal operating speed of 258 rpm and a diameter of 53 ft 8 in. The blades have an equivalent -18° twist and combine two airfoil sections. The blade segments between approximately 49 and 83% span have an SC1094 R8 section of 21-inch chord; the remaining segments have an SC1095 section of 20.75-inch chord. The blade tips (outer 21 in.) are swept aft 20°. The SC1094 R8 has the same section as the SC1095, except for a "droop-snoot" contour for the leading edge. Since this addition extends the nose forward slightly, it reduces the thickness-to-chord ratio. Before 1984, the literature referred to the "droop-snoot" section as an SC1095 R8 but it has since been redesignated as an SC1094 R8 to indicate the correct ratio.

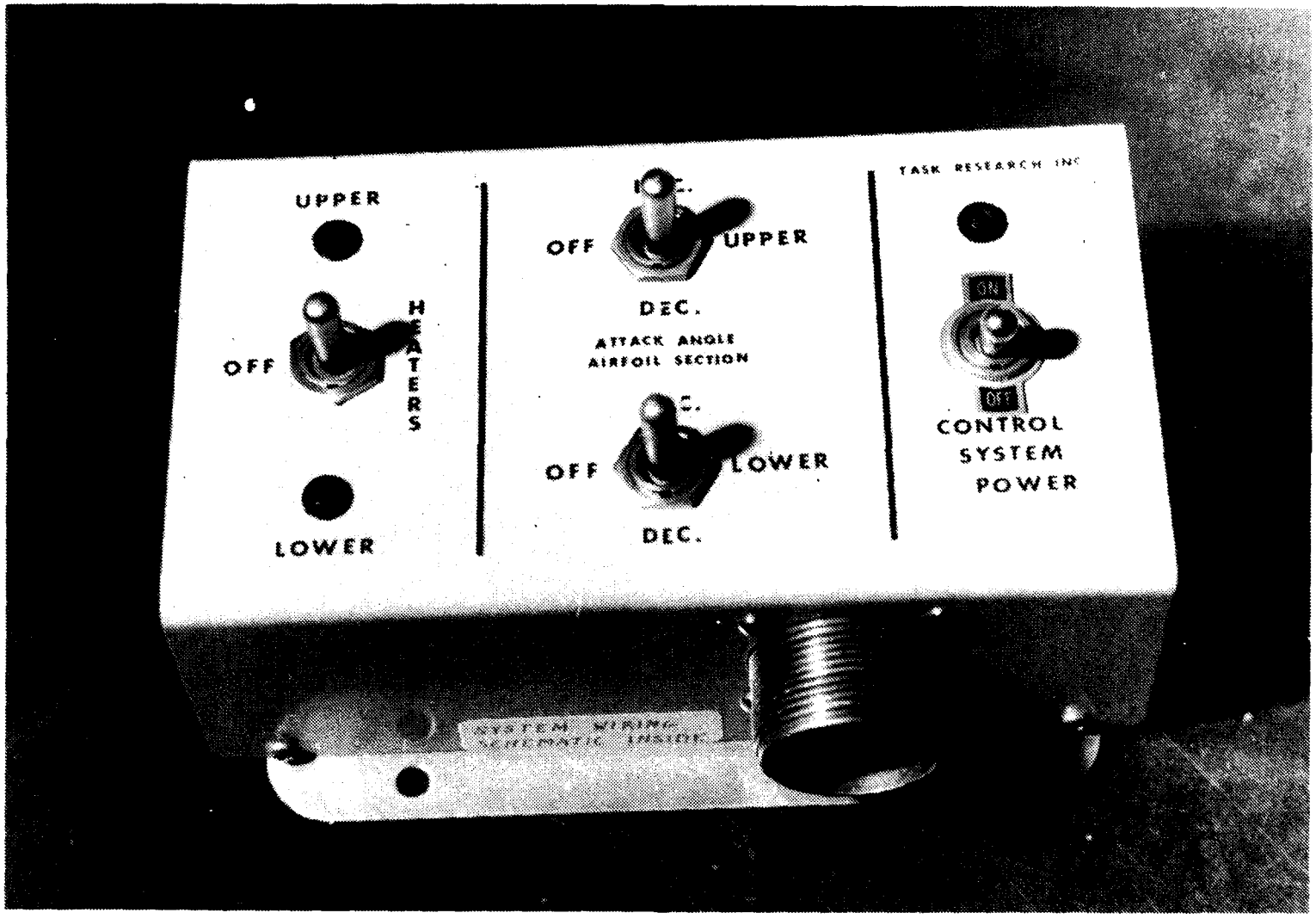

Figure B-5. ASA Control Panel

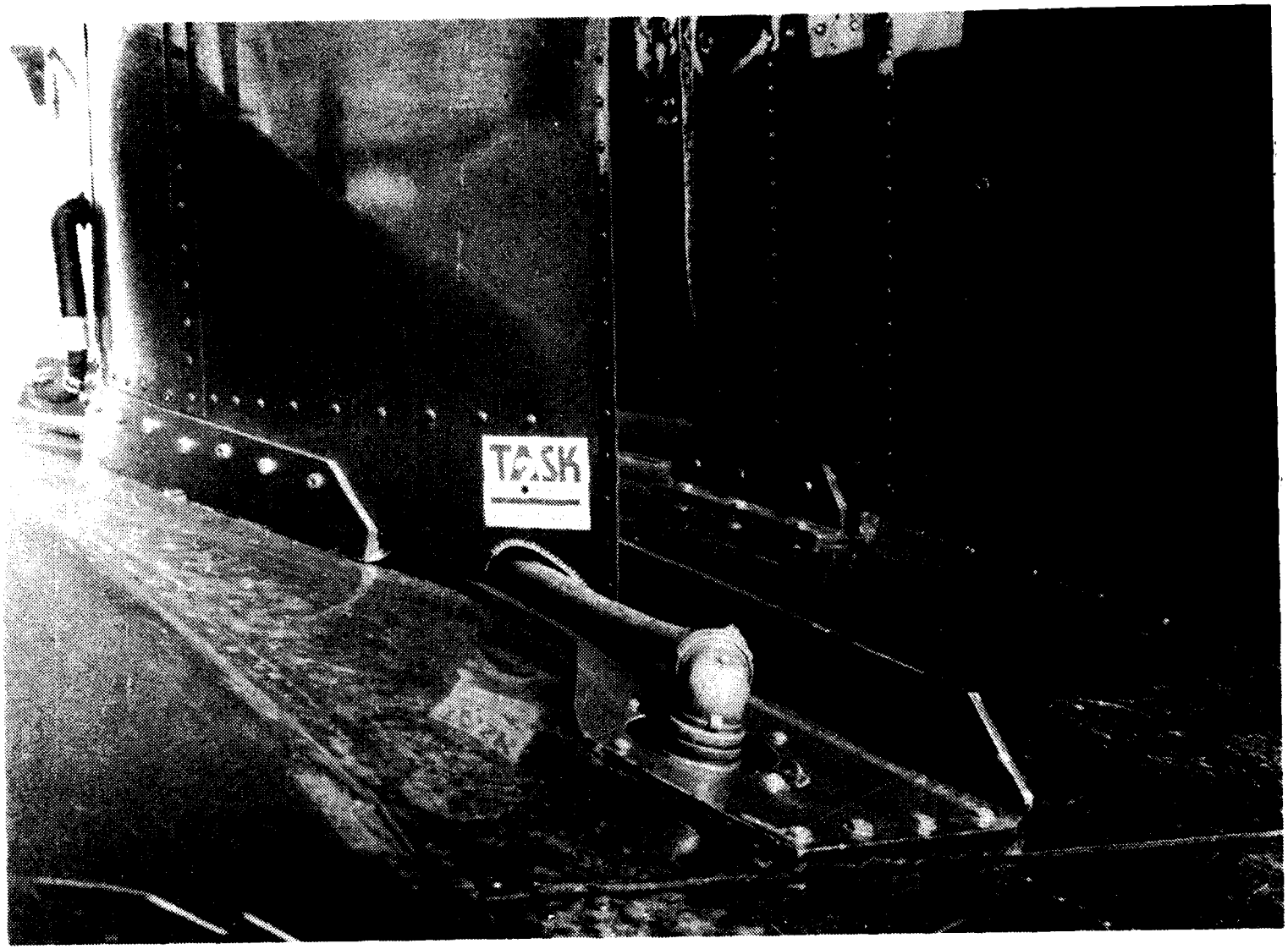

Figure B-6. Base of Outboard Pylon Showing Pneumatic Boot Connection at Front and Electrical Connector At Rear

8. The comparative blade section profiles shown in figure B-7 are taken from reference 24, appendix A, which presents wind tunnel data with aerodynamic characteristics of all three airfoils. The NACA 0012 section is a symmetrical airfoil with a maximum 12% thickness and a leading edge radius of 1.58% chord. The SC sections are cambered airfoils. The SC1095 has a 9.5% thickness with a leading edge radius of 0.83% chord, and the SC1094 R8 has a 9.4% thickness and an effective 1.75% leading edge radius. Task Research fabricated the ASA test airfoils from fiberglass over a steel spar in three scales, with chord sizes of 21 in. (full scale), 15.75 in. (3/4 scale) and 6 in. All airfoils had an 18-in. span. Figure B-8 shows the test airfoils as well as actual rotor blade sections for comparison.

9. Electrical heating blankets were imbedded in the test airfoil leading edges to 10% chord on the upper surface and 15% on the lower. The heater blankets were covered with 0.012 in. thick aluminum cladding blended into the airfoil contour to provide a painted surface texture representative of actual rotor blades. A power density of 25 watts per square inch was used on the 6-in. chord and 3/4-scale airfoils. Because of power considerations for single-generator electrical system operation of the JU-21A, the full-size airfoil heaters had a reduced power density of 20 watts per square inch. The electrical connectors and pivot mounting bolt provisions for each airfoil were centered on the quarter chord points.

10. An end plate attached to each airfoil, flush with the outboard support mast, was marked with a half-inch grid to provide a background for viewing the ice formations. Index marks on the end plates indicated airfoil incidence angle by position relative to stripes painted on the outboard support mast.

UNIVERSITY OF WYOMING SUPER KING AIR

11. The aircraft used to obtain cloud measurement comparison data was a Beech Aircraft Corporation Super King Air Model 200T, civil registration N2UW, operated by the University of Wyoming Department of Atmospheric Science, shown in figure B-9. It is a pressurized, low wing, all metal, twin engine airplane with retractable tricycle landing gear and a maximum takeoff gross weight of 14,000 lb. The aircraft has a wingspan of 55 ft, 6 in. and a length of 43 ft, 9 in. Power is provided by two Pratt and Whitney PT6A-41 turboprop engines rated at 840 shaft horsepower. The aircraft is certified for flight into known icing conditions and is equipped with a full complement of ice protection systems. The outer wing panels are reinforced to accommodate wing-tip

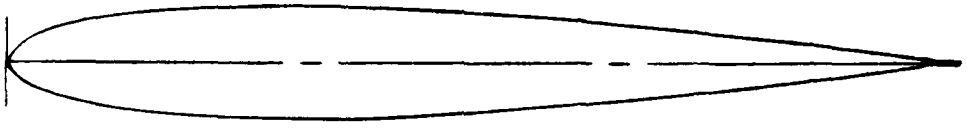

NACA 0012 (0° Tab)

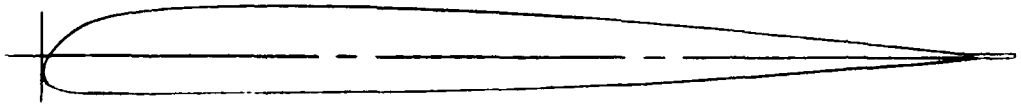

SC 1094-R8

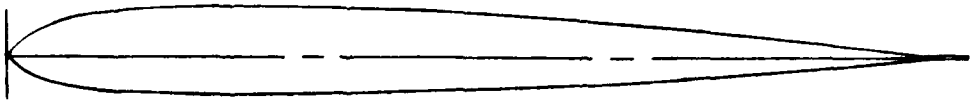

SC 1095

Figure B-7. Airfoil Blade Section Profiles (ref 24)

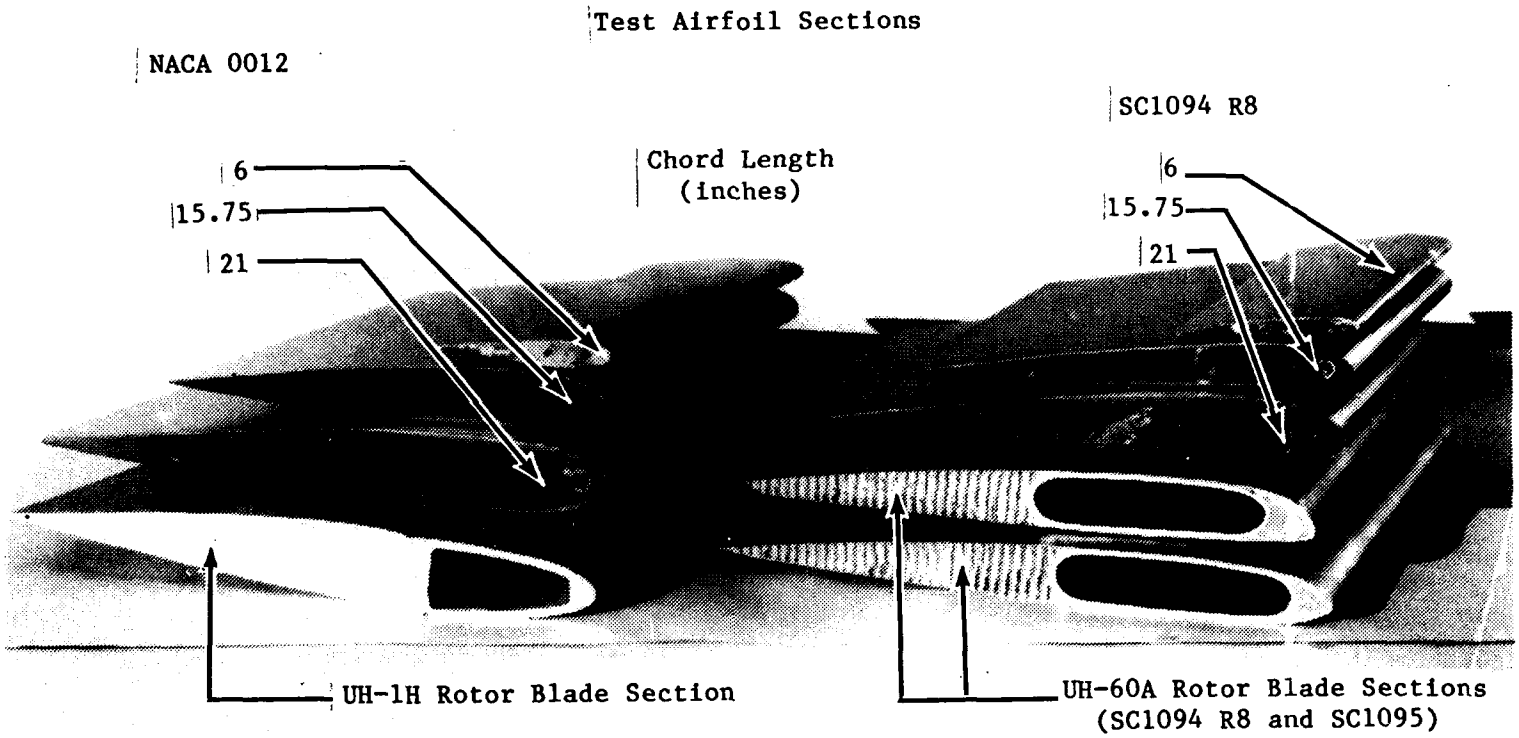

Figure B-8. ASA Test Airfoils and Actual Rotor Blade Sections

Figure B-9. University of Wyoming Super King Air N2UW

pylons for instrumentation mounts, and a Saunders Failsafe™ spar strap is installed between the outer wing panels beneath the fuselage. The aircraft is used as a cloud physics research test bed for various icing environment, cloud seeding, and storm climatology studies. Projects are sponsored by the FAA and the Bureau of Reclamation, Department of the Interior (e.g., High Plains Cooperative Experiment (HIPLEX) and Sierra Cooperative Pilot Project (SCPP) programs). The instrumentation and data systems installed are described in appendix C.

HELICOPTER ICING SPRAY SYSTEM (HISS)

12. The HISS is installed in a modified Boeing Vertol JCH-47C helicopter, US Army S/N 68-15814, with fiberglass rotor blades. It is a twin-engine, turbine-powered tandem-rotor helicopter with a maximum gross weight of 48,000 lb. Power is provided by two Lycoming T55-L-11 turboshaft engines. Each engine has an installed power rating of 3,750 shaft horsepower at standard day sea level conditions. (Since the completion of the project T55-L-712 engines have been installed). Each rotor system is 60 ft in diameter and is equipped with three fiberglass blades with 32 in. chords. Normal operating rotor speed is 225 rpm. Fuselage length is 50 ft 9 in., and distance between the fore and aft rotor hubs is 39 ft 2 in. A hydraulically powered loading ramp is located at the rear of the cargo compartment.

13. The HISS installation was initially developed under contract by the All American Engineering Co. and has been used for artificial icing evaluations since 1973. Various modifications from the original configuration have included a dual-trapeze spray boom incorporated in 1975, replacement of the original atomizers with Sonicore nozzles in 1979, addition of a gas-turbine bleed air source in 1981, and air and water plumbing improvements to the cabin and extenal boom assemblies since 1982. The present system is described in reference 13, appendix A, and side and rear views of the overall arrangement are shown in figure B-10. The internally mounted aluminum water tank has an 1800 gallon capacity, and when deployed the spray boom assembly is suspended 19 ft beneath the aircraft from a torque tube through the cargo compartment. Hydraulic actuators rotate the torque tube to raise and lower the boom assembly, and mechanical latches hold the boom assembly locked in either the fully deployed or retracted positions. Both the external boom assembly and the internal water supply can be jettisoned in an emergency.

14. The boom assembly consists of two parallel 27-ft trapeze sections with 5 ft vertical separators, and two 17.6-ft outriggers

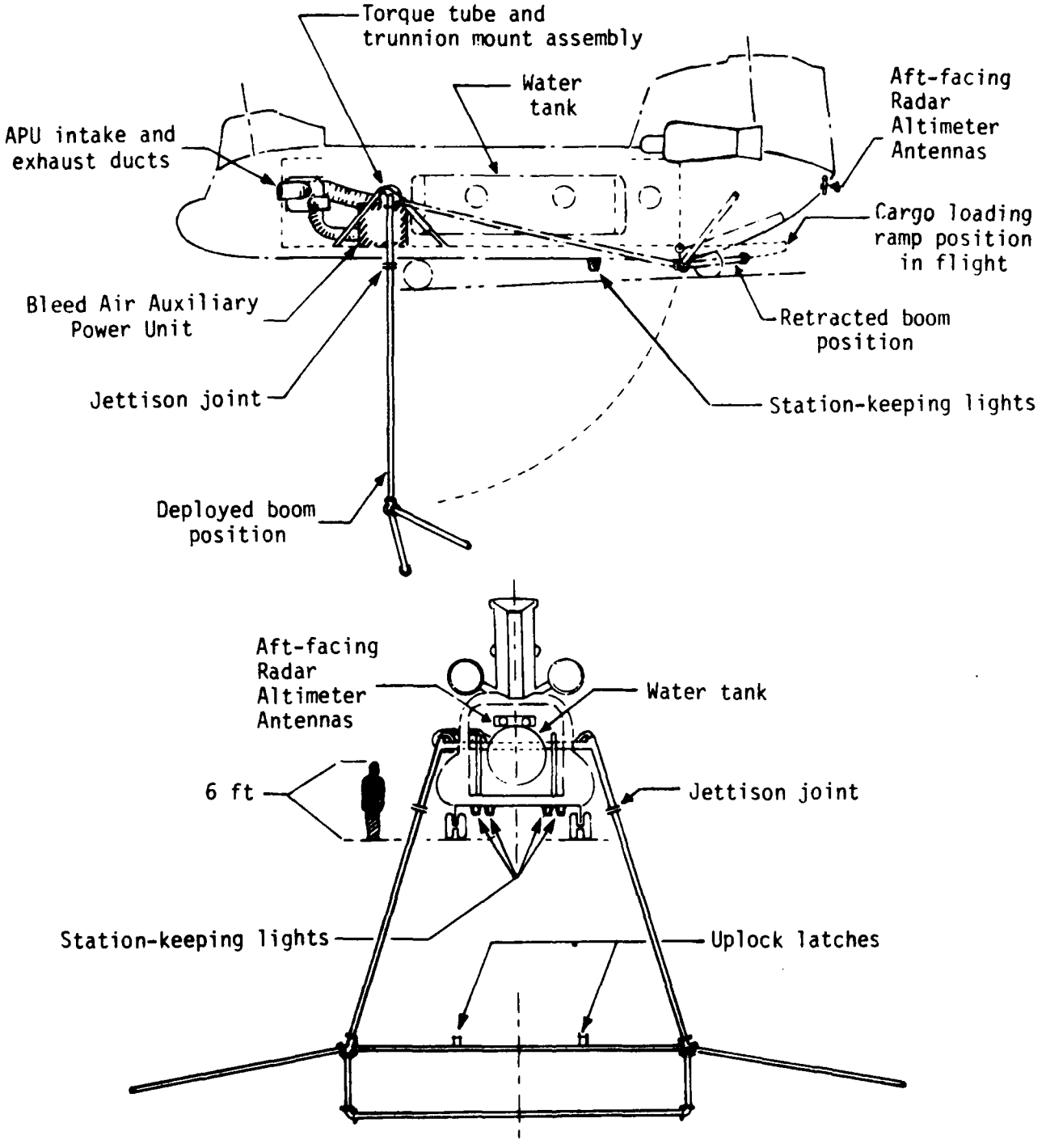

Figure B-10. Helicopter Icing Spray System
Side and Rear View Schematic

attached by 4-way junctions to the upper trapeze. When lowered, the outriggers are swept aft 20° and angled down 10° giving a tip-to-tip boom width of 60 ft. The boom is constructed of concentric metal pipe. The outer pipe (4 in. diameter) is the structural trapeze and outrigger assembly and provides a passage for bleed air. Water is pumped through the inner pipe at selected flow rates from the tank to the nozzles on the boom assembly. Aircraft engine compressor bleed air mixed with bleed air from a Solar T-62T-40C2 auxiliary power unit (APU) are supplied through the outer pipe to the nozzles for atomization. Sonic Development Corporation Model 125-H Sonicore nozzles are installed at 97 locations on the center trapeze sections only. The outriggers are retained for structural reasons but are isolated from the water and bleed air supply. At the nominal 180 feet distance from the booms used for icing tests, the size of the visible spray cloud cross-section is approximately 8 feet high and 36 feet wide.

15. To produce a selected LWC, the initial water flow rate is set to a value calculated from the relationship between water volume, airspeed, and cloud cross-sectional area that assumes an homogeneous spray dispersion and no water loss from evaporation:

$$LWC = \frac{1320.06 \times \text{flow rate}}{\text{airspeed} \times \text{area}}$$

Where:

LWC = liquid water content of drops within a volume of air, gm/m^3
flow rate = gallons/minute
airspeed = knots true airspeed (KTAS)
cross-sectional cloud area = ft^2 ($288\ ft^2$ for the 8 x 36 ft HISS spray)
1320.06 = conversion factor for units shown; water density taken as 1 gm/cm^3

This function provides a calculated average of LWC over the entire cloud cross-sectional area. Adjustments to the flow rate are made after the instrumented JU-21A samples the spray and obtains a measured value for LWC.

16. To provide visual cues to the test aircraft for maintaining standoff position, aft-facing radar altimeter antennas are mounted at the rear of the HISS which activate red and yellow lights on the fuselage. A calibrated Rosemount air temperature probe and a Cambridge dew point hygrometer with cockpit displays provide ambient temperature and humidity measurement. To enhance

photographic detail during icing operations, yellow dye is added to the water (calcocid uranine yellow No. 73, in approximate proportions of 7 ounces per 1500 gallons).

APPENDIX C. INSTRUMENTATION

JU-21A CLOUD MEASUREMENTS

1. The cloud measurement package installed on the JU-21A consisted of the following equipment: a Particle Measuring Systems, Inc. (PMS) forward-scattering spectrometer probe (model FSSP-100), a PMS optical array cloud droplet spectometer probe (model OAP-200X), Rosemount total temperature sensor and display, Cambridge model 137 chilled mirror dew point hygrometer and display, Cloud Technology Inc. model LWH-1 (Johnson Williams type) liquid water content (LWC) indicator system (installed after the cloud measurement comparison tests), and the Small Intelligent Icing Data System (SIIDS). Figure C-1 shows the exterior of the aircraft with the probes in place; figure C-2 shows the interior instrumentation rack with displays.

2. The PMS spectrometers provide a measurement of the drop size population found in the cloud. Each probe projects a collimated helium-neon laser beam normal to the airflow across a small sample area. In forward flight, particles passing through the beam (sample area) are counted and measured into 15 size channels per probe, each probe operating over a different size range. While these probes are primarily intended as particle sizing de ices, a LWC can be calculated from the drop size measurement and number count within the sample volume relative to airspeed. The FSSP-100 determines particle size by measuring the amount of light scattered into the collecting optics aperture as the particles pass through the laser beam, and resolves diameter from 2 to 47 μm into 15 3- μm increments. It is capable of sizing particles having velocites of 20 to 125 meters/ sec (39 to 243 knots). The OAP-200X determines particle size using a linear array of photodiodes to sense the shadowing of array elements. Particles passing through the field of view illuminated by its laser are imaged as shadowgraphs on the array, and size is given by the number of elements darkened by a particle's passage, the size of each array element, and the optical magnification. Magnification is set for a size range of 20 to 300 μm, and 24 active photodiode elements divide particles into 15 size channels, each 20 μm wide. It is capable of sizing particles with velocities of 5 to 100 meters/sec (10 to 194 knots).

3. The SIIDS was designed by Meteorology Research Inc. and is a data acquisition system programmed specifically for icing studies. A more complete description appears in the user's guide (ref 25, app A). It consistes of four main components: a microprocessor, Techtran data cassette recorder, Axiom printer, and an operator control panel. The SIIDS has three operational modes: (1) data acquisition, in which averaged raw data are recorded on cassette tape and engineering units are displayed on the printer, (2) a

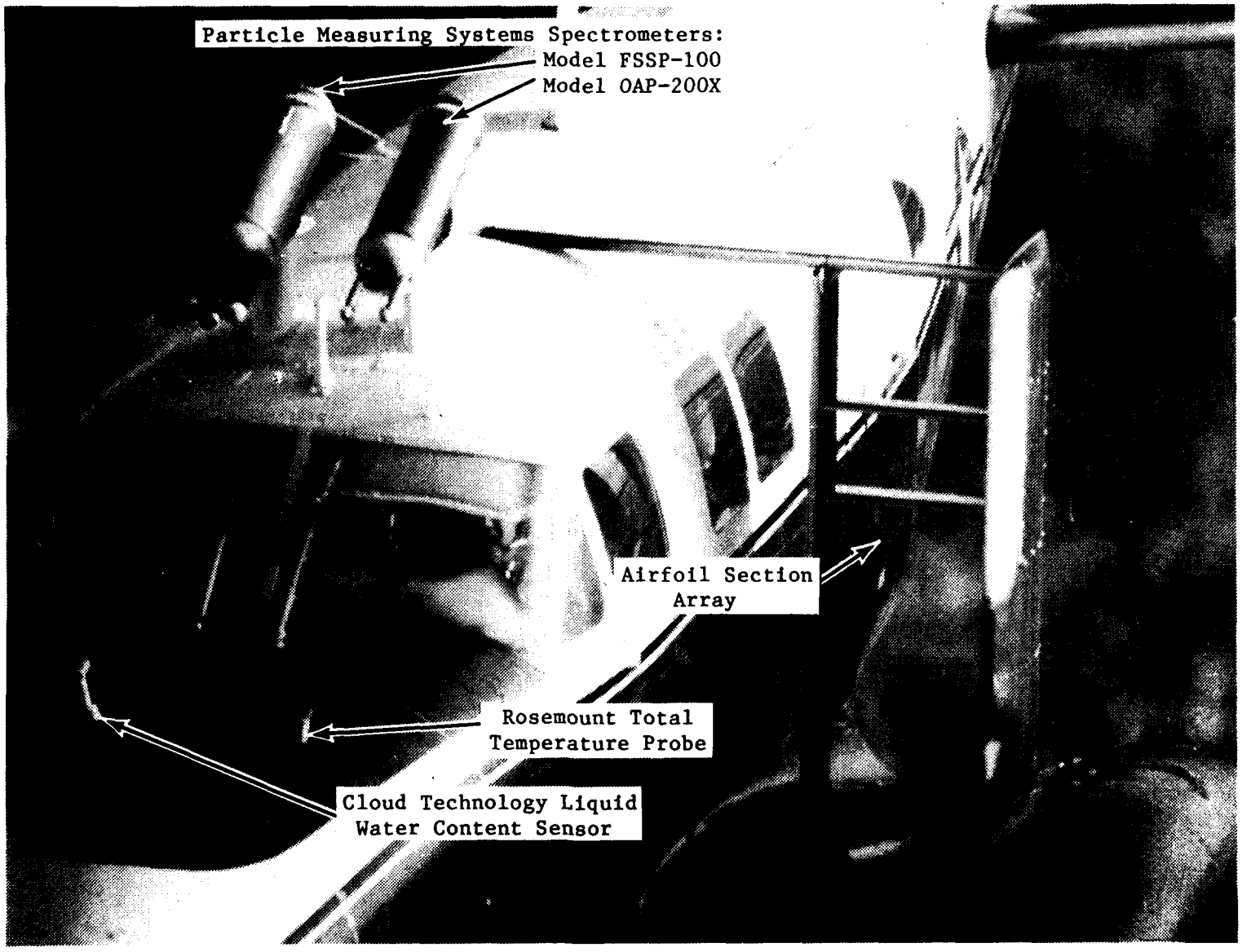

Figure C-1. Cloud Measuring Instrumentation on JU-21A

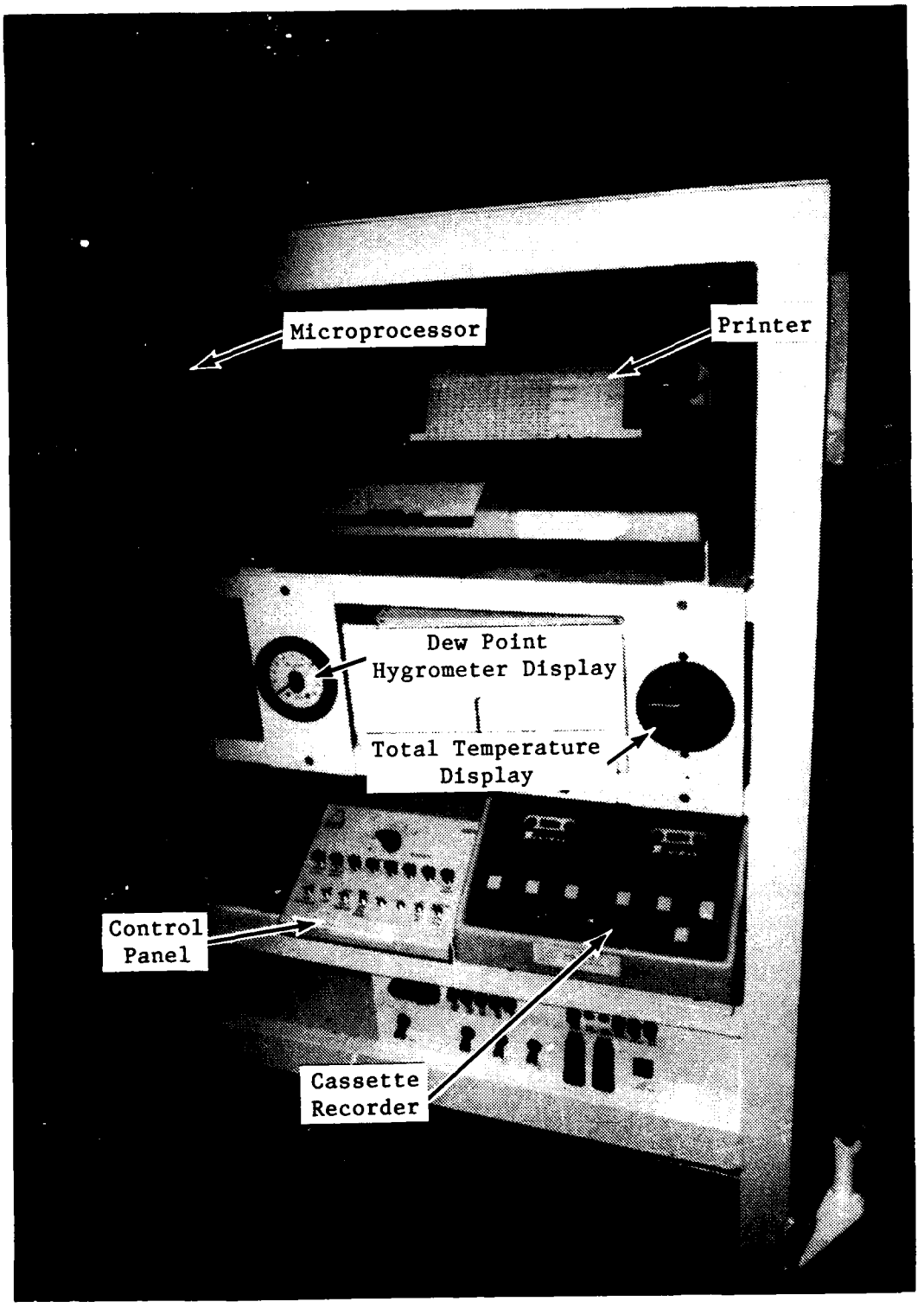

Figure C-2. SIIDS Display Rack

playback mode in which raw averaged data read from the cassette are converted to engineering units displayed on the printer, and (3) a monitor mode used to set the calendar clock and alter programmed constants. During data acquisition, the operator may select an averaging period of 1/2, 1, 2, 5 or 10 seconds. The following parameters are displayed on the SIIDS printer in engineering units.

a. calendar: year, month, day, hour, minute, and second

b. pressure altitude (feet)

c. airspeed (knots)

d. outside air temperature (°C)

e. dew point (°C)

f. total LWC observed by the FSSP (gm/m^3)

g. total LWC observed by both FSSP and OAP (gm/m^3)

h. median volumetric diameter (μm)

i. amount of LWC observed for each channel (total 30) of both probes (gm/m^3).

SUPER KING AIR CLOUD MEASUREMENTS

4. The data system installed in the University of Wyoming Super King Air was specifically designed for cloud physics research. Data acquisition is controlled by a microprocessor linked to an onboard computer. The computer converts the data to engineering units for display in the aircraft, while the microprocessor controls data recording on magnetic tape. Measurements available include a range of aircraft positioning and performance parameters in addition to the meteorological equipment and hydrometeor particle sensors. The instrumentation used for icing studies is discussed in some detail in reference 26, appendix A, and the data system output is described in reference 27. The data comparisons for this project used a particle spectrometer and two LWC sensors. The spectrometer is a PMS FSSP-100 instrument that provides drop size spectra in the 2- to 47-μm range in 15 size increments, as described in paragraph 2. The Bacharach Instruments model LWH Johnson-Williams sensor is a hot-wire device that provides an LWC measurement using the change in resistance of a heated wire exposed to the airstream. The second device uses a

design developed by the Australian Commonwealth Scientific and Industrial Research Organization (CSIRO). This device maintains a heated wire-wound cylinder at a constant temperature. LWC is proportional to the power supplied to the heated wire. Data from these probes were provided at a sample rate of one per second.

AIRFOIL SECTION ARRAY (ASA)

5. Ice accretions on the ASA were photographed using two 35mm Minolta model X-700 cameras fitted with Minolta 50mm focal length f/3.5 macro lenses. The lenses allowed focusing to within 9 in. of the film plane. Both cameras were fitted with motor drives and multifunction backs to allow automatic sequencing of exposures at preset intervals, and imprinted an LED time display (hr/min/sec) on each image. Kodacolor VR 400 color negative (print) film was used without any filters. The lenses were set for an f/8 aperture in automatic exposure mode during the sequence photos, resulting in shutter speeds ranging between 1/250 and 1/500 of a second over the cloud shrouded (natural) and sunlit (artificial) icing conditions encountered.

6. The cameras were mounted in the aircraft cabin on a bracket attached below the left forward window (fig. C-3), positioning the camera film planes approximately 35 3/4 inches from the test airfoil reference grid surface. The bracket held the cameras one above the other to sight along the leading edge of each test airfoil. The same lens and camera combinations were used for the respective upper and lower bracket locations throughout the program. The bracket design permitted lateral and vertical positioning and tilt adjustment of each camera to accommodate required changes in field of view resulting from test airfoil selection or size of ice accretion.

7. An end plate attached to each airfoil, flush with the outboard support mast, was marked with a half-inch grid (red and white checkerboard self-adhesive Trim Monokote™) to provide a background for viewing the ice formations. Index marks on the end plates indicated airfoil incidence angle by position relative to stripes painted on the outboard support mast. Tufts were attached at various locations on the inboard surface of the outer ASA pylon to provide an indication of local flow angle. Date, flight number, and airfoil information were written directly on the ASA pylon with a grease pencil to assist identification of the resulting photographs. A small piece of black tape was positioned on the aircraft window to darken the lower right frame corner of each camera for better visibility of the time display appearing on the exposed negative.

8. A hand held probe equipped with pitot and static ports (fig. C-4) connected to a separate calibrated aircraft airspeed indicator was fabricated for this program. The probe could be extended from the aircraft cabin through a hole in the fuselage (fig. C-5) to obtain airspeed measurements at various locations around the ASA assembly.

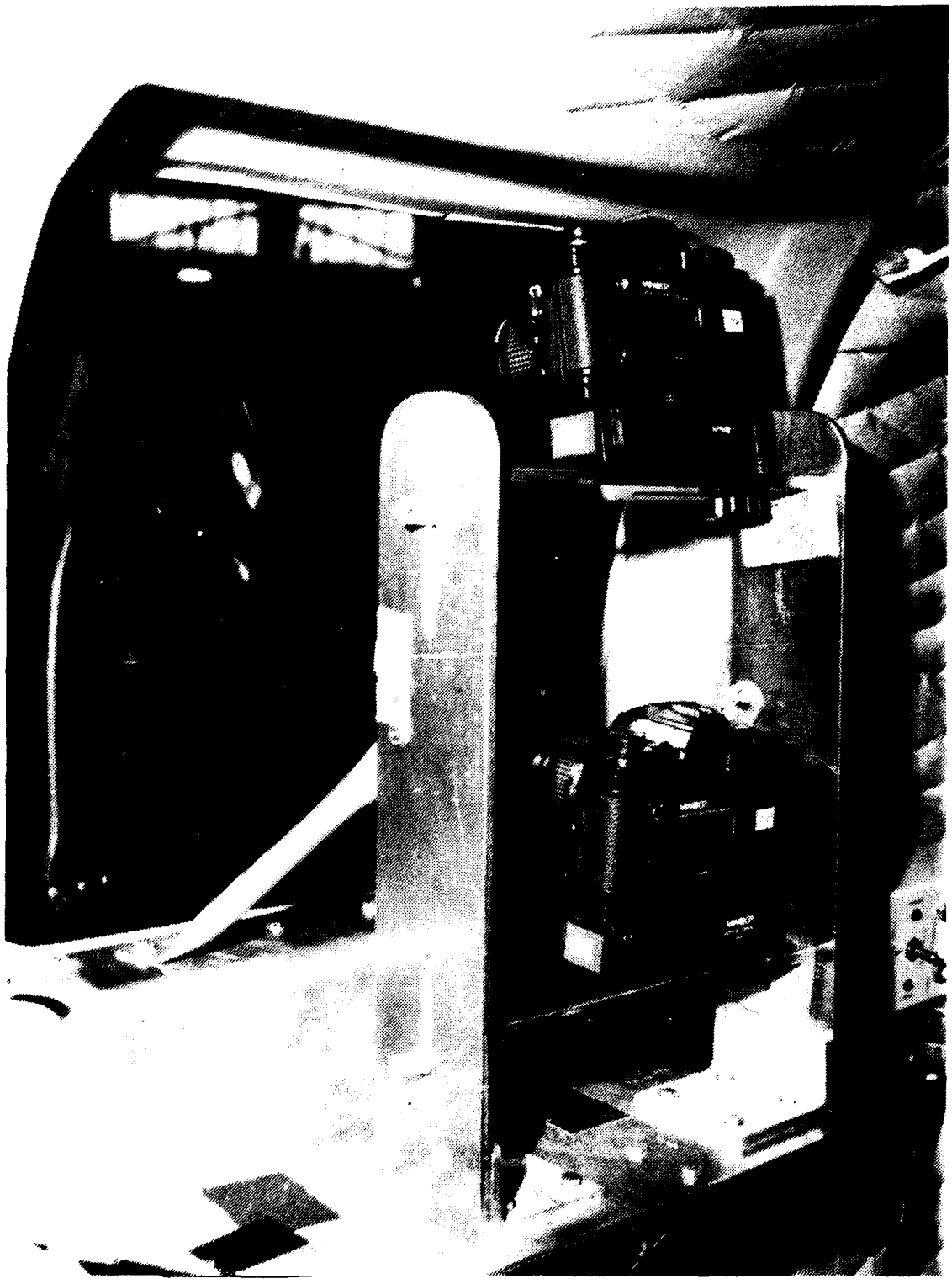

Figure C-3. Cameras Installed on Mounting Bracket Next to Cabin Window

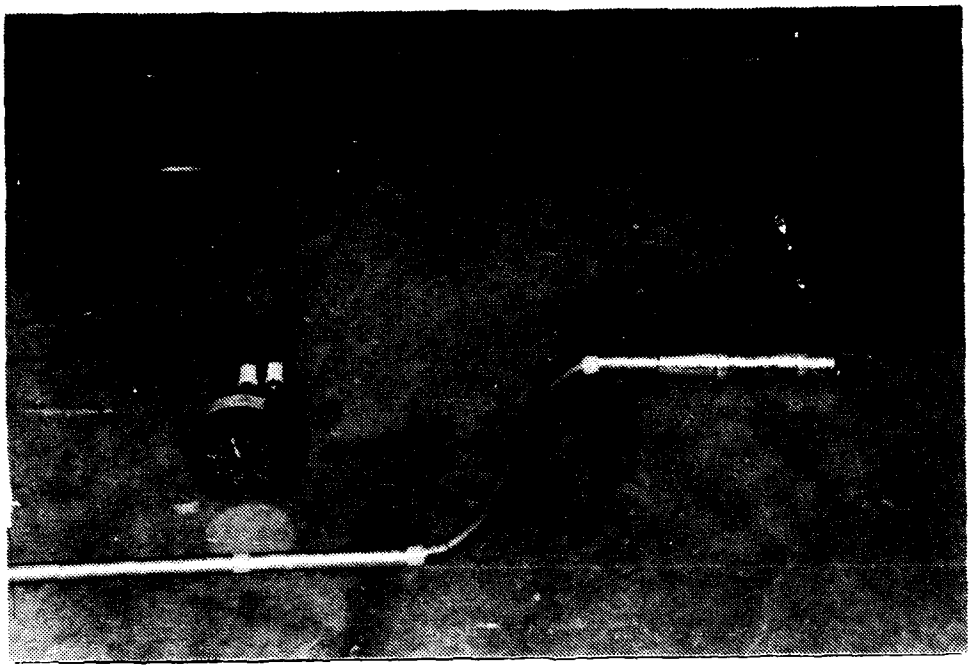

Figure C-4. Hand-Held Airspeed Probe and Indicator

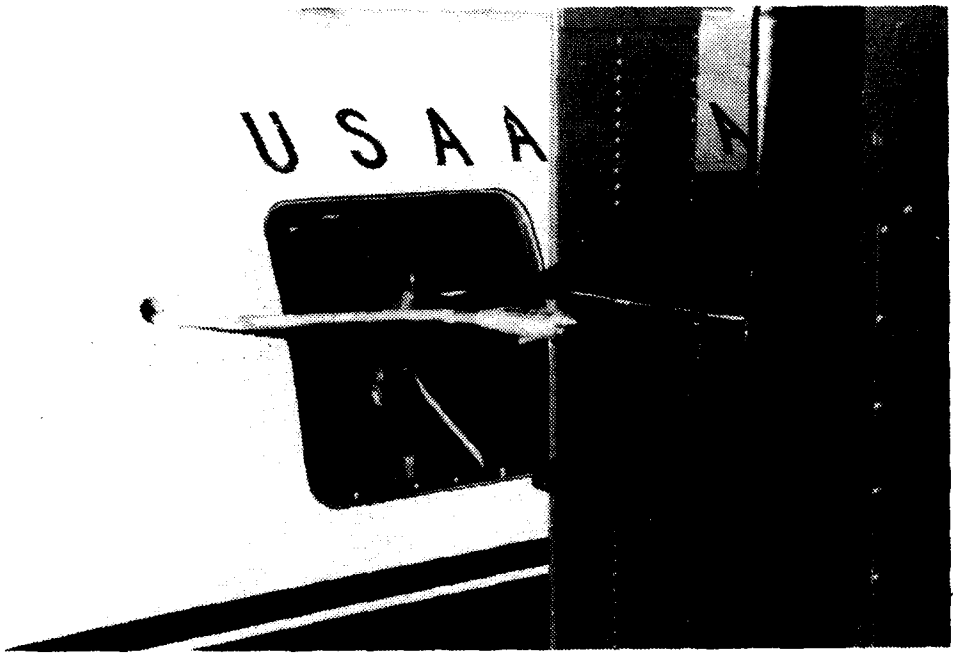

Figure C-5. Airspeed Probe Extended Through Fuselage Opening Ahead of Test Airfoils

APPENDIX D. TEST TECHNIQUES AND DATA ANALYSIS METHODS

CLOUD MEASUREMENT COMPARISON

1. Comparative cloud measurements from the JU-21A and the University of Wyoming Super King Air were made in orographic cumuliform clouds under conditions of 60 to 80% sky coverage near Sacramento, California. Sampled clouds varied from one to four miles in horizontal extent, and 3000 to 6000 ft in depth. Airpeeds flown were from 160 to 200 KTAS. The Super King Air served as lead aircraft and its weather radar was used to assist in cloud selection. The JU-21A followed in trail formation approximately three nautical miles to the rear. At cloud entry, the Super King Air announced heading, altitude and airspeed for the penetration and held them constant. The JU-21A followed at the same altitude and heading but several knots slower to avoid closure. When both aircraft had exited the cloud, they resumed trail formation and penetrated additional clouds in the same manner.

2. Data taken during these cloud penetrations were made available in a one-sample-per-second format. Since the cloud entry and exit times for the two aircraft were different, the time scales were adjusted to allow comparison between measurements. This was done using elapsed time spent within the cloud by the Super King Air as the baseline, and assuming that the JU-21A flew the same path through the cloud. The JU-21A data time scale between cloud entry and exit was compressed to match total duration of the Super King Air exposure to allow comparison over the extent of the cloud.

ASA AIRWORTHINESS EVALUATION

3. Before conducting icing operations of the JU-21A equipped with the ASA assembly and test airfoils, airworthiness was established by a combination of engineering analysis and flight envelope expansion. Task Research Inc. provided an initial structural analysis as part of the ASA contract. Additional flight loads and stress calculations were performed at AEFA and AVSCOM to determine safety margins and suitable operating limits. These analyses identified several features of the original ASA design and hardware that required modification to satisfy structural integrity and airworthiness criteria. The contract was amended appropriately and Task Research rebuilt the ASA assembly to reinforce portions of the structure and strengthen the mounting provisions.

4. Before first flight, a series of high-speed taxi runs to rotation speed (93 KIAS), including nose wheel liftoff, using several test airfoil combinations verified satisfactory ASA

operation and pre-takeoff characteristics. Takeoff on the first flight with the ASA was intentionally limited to lifting off to several feet above the runway and descending again to touchdown before resuming forward acceleration for normal takeoff and climbout. A chase aircraft flew formation with the JU-21A to observe takeoffs, landings, and in-flight maneuvers during the airworthiness evaluation. Tufts were applied to the left side of the JU-21A fuselage, wing, and empennage to provide visual indication of airflow patterns aft of the ASA assembly. Data onboard the JU-21A were hand recorded using standard aircraft instrumentation and cockpit indicators.

5. The flight envelope expansion followed a build-up sequence, proceeding from small to large ASA blade sections, progressive incidence angle variation, increasing aircraft weight, and finally addition of the roof mounted PMS probes. The evaluation considered aircraft configurations and maneuvers used throughout each phase of an icing flight profile, to include possible emergency situations. These configurations (takeoff, cruise, 35% flaps, approach, and landing) are described in table D-1 and the maneuvers evaluated are shown in table D-2. For comparison, baseline (no ASA) handling qualities flights were conducted before the airworthiness evaluation and again after the icing tests. The evaluation was performed using established flight test techniques (ref 8, app A).

6. For each configuration, lateral-directional stability characteristics were qualitatively evaluated by establishing steady heading sideslips and noting the required control forces and deflections. Aircraft response after release from sideslip by returning the controls to trim provided frequency and damping characteristics of the resulting oscillations. Since sideslip angle was not displayed in the cockpit, the turn and slip (ball) indicator was used as a reference. Ball displacement could be correlated with sideslip angle as estimated from the position of a yaw string relative to angle markings on the aircraft nose and windshield. One ball width, of displacement was produced by approximately 15 degrees of sideslip at 120 KTAS and 5 degrees at 200 KTAS.

7. The stability evaluations were conducted in climb, descent and level flight over airspeed ranges appropriate for an operational icing mission. Standard maneuvers such as turns, pull-ups, and pushovers were performed to determine any effects of the ASA on handling qualities. Integrity of the ASA installation was verified to a maximum airspeed of 200 KTAS for use during icing flight operations.

Table D-1. JU-21A Aircraft Configurations for ASA Airworthiness Evaluation

Configuration	Landing Gear Position	Flap Setting	Propeller Speed (rpm)
Takeoff	Down	Zero	2200
35% Flaps	Up	35%	1900
Clean		Zero	
Approach	Down	35% to full down	2200
Landing	Down	Full Down	2200

Table D-2. JU-21A Tests for ASA Airworthiness Evaluation

Maneuver	Aircraft Configuration	Airspeed	Remarks
Climb	35% Flaps, Clean	115 to 140 KIAS[1]	Climb to test altitude of 9000 feet H_P, sideslip to 1 1/2 ball width
Descent	35% Flaps	140 KIAS	500 ft/min descent, sideslip to 1 1/2 ball width
	Clean	160 KIAS	
Level Flight	35% Flaps	105 to 125 KIAS	Vary ASA angle of attack, turns to 45° bank angle, sideslip to 1 1/2 ball width, pull-ups to 1.5 g, pushovers 0.5 g
	Clean	140 to 160 KIAS	
V_H[2]	35% Flaps	173 KIAS	ASA angles neutral, sideslip to 1 ball width
	Clean	200 KTAS[3]	
Stall Characteristics	3% Flaps, Takeoff, Approach, Landing	From 1.2 V_{sl}[4]	ASA angles neutral, power OFF and 50% power settings
Simulated Single-Engine Failure	35% Flaps	120 KTAS	Left and right engine throttle chops, autopilot ON
	Clean	160 KTAS	
Static V_{mc}[5]	35% Flaps, Takeoff, Approach, Landing	From V_{yse}[6]	Autopilot OFF, left engine set at zero thrust, right engine at takeoff power
Dynamic V_{mc}	35% Flaps, Takeoff, Approach, Landing	From Static V_{mc} +20	Autopilot OFF, left engine throttle chop to idle

NOTES:

[1]KIAS: Knots indicated airspeed.
[2]V_H : Maximum level flight airspeed as limited by the Airworthiness Release.
[3]KTAS: Knots true airspeed.
[4]V_{sl} : Stall airspeed for a specific aircraft configuration without the ASA installed.
[5]V_{mc} : Minimum airspeed at which control can be maintained with the left (critical) engine set at zero thrust.
[6]V_{yse} : Single-engine best rate of climb airspeed.

8. Stalls were performed at 50% of maximum available power and with idle power. Trim airspeeds were 1.2 times stall speed of the baseline aircraft (no ASA) in each configuration, and the stall condition was approached by reducing airspeed by one knot per second or less. Stall warning, buffet, stall break, poststall gyrations, and control margins were noted for each aircraft configuration to evaluate stall characteristics.

9. Simulated single-engine failures in level flight at 120 and 155 KTAS were performed by reducing rapidly the power lever of the right and left engine to determine aircraft reaction and recovery characteristics.

10. Minimum single-engine control speed (static V_{mc}) tests were conducted with the left (critical) engine set at approximately zero thrust and the right engine at takeoff power. The aircraft was trimmed at single-engine best rate of climb airspeed (V_{yse}) and then slowed by one knot per second or less while maintaining a zero turn rate and a 5-degree bank angle into the operating engine. The airspeed at which lateral or directional control limits were reached or when the aircraft stalled was defined as static V_{mc}.

11. Minimum control speed after sudden engine failure (dynamic V_{mc}) was evaluated from trimmed symmetrical test day maximum power climb by rapidly reducing the left engine power to idle. Controls were held fixed for one second or until roll attitude or heading changed more than 20°. All controls were then used to return the aircraft to stabilized flight at the trim airspeed without reducing power on the operating engine or adding power to the idling engine. These tests were repeated at increasingly lower trim airspeeds. The airspeed at which aircraft heading or roll attitude changes exceeded 20° or stall was encountered was defined as dynamic V_{mc}.

ASA ICING TESTS

12. The ASA icing evaluation was conducted by flying the JU-21A in both natural clouds and in the artificial clouds produced by the HISS. Cloud immersion resulted in accretion of ice on the aircraft and test airfoils. The JU-21A ice protection systems were activated as required during the icing flights in accordance with procedures in the operator's manual. The initial icing tests were flown using the HISS cloud to gain experience with the ASA in icing conditions and to verify satisfactory operation. Subsequently, the natural and artificial phases were flown concurrently during the test period, depending on weather conditions.

As described in reference 13, appendix A, the JU-21A also supported other icing programs as a scout and chase aircraft during the test period, and conducted an evaluation of HISS spray cloud characteristics.

13. The natural icing tests were generally flown in stratiform clouds in instrument meteorological conditions (IMC) under instrument flight rules (IFR). Coordination with air traffic control to find and stay in the icing environment was accomplished using a combination of radar vectoring, navigational aid holding, and block airspace assignment. Icing immersion was initiated by descending into the cloud tops and remaining within the upper 200 ft of the layer, seeking exposure to the highest LWC available. Average airspeed was generally maintained between 150 and 155 KTAS in a clean (zero flaps) aircraft configuration. Immersion was terminated by climbing above the cloud.

14. Artificial icing tests were conducted by flying in the spray cloud produced by the HISS. The cloud was entered from a position beneath the spray plume, and standoff distance was maintained at 180 ft behind the spray booms by using the HISS radar altimeter and positioning light arrangement. For all artificial icing flights, airspeed was held at 120 KTAS and a water flow rate of 13 gal/min was used to produce a nominal LWC of 0.5 gm/m^3. An approach flaps setting (35%) was used to provide a fuselage attitude as nearly level as practicable at this airspeed.

15. Two test airfoils were installed one above the other in the ASA assembly on the JU-21A. When airfoils of different chord were used, the smaller one was placed in the top location. During flight in icing conditions, airfoil ice accretions were photographed using two 35mm cameras, each positioned to sight along the leading edge of one airfoil through the cabin window. The cameras were started simultaneously on cloud entry, and automatically took a series of sequence photographs throughout the immersion at preset intervals of 15 seconds to one minute between exposures. Immersion duration was normally sufficient to provide an ice thickness great enough to allow reasonable indication of shape and accretion. A hand held 35mm camera was also used during the icing encounters to obtain different views of the ASA and photograph ice accretion on portions of the airframe.

16. The HISS cloud was always set to spray at 13 gpm for a nominal LWC of 0.5 gm/m^3 at the 120 KTAS airspeed flown (para 15, app B). This flow rate was selected as a moderate icing severity condition that produced satisfactory atomization (well below nozzle breakdown at high water to air pressure ratios that occur at flow rates greater than 30 gpm) and provided a uniform spray pattern

throughout the boom array (without sputtering or flow imbalance problems at flow rates less than 8 gpm). Since relative humidity was 50% or higher in all cases, evaporative effects that tend to drive MVD upward were assumed to be moderate. Previous experience with the HISS (ref 13, app A) indicates a drop size spectrum that peaks between 15 and 25 μm but includes drop diameters as large as 200 μm, resulting in an MVD near 35 μm for this flow rate. The artificial icing cloud for this program was assumed to have an LWC of 0.5 gm/m^3 and an MVD of 35 μm.

17. The natural icing conditions were more difficult to categorize without reliable data. The LWC of the stratiform clouds typically encountered near Duluth during scouting flights have most frequently ranged between 0.1 and 0.2 gm/m^3. Since this is near the low end of the desired LWC range, natural clouds with higher values are actively sought during icing programs. LWC values from 0.25 to 0.50 gm/m^3 and higher are less frequent, which contributes to the length of time commonly required for icing projects. The most common condition considered acceptable for icing flights generally produces LWC values that fluctuate from 0.1 to 0.3 gm/m^3, averaging near 0.2. The most frequent drop sizes encountered near Duluth (for 0.1 to 0.2 gm/m^3) occur in an MVD range from 10 to 18 μm. A correlation with temperature is frequently seen, with smaller drops occurring at lower temperatures. However, larger drop size averages are often measured at the higher LWC values flown, and MVD sizes as high as 25 μm are not uncommon. Selecting a single figure as representative of all natural conditions is subject to limitations, but values around 18 to 20 μm appear most appropriate. The natural icing clouds for this program were assumed to have an LWC of 0.2 gm/m^3 and an MVD of 20 μm.

18. The nominal drop size distributions corresponding to these assumed values are compared in figure D-1. These curves show the normalized drop mass (LWC) distributions estimated as representative of the natural and artificial icing clouds encountered by the JU-21A in this program, and were derived from cloud measurements presented in reference 13, appendix A.

19. After cloud exit, the test airfoils and ASA structure were deiced as far as practicable with the pneumatic boot on the outboard support pylon and the leading edge heaters on the test airfoils. A hand held bent metal tube was then extended through an opening in the cabin wall and used to scrape ice from the inboard pylon and clear away residual formations on the test airfoils and outer pylon. When deicing was complete and the cameras reloaded if required, the airfoils were reconfigured for the next immersion at a new incidence angle. Three complete

Figure D-1

NOMINAL CLOUD SPECTRA

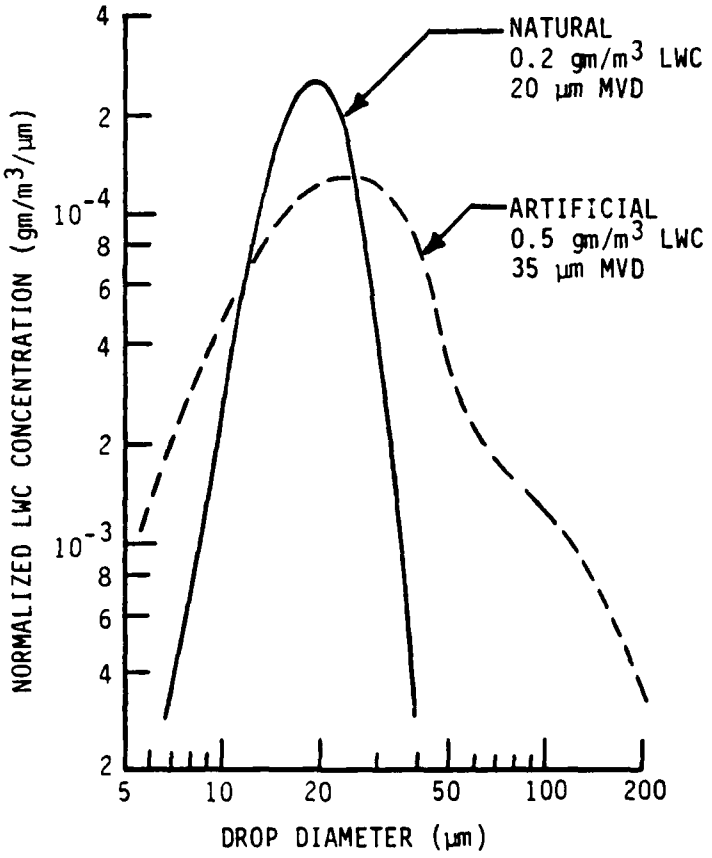

immersions were generally accomplished per flight, at airfoil incidence angles of 0°, 6° and 9°, with an occasional fourth immersion at a 3° angle on some flights. Selecting and installing different pairs of test airfoils from the six available was accomplished on the ground between flights, based on test conditions anticipated for the next flight.

20. Determination of ice shapes from the ASA sequence photographs was accomplished by projecting the original 35mm negatives with a darkroom enlarger onto 1/4-inch grid graph paper. Size of the image was carefully adjusted to align the original 1/2-inch end plate background grid with the graph paper. Reference marks on the images were provided by the edges of the end plate, the index and angle alignment marks, and triangular tape pieces that attached tufts to the pylon, allowing repeatable alignment and overlay from one negative to the next. The initial photo of an icing sequence showed the leading edge outline of the clean airfoil section, and subsequent overlaid photos provided silhouettes of the growing ice accretion. These outlines were traced by hand onto the graph paper. Usable profile visibility was limited to the forward portions of the ice shapes due to perspective effects (R&D section, para 41). The airfoil contours shown aft of the leading edge were obtained from correctly scaled 2 dimensional drawings. A time display was imprinted on each negative during exposure. The time interval between photographs was usually 30 or 45 seconds for artificial and 60 seconds for natural icing. Only a portion of the photographs are presented in this report, therefore, the elapsed time between the ice shape tracings shown is greater.

ICING SIMILITUDE

21. Several flight and wind tunnel investigations have studied ice accretion on rotorcraft airfoils in recent years. Artificial ice formations on actual UH-1H rotors were obtained during two programs: in hover conditions at the Ottawa Icing Spray Facility during 1983 (ref 28, app A) and in forward flight at 90 KTAS behind the HISS during 1984 (ref 21). The ice formations were obtained by making silicone rubber molds after landing. The aerodynamic characteristics of castings made in these molds were then evaluated at the Fluidyne Engineering Corp. transonic wind tunnel (ref 29 and 30). A full-scale UH-1H main rotor section was tested at the NASA-Lewis Icing Research Tunnel (ref 31). This test investigated the effects of incidence angle, temperature, airspeed, LWC, MVD, and exposure time. Several 6-inch chord airfoils (including the NACA 0012 and SC1094 R8 sections) were tested and molds were made at the Canadian National Research

Council High Speed Icing Tunnel in Ottawa (ref 32). Aerodynamic characteristics of these ice shape castings were further evaluated at the Ohio State University Transonic Airfoil Facility tunnel, and the combined results are described in references 33, 34 and 35. Effects considered included Reynolds number, surface roughness, rime feathers, and turbulence.

22. A general engineering summary of technical data related to ice accretion characteristics is given by reference 22. Effects of airspeed, temperature, pressure, drop size, LWC, body size and geometry are discussed as they relate to airfoil icing parameters such as drop trajectories, impingement limits, collection efficiency, freezing fraction, and ice shapes. Nondimensional icing parameters are used to simplify correlation of variables. Advances in computer technology since reference 21 was published (1964) have expedited the application of numerical solutions to complex algorithms.

23. A number of terms in general use for icing analysis are used in this report. The parameters described below appear in the engineering data summary of reference 22, appendix A, the more recent analyses in references 36 through 38, and the scaling comparisons used for the similitude computer code in reference 23:

a. Local Impingement Efficiency (β) is the ratio of the mass flux of water striking the airfoil surface to the mass flux contained in the free stream. It applies to a particular point on the airfoil contour, and values for β vary over the surface arc, with the maximum value usually near the stagnation point.

b. Modified Inertia Parameter (Ko) is a function of airspeed, drop diameter, and drop density divided by airfoil chord, air density, and air viscosity. It includes Reynolds number and affects the flow field and drop trajectories over the airfoil. Ko increases with larger drop diameter, greater airspeeds, lower air density, or smaller chord size.

c. Accumulation Parameter (Ac) represents the potential ice accumulation thickness that would accrete during a given icing immersion if the overall collection efficiency were 1.0 and all the water drops froze. It is nondimensionalized to a fraction of chord length and is a product of LWC, airspeed, and immersion time divided by density of the ice accreted.

d. Freezing Fraction (n) defines the fraction of impinging liquid which freezes in the region of impingement, and involves energy and heat transfer relationships between the liquid water

drops and body surface. Factors affecting n include static temperature, airspeed, LWC, and static pressure.

e. Relative Heat Factor (b) measures the ratio sensible heat absorbing capacity of the impinging water to the body convective heat-dissipating capacity per unit surface area. Factors affecting b include LWC, airspeed, local impingement efficiency, specific heat of water, and body geometry.

f. Energy Transfer Potentials for the water drops (ϕ) and surrounding air (θ) have units of temperature difference and are a measure of their convective heat flux transfer driving potentials. ϕ is related to the total enthalpy (heat content) of the impinging water. Static pressure, temperature, airspeed and LWC terms are included.

24. References 36, 37 and 38 describe more recent studies that used an analytical approach to explore the effects of airfoil geometry on rime icing characteristics. With this approach, the flow field over an airfoil is first calculated to derive the drop trajectories and their impingement locations. When ice accretion begins to change the profile, an iterative procedure is then used to recalculate the flow field for successive stages of ice build-up. By changing separate variables in the calculations, their relative effects on icing parameters can be compared analytically. An additional parameter, the overall collection efficiency, is the ratio of vertical distance between upper and lower surface impingement limits on the airfoil (the drop tangent trajectories) and the total projected height of the airfoil.

25. The effects of airfoil characteristics and free stream conditions on the icing parameters are described in references 37 and 38. Larger drop diameters increase the collection efficiency, maximum impingement efficiency, and area of impingement. The modified inertia parameter is directly proportional to airspeed, drop diameter, and inversely proportional to chord length. Higher values of modified inertia parameter increase local and maximum impingement efficiencies, overall collection efficiency, and extend upper and lower surface limits of impingement. Increasing incidence angle decreases the upper limit of impingement and increases the lower limit. Increasing incidence angle also tends to increase overall collection efficiency at higher values of modified inertia parameter. Decreasing leading edge radius increases maximum impingement efficiency, but can increase or decrease overall collection efficiency depending on incidence angle. Decreasing airfoil thickness increases overall collection efficiency, but does not greatly affect maximum impingement

efficiency. Increasing camber appears to move the impingement area toward the upper surface of the airfoil for a given lift coefficient. Decreasing airfoil thickness and increasing airfoil camber each tend to allow limits of impingement on the lower surface to reach the airfoil trailing edge at lower incidence angles.

26. To achieve similar icing characteristics for different scale airfoils, the flow fields and drop trajectories must be comparably scaled. This can be obtained by holding the modified inertia parameter constant, and assumes similar scaling of viscous and boundary layer effects. To maintain proper scaling between total accretion for a given immersion, test conditions must also produce the same accumulation parameter (nondimensionalized ice thickness). Reference 23 presents an analysis of factors that affect similitude relationships, i.e., the interaction of variables required to produce proportionately scaled ice formations of correct shape for different size airfoil models. This study verified such relationships in the Arnold Engineering Development Center Engineering Test Facility icing tunnel using different sized cylinders and airfoil sections.

27. Icing similitude implies that correctly scaled ice shapes will be produced on different size bodies by selecting test conditions to keep appropriate nondimensional parameters constant. In addition to the modified inertia and accumulation parameters, stagnation-line thermodynamic factors were considered to maintain corresponding rime and glaze characteristics. The icing tunnel tests of reference 23 compared several combinations of similitude parameters and found that holding Ko, Ac, n, ϕ, and θ constant gave consistent results within the accuracy of the measurement technique. Reference 23 also presents a computer program (SIMICE) that calculates values of the scaling parameters for a given set of test conditions, and generates scaled conditons required to preserve similitude for alternate choices of airfoil chord and airspeed (different LWC, MVD, ambient temperature and pressure). The SIMICE routine was applied to the JU-21A conditions flown in this program to calculate scaling parameters (para 66, R & D section).

APPENDIX E. TEST DATA

INDEX

FIGURE E-1

CLOUD MEASURING INSTRUMENTATION COMPARISON

NOTES: 1. Orographic cumuliform clouds measured in 1983 near Sacramento, CA
2. USAAEFA JU-21A flown in trail formation 3 miles behind University of Wyoming Super King Air
3. Time scale for JU-21A data adjusted to match duration of King Air cloud exposure
4. Median volumetric drop diameters calculated from Particle Measuring Systems, Inc FSSP laser spectrometer data

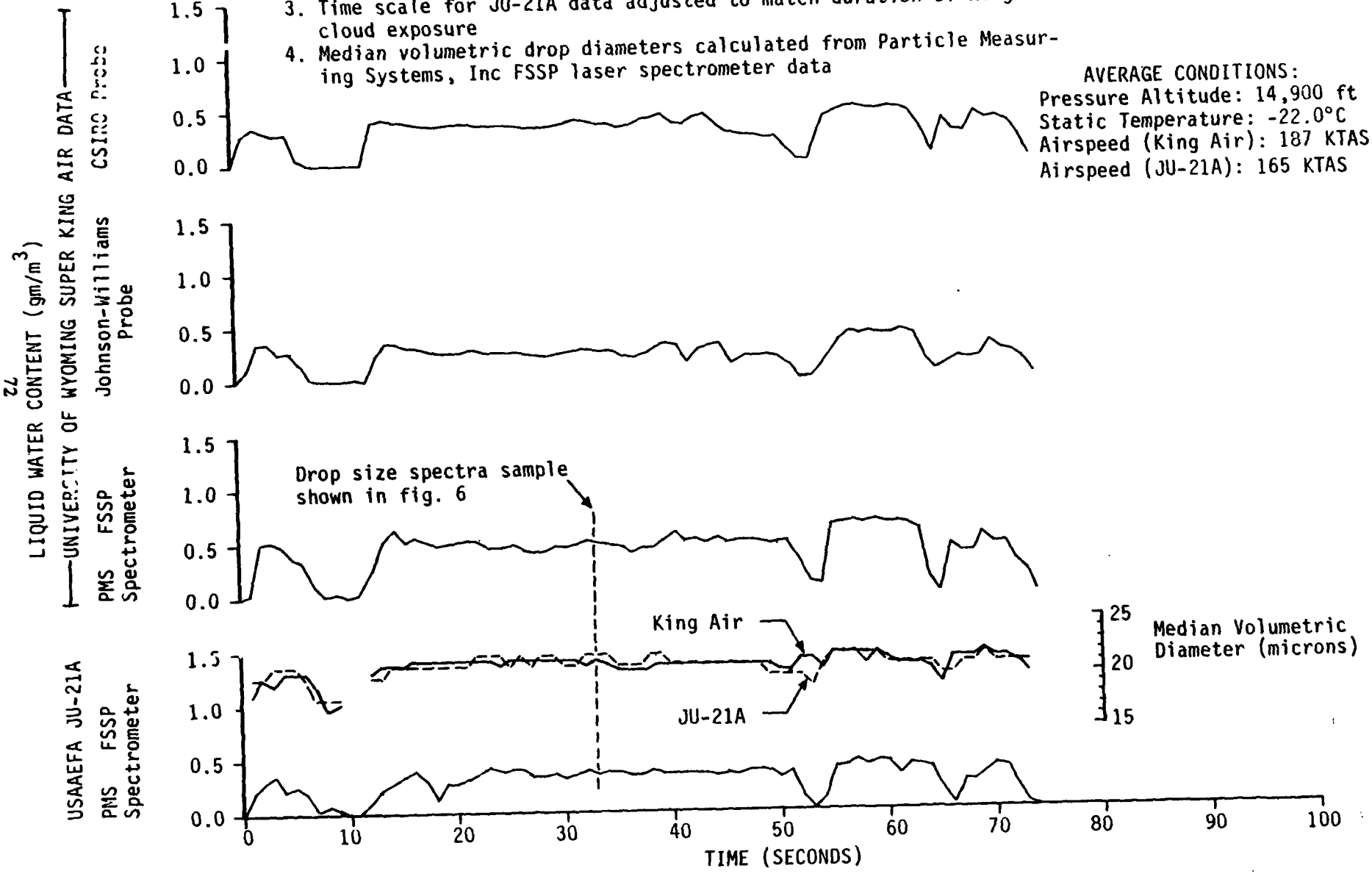

AVERAGE CONDITIONS:
Pressure Altitude: 14,900 ft
Static Temperature: -22.0°C
Airspeed (King Air): 187 KTAS
Airspeed (JU-21A): 165 KTAS

FIGURE E-2

CLOUD MEASURING INSTRUMENTATION COMPARISON

NOTES: 1. Orographic cumuliform clouds measured in 1983 near Sacramento, CA
2. USAAEFA JU-21A flown in trail formation 3 miles behind University of Wyoming Super King Air
3. Time scale for JU-21A data adjusted to match duration of King Air cloud exposure
4. Median volumetric drop diameters calculated from Particle Measuring Systems, Inc FSSP laser spectrometer data

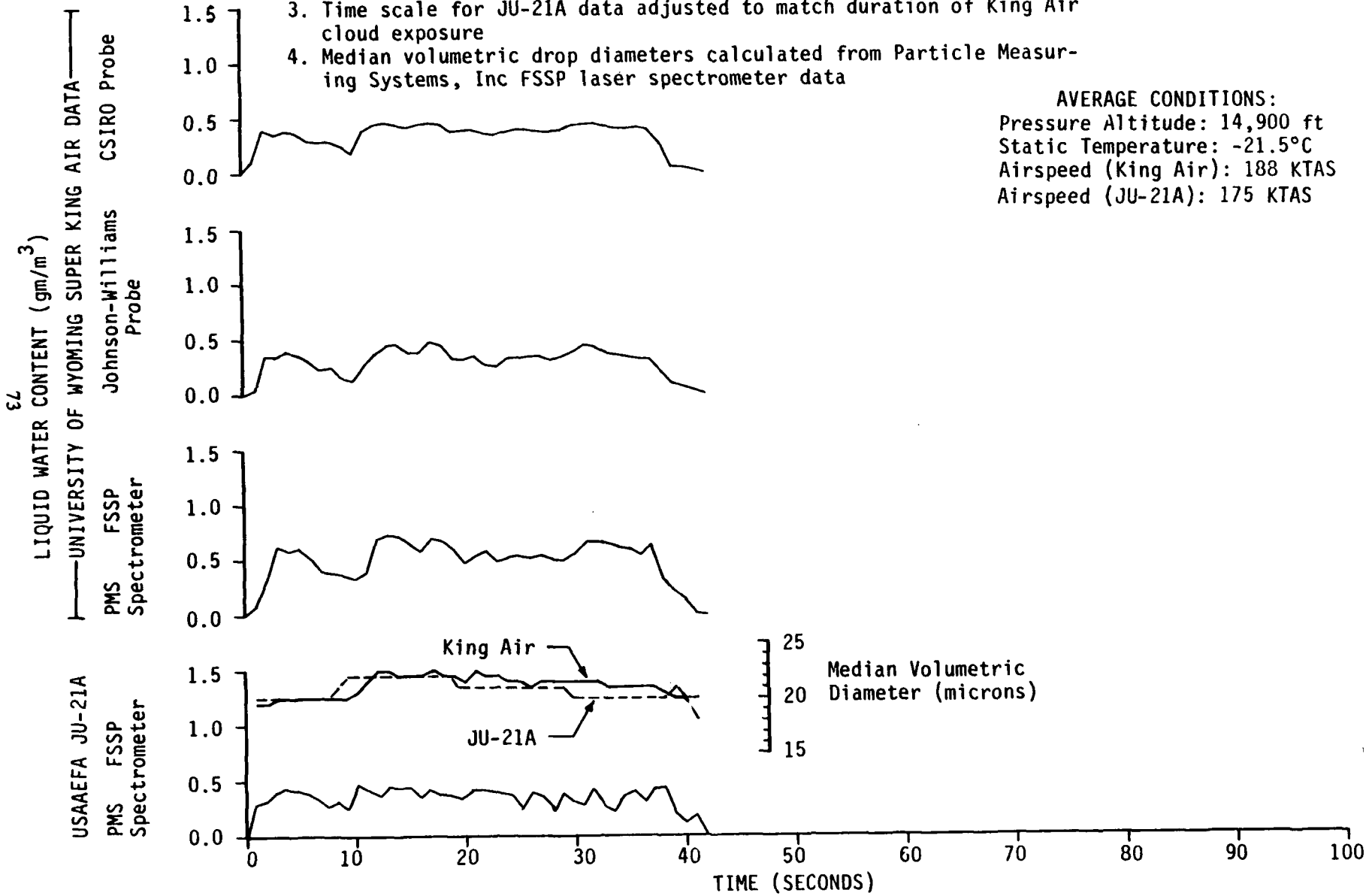

FIGURE F-3

CLOUD MEASURING INSTRUMENTATION COMPARISON

NOTES: 1. Orographic cumuliform clouds measured in 1983 near Sacramento, CA
2. USAAEFA JU-21A flown in trail formation 3 miles behind University of Wyoming Super King Air
3. Time scale for JU-21A data adjusted to match duration of King Air cloud exposure
4. Median volumetric drop diameters calculated from Particle Measuring Systems, Inc FSSP laser spectrometer data

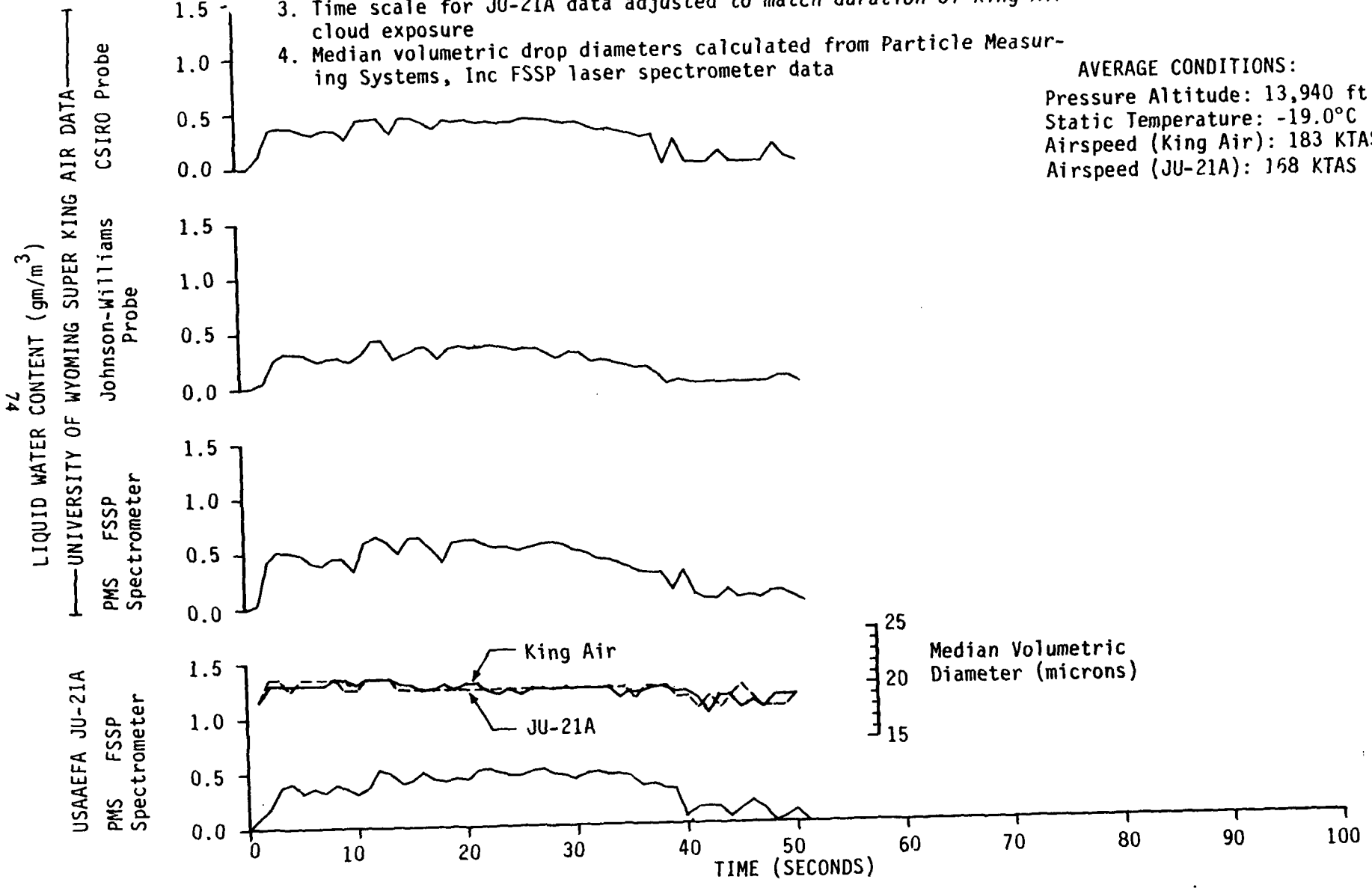

FIGURE E-4
CLOUD MEASURING INSTRUMENTATION COMPARISON

NOTES: 1. Orographic cumuliform clouds measured in 1983 near Sacramento, CA
2. USAAEFA JU-21A flown in trail formation 3 miles behind University of Wyoming Super King Air
3. Time scale for JU-21A data adjusted to match duration of King Air cloud exposure
4. Median volumetric drop diameters calculated from Particle Measuring Systems, Inc FSSP laser spectrometer data

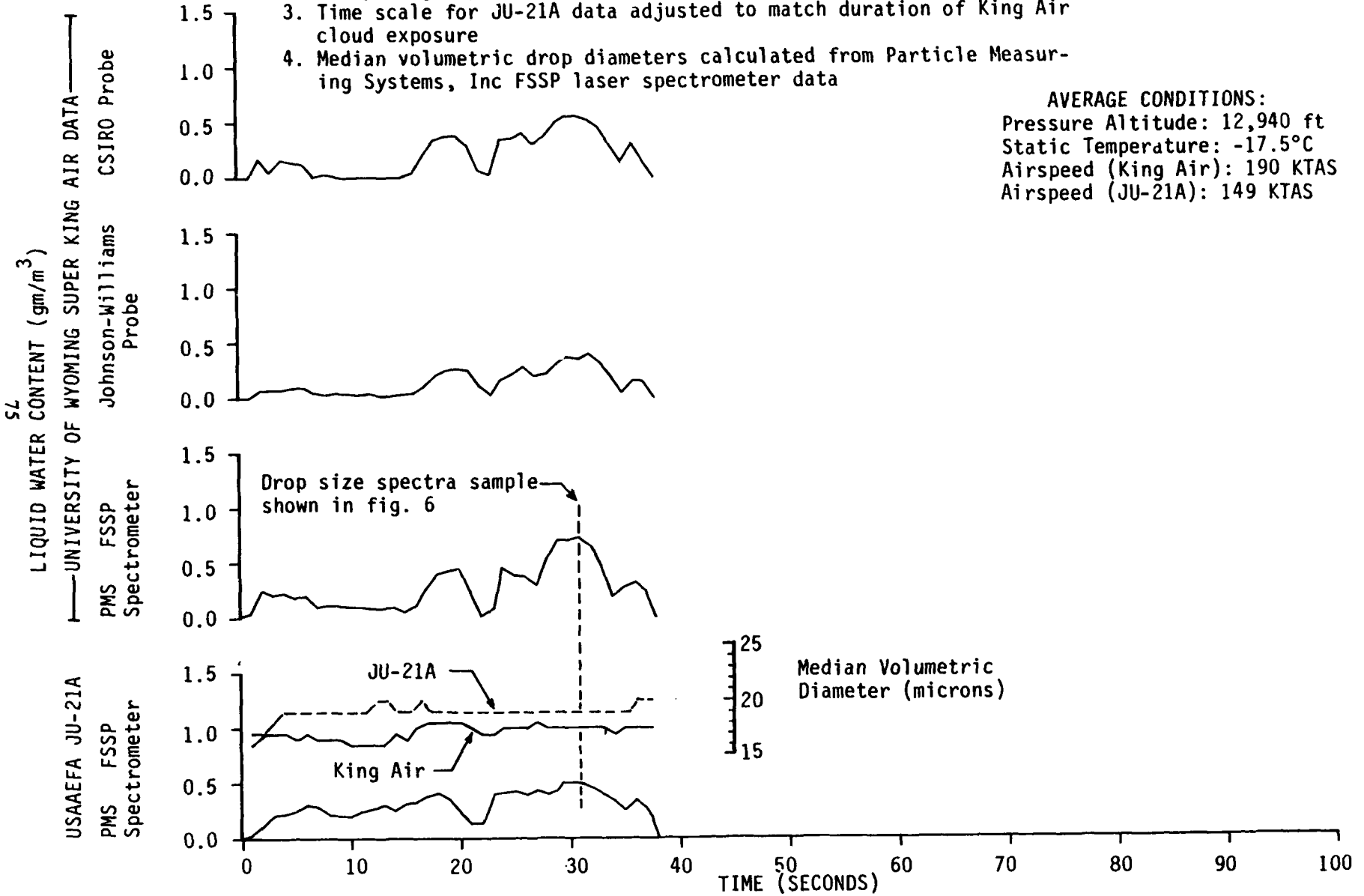

FIGURE F-5

CLOUD MEASURING INSTRUMENTATION COMPARISON

NOTES: 1. Orographic cumuliform clouds measured in 1983 near Sacramento, CA
2. USAAEFA JU-21A flown in trail formation 3 miles behind University of Wyoming Super King Air
3. Time scale for JU-21A data adjusted to match duration of King Air cloud exposure
4. Median volumetric drop diameters calculated from Particle Measuring Systems, Inc FSSP laser spectrometer data

AVERAGE CONDITIONS:

Pressure Altitude: 11,180 ft
Static Temperature: -6.5°C
Airspeed (King Air): 190 KTAS
Airspeed (JU-21A): 175 KTAS

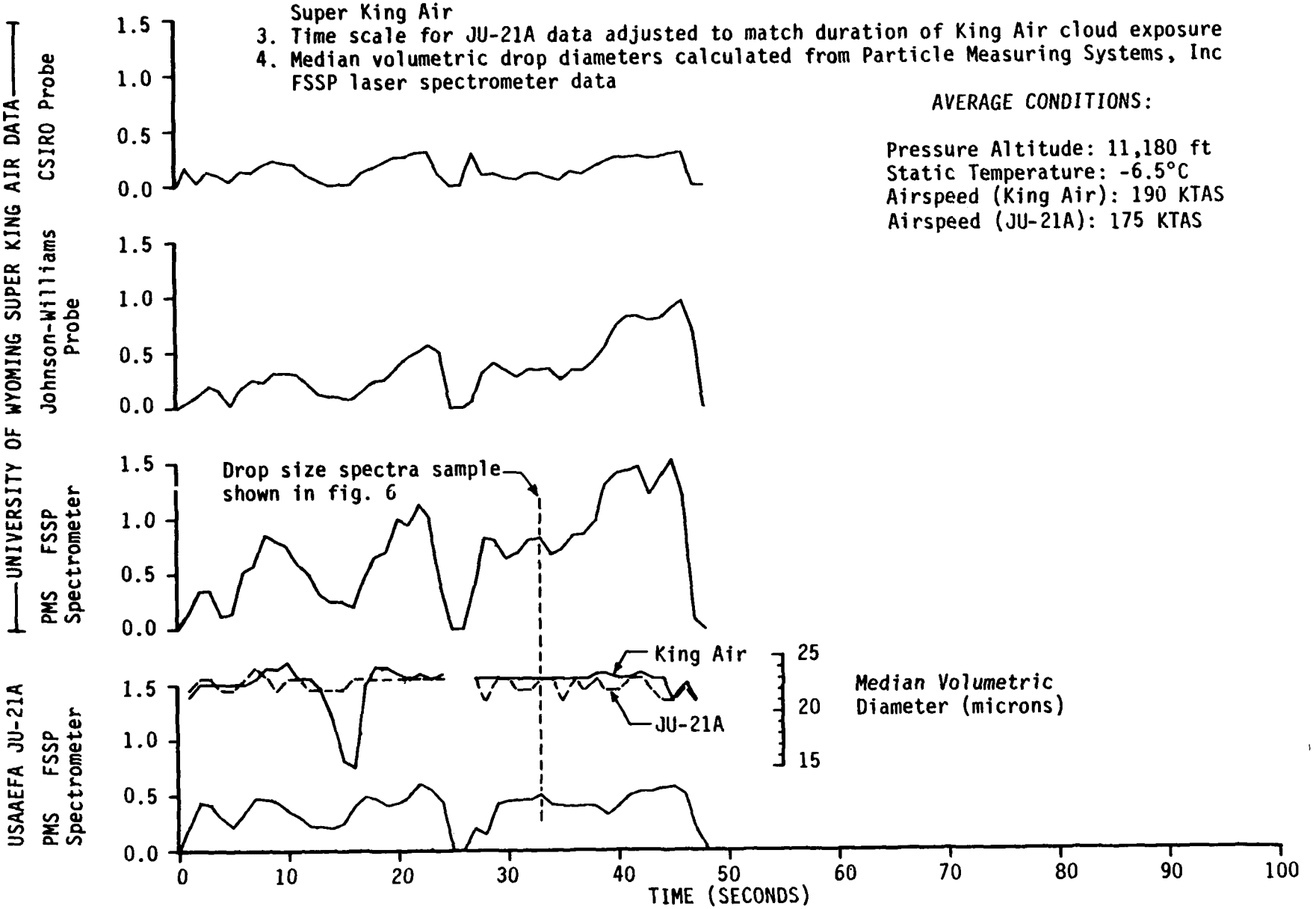

FIGURE E-6

NATURAL CUMULIFORM CLOUD DROP
MASS DISTRIBUTION COMPARISON

NOTES: 1. Data obtained using Particle Measuring Systems, Inc., laser spectrometers
2. One-second samples selected from figures 1, 4, and 5
3. Clouds measured in 1983 near Sacramento, CA; JU-21A flown in trail formation 3 miles behind King Air

—○— University of Wyoming Super King Air data
---△--- USAAEFA JU-21A data

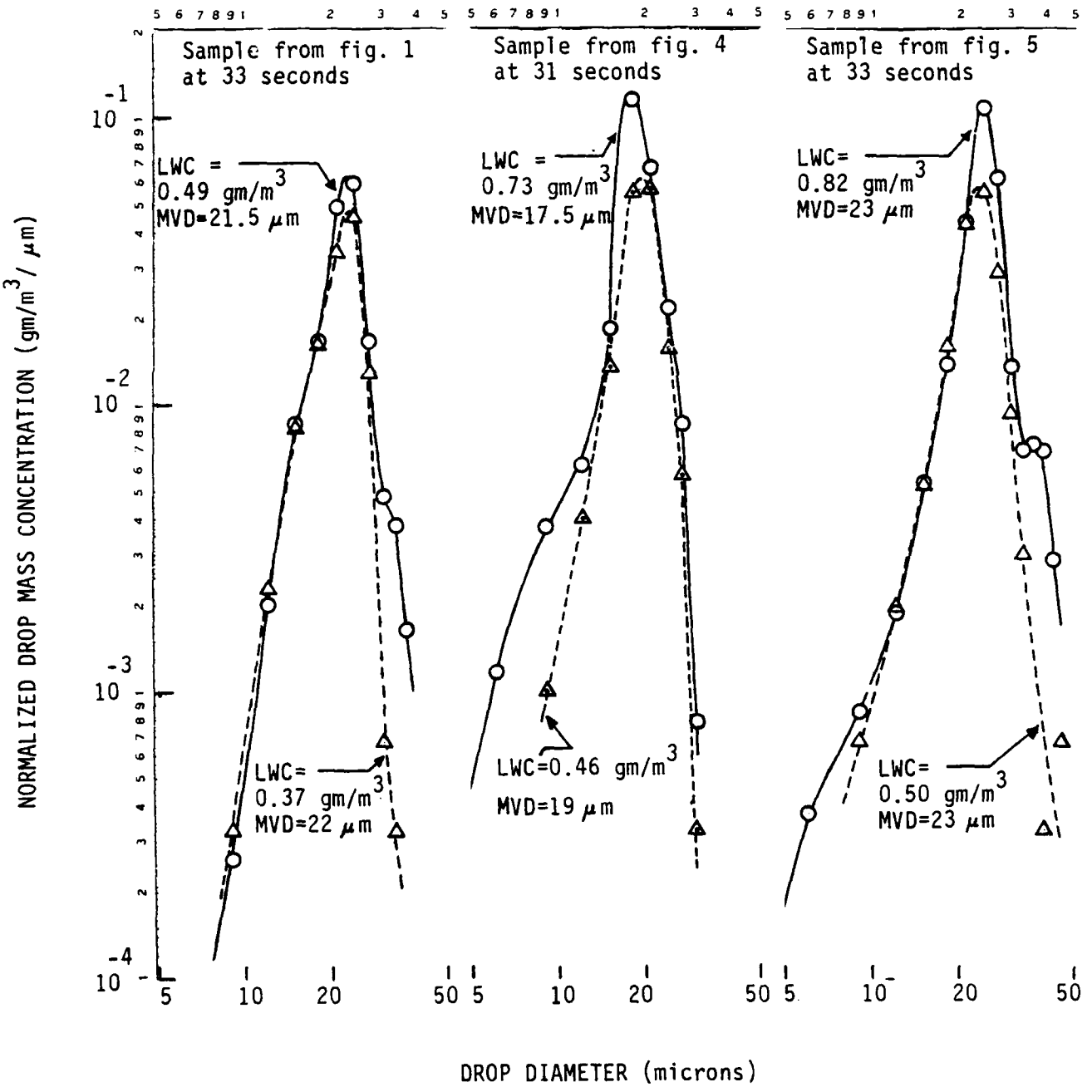

FIGURE E-7

AIRFOIL SECTION ICE SHAPE PROFILES

Notes: 1. Natural icing condition, measured LWC and MVD not available
2. Both airfoil sections of 18-inch span mounted above left wing of JU-21A
3. Successive profiles show ice accretion near outboard edge for indicated minutes duration
4. Grid scale = 0.5 inch squares
5. Flight No. 23

NACA 0012 Airfoil with 6 inch chord

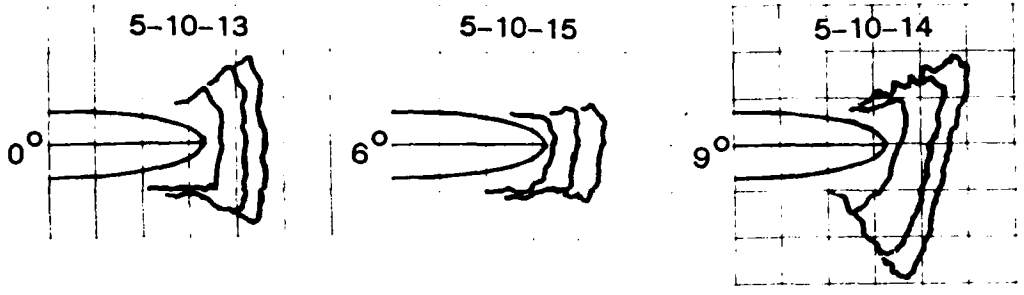

Average Flight Conditions:			
Static temp (°C)	-7.4	-5.8	-7.2
Airspeed (KTAS)	154	156	153
Press. Alt. (ft)	3400	3460	3700

SC1094 R8 Airfoil with 6 inch chord

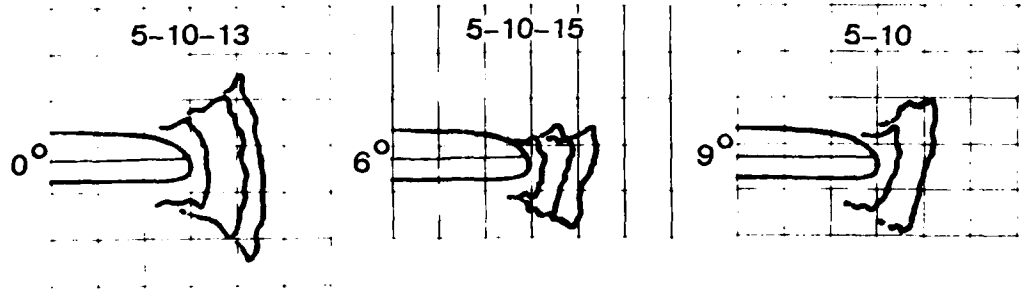

FIGURE E-8

AIRFOIL SECTION ICE SHAPE PROFILES

Notes: 1. Natural icing condition, measured LWC and MVD not available
2. Both airfoil sections of 18-inch span mounted above left wing of JU-21A
3. Successive profiles show ice accretion near outboard edge for indicated minutes duration
4. Grid scale = 0.5 inch squares
5. Flight No. 22, 21

NACA 0012 Airfoil with 21 inch chord

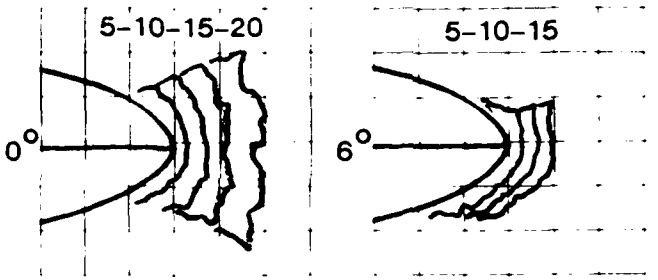

Average Flight Conditions:		
Static temp (°C)	-6.9	-7.0
Airspeed (KTAS)	153	154
Press. Alt. (ft)	4000	3960

SC1094 R8 Airfoil with 21 inch chord

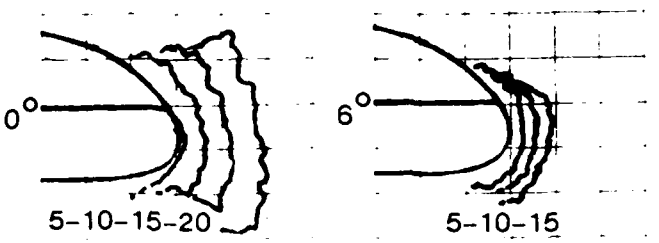

FIGURE E-9

AIRFOIL SECTION ICE SHAPE PROFILES

Notes: 1. Natural icing condition, measured LWC and MVD not available
2. Both airfoil sections of 18-inch span mounted above left wing of JU-21A
3. Successive profiles show ice accretion near outboard edge for indicated minutes duration
4. Grid scale = 0.5 inch squares
5. Flight No. 20

NACA 0012 Airfoil with 21 inch chord

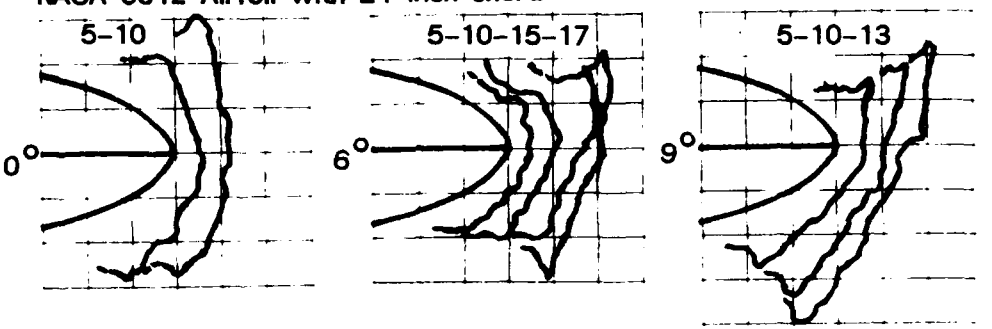

Average Flight Conditions:			
Static temp (°C)	-6.9	-7.2	-6.8
Airspeed (KTAS)	154	154	153
Press. Alt. (ft)	3220	3040	2980

SC1094 R8 Airfoil with 21 inch chord

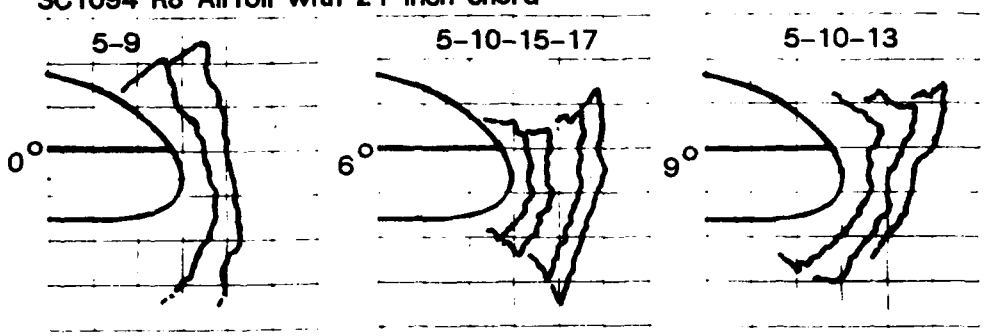

FIGURE E-10

AIRFOIL SECTION ICE SHAPE PROFILES

Notes: 1. Natural icing condition, measured LWC and MVD not available
2. Both airfoil sections of 18-inch span mounted above left wing of JU-21A
3. Successive profiles show ice accretion near outboard edge for indicated minutes duration
4. Grid scale = 0.5 inch squares
5. Flight No. 13

NACA 0012 Airfoil with 6 inch chord

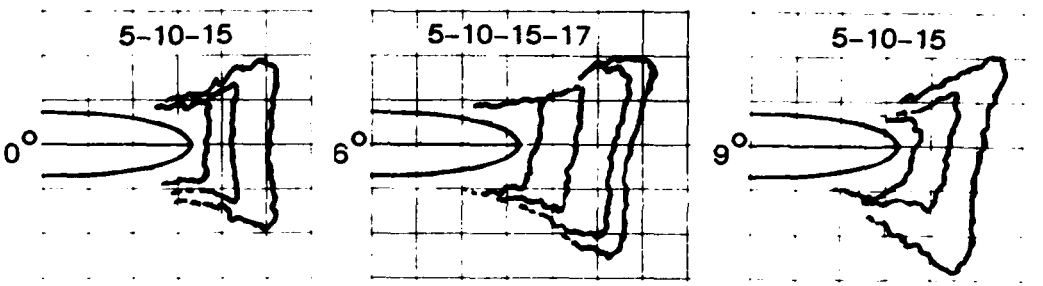

Average Flight Conditions:			
Static temp (°C)	-7.1	-7.1	-6.6
Airspeed (KTAS)	154	155	154
Press. Alt. (ft)	5060	5000	5060

NACA 0012 Airfoil with 21 inch chord

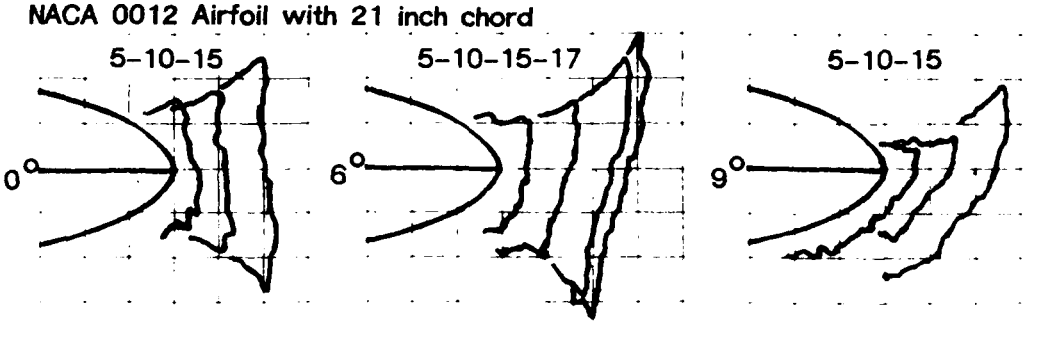

FIGURE E-11

AIRFOIL SECTION ICE SHAPE PROFILES

Notes: 1. Natural icing condition, measured LWC and MVD not available
2. Both airfoil sections of 18-inch span mounted above left wing of JU-21A
3. Successive profiles show ice accretion near outboard edge for indicated minutes duration
4. Grid scale = 0.5 inch squares
5. Flight No. 19

SC1094 R8 Airfoil with 6 inch chord

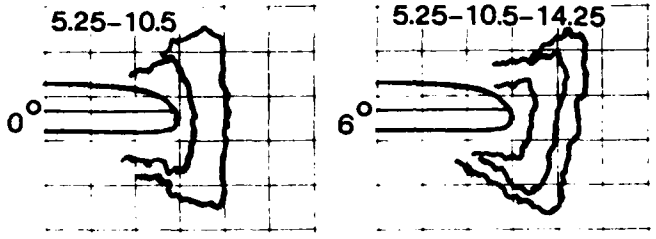

Average Flight Conditions:		
Static temp (°C)	-7.9	-6.6
Airspeed (KTAS)	149	147
Press. Alt. (ft)	3300	3080

SC1094 R8 Airfoil with 21 inch chord

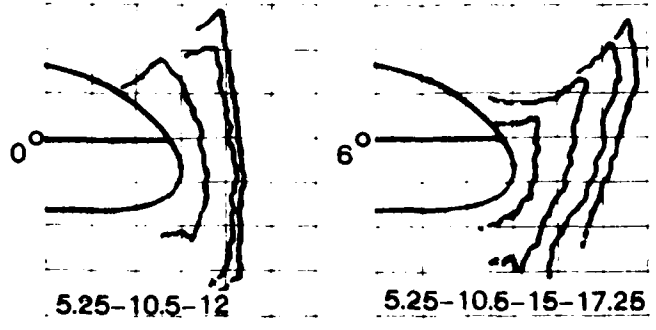

FIGURE E-12

AIRFOIL SECTION ICE SHAPE PROFILES

Notes: 1. Natural icing condition, measured LWC and MVD not available
2. Both airfoil sections of 18-inch span mounted above left wing of JU-21A
3. Successive profiles show ice accretion near outboard edge for indicated minutes duration
4. Grid scale = 0.5 inch squares
5. Flight No. 24

NACA 0012 Airfoil with 15.75 inch chord

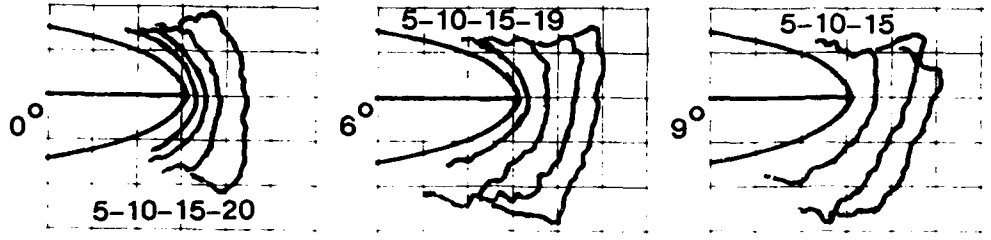

Average Flight Conditions:			
Static temp (°C)	-8.7	-9.1	-9.2
Airspeed (KTAS)	157	156	153
Press. Alt. (ft)	4460	4600	4140

SC1094 R8 Airfoil with 15.75 inch chord

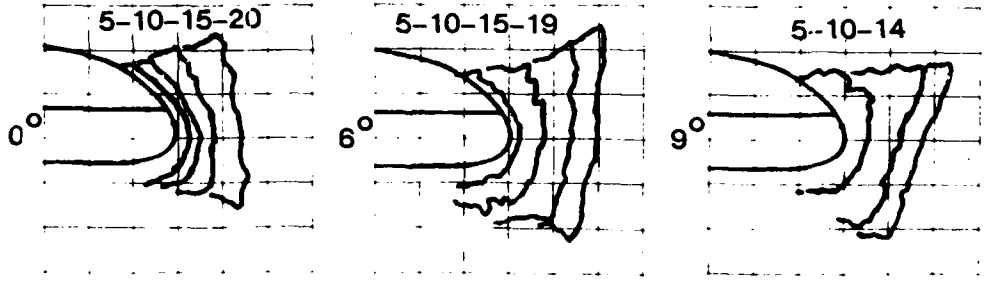

FIGURE E-13

AIRFOIL SECTION ICE SHAPE PROFILES

Notes: 1. Natural icing condition, measured LWC and MVD not available
2. Both airfoil sections of 18-inch span mounted above left wing of JU-21A
3. Successive profiles show ice accretion near outboard edge for indicated minutes duration
4. Grid scale = 0.5 inch squares
5. Flight No. 9

NACA 0012 Airfoil with 6 inch chord

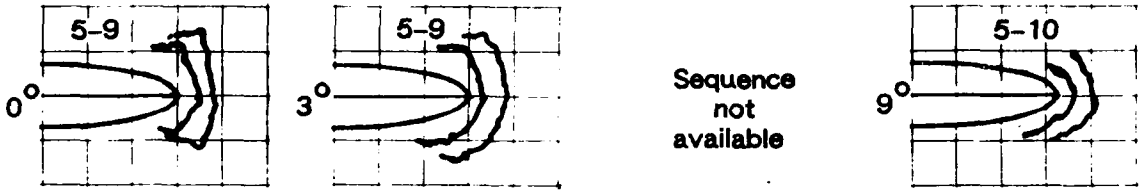

Average Flight Conditions:				
Static temp (°C)	-8.6	-9.0	-9.1	-10.5
Airspeed (KTAS)	151	153	149	151
Press. Alt. (ft)	4240	5000	4120	4880

NACA 0012 Airfoil with 15.75 inch chord

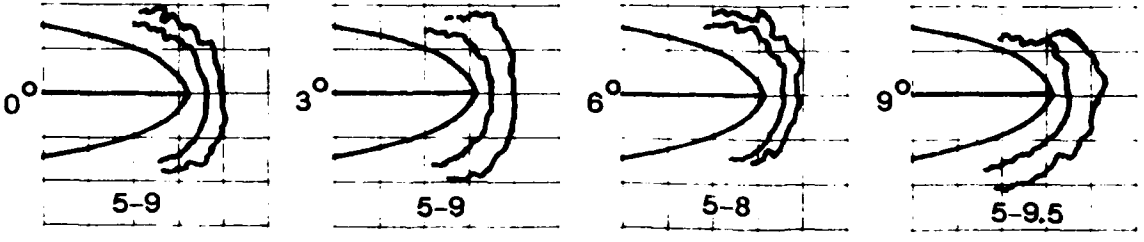

FIGURE E-14

AIRFOIL SECTION ICE SHAPE PROFILES

Notes: 1. Natural icing condition, measured LWC and MVD not available
2. Both airfoil sections of 18-inch span mounted above left wing of JU-21A
3. Successive profiles show ice accretion near outboard edge for indicated minutes duration
4. Grid scale = 0.5 inch squares
5. Flight No. 7

NACA 0012 Airfoil with 6 inch chord

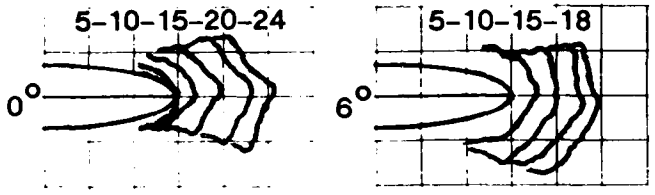

Average Flight Conditions:		
Static temp (°C)	-11.6	-12.2
Airspeed (KTAS)	146	148
Press. Alt. (ft)	3960	4040

SC1094 R8 Airfoil with 6 inch chord

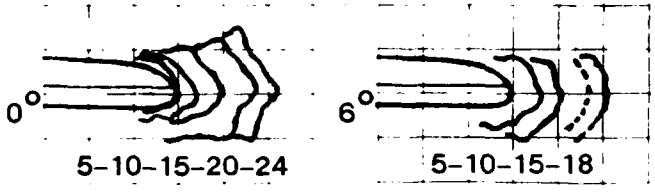

FIGURE E-15

AIRFOIL SECTION ICE SHAPE PROFILES

Notes: 1. Natural icing condition, measured LWC and MVD not available
2. Both airfoil sections of 18-inch span mounted above left wing of JU-21A
3. Successive profiles show ice accretion near outboard edge for indicated minutes duration
4. Grid scale = 0.5 inch squares
5. Flight No. 10A

NACA 0012 Airfoil with 15.75 inch chord

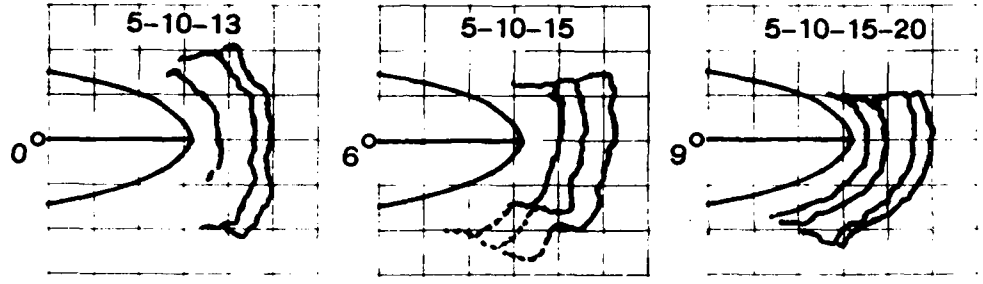

Average Flight Conditions:			
Static temp (°C)	-12.1	-11.9	-12.1
Airspeed (KTAS)	154	153	163
Press. Alt. (ft)	11340	11540	11160

SC1094 R8 Airfoil with 15.75 inch chord

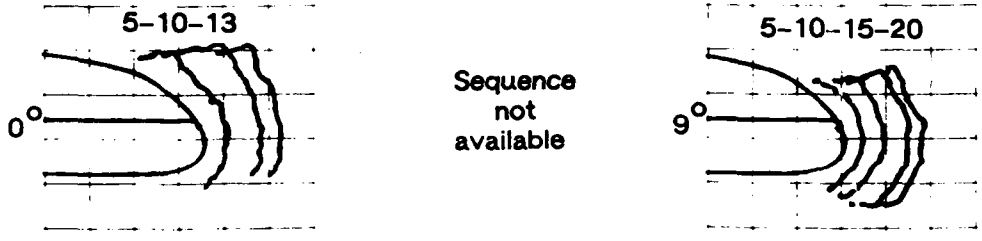

FIGURE E-16

AIRFOIL SECTION ICE SHAPE PROFILES

Notes: 1. Natural icing condition, measured LWC and MVD not available
2. Both airfoil sections of 18-inch span mounted above left wing of JU-21A
3. Successive profiles show ice accretion near outboard edge for indicated minutes duration
4. Grid scale = 0.5 inch squares
5. Flight No. 7A

SC1094 R8 Airfoil with 6 inch chord

Incidence angle:

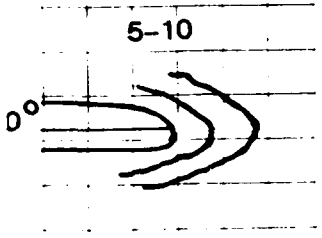

Average Flight Conditions:

Static temp (°C)	-21.0
Airspeed (KTAS)	159
Press. Alt. (ft)	8800

NACA 0012 Airfoil with 6 inch chord

Incidence angle:

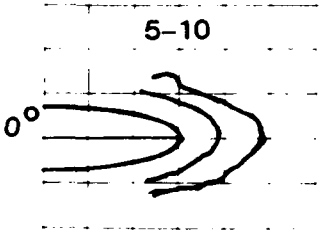

FIGURE E-17

AIRFOIL SECTION ICE SHAPE PROFILES

Notes: 1. Natural icing condition, measured LWC and MVD not available
2. Both airfoil sections of 18-inch span mounted above left wing of JU-21A
3. Successive profiles show ice accretion near outboard edge for indicated minutes duration
4. Grid scale = 0.5 inch squares
5. Flight No. 11

SC1094 R8 Airfoil with 6 inch chord

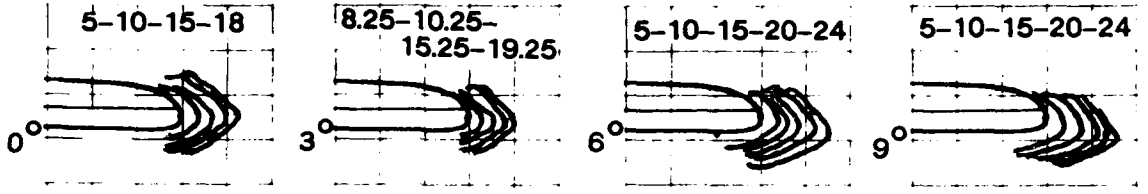

Average Flight Conditions:				
Static temp (°C)	-23.8	-23.5	-23.8	-24.7
Airspeed (KTAS)	158	159	158	160
Press Alt. (ft)	13220	13040	13160	13620

SC1094 R8 Airfoil with 15.75 inch chord

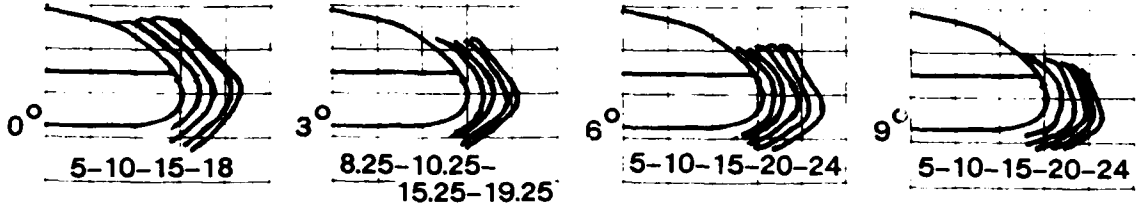

FIGURE E-18

AIRFOIL SECTION ICE SHAPE PROFILES

Notes: 1. Artificial icing condition, HISS set at 13 gpm flow rate for nominal LWC of 0.5 gm/m^3
2. Both airfoil sections of 18-inch span mounted above left wing of JU-21A
3. Successive profiles show ice accretion near outboard edge for indicated minutes duration
4. Grid scale = 0.5 inch squares
5. Flight No. 17

SC1094 R8 Airfoil with 21 inch chord

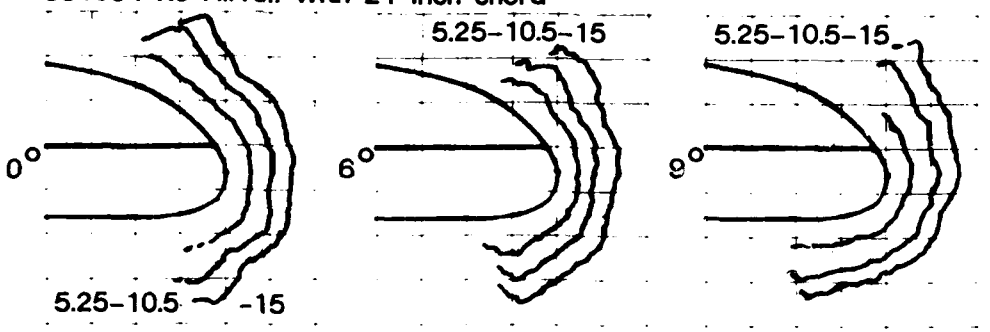

Average Flight Conditions:			
Static temp (°C)	-5.6	-5.5	-5.7
Airspeed (KTAS)	119	120	120
Press. Alt. (ft)	8800	8860	8900

NACA 0012 Airfoil with 21 inch chord

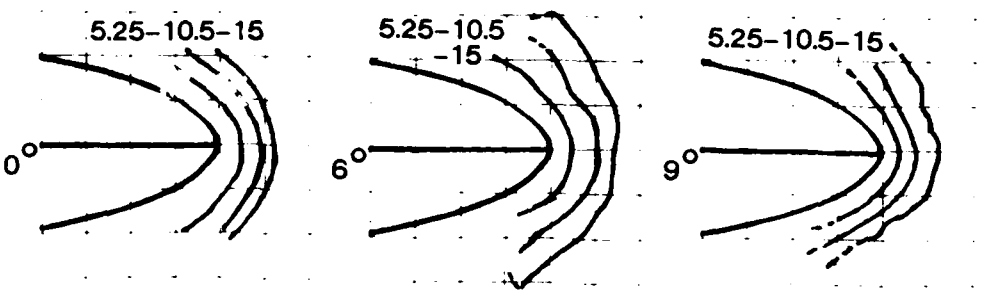

FIGURE E-19

AIRFOIL SECTION ICE SHAPE PROFILES

Notes: 1. Artificial icing condition, HISS set at 13 gpm flow rate for nominal LWC of 0.5 gm/m^3
2. Both airfoil sections of 18-inch span mounted above left wing of JU-21A
3. Successive profiles show ice accretion near outboard edge for indicated minutes duration
4. Grid scale = 0.5 inch squares
5. Flight No. 15

NACA 0012 Airfoil with 6 inch chord

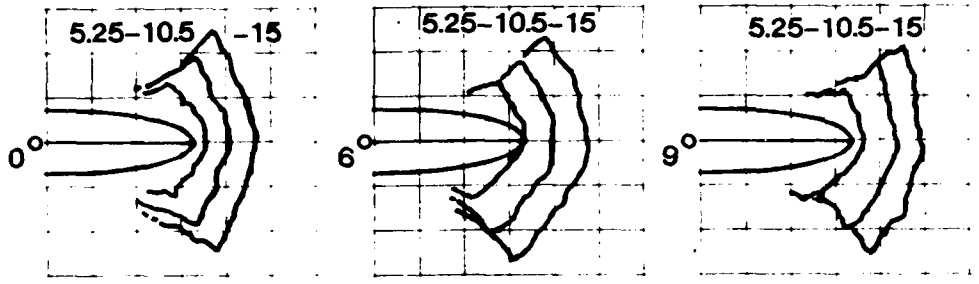

Average Flight Conditions:			
Static temp (°C)	-6.5	-6.5	-7.3
Airspeed (KTAS)	120	118	118
Press. Alt. (ft)	7300	7320	7060

NACA 0012 Airfoil with 21 inch chord

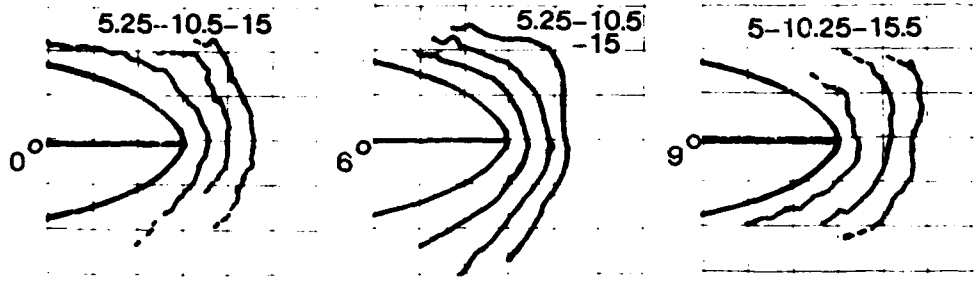

FIGURE E-20

AIRFOIL SECTION ICE SHAPE PROFILES

Notes: 1. Artificial icing condition, HISS set at 13 gpm flow rate for nominal LWC of 0.5 gm/m^3
2. Both airfoil sections of 18-inch span mounted above left wing of JU-21A
3. Successive profiles show ice accretion near outboard edge for indicated minutes duration
4. Grid scale = 0.5 inch squares
5. Flight No. 18

SC1094 R8 Airfoil with 6 inch chord

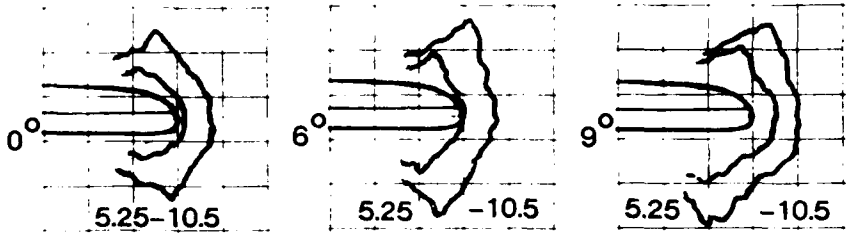

Average Flight Conditions:			
Static temp (°C)	-5.7	-6.7	-6.6
Airspeed (KTAS)	121	122	121
Press. Alt. (ft)	8040	8440	8460

SC1094 R8 Airfoil with 21 inch chord

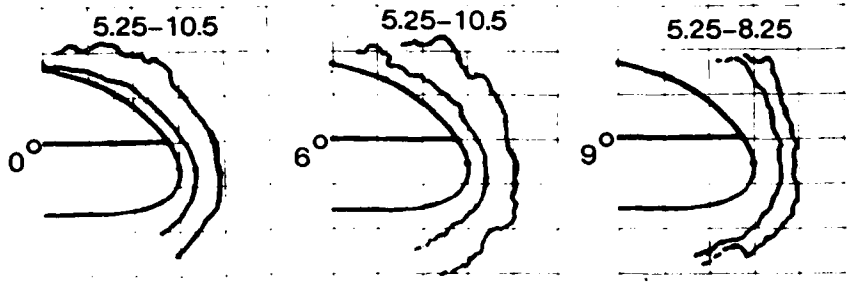

FIGURE E-21

AIRFOIL SECTION ICE SHAPE PROFILES

Notes: 1. Artificial icing condition, HISS set at 13 gpm flow rate for nominal LWC of 0.5 gm/m^3
2. Both airfoil sections of 18-inch span mounted above left wing of JU-21A
3. Successive profiles show ice accretion near outboard edge for indicated minutes duration
4. Grid scale = 0.5 inch squares
5. Flight No. 14

NACA 0012 Airfoil with 6 inch chord

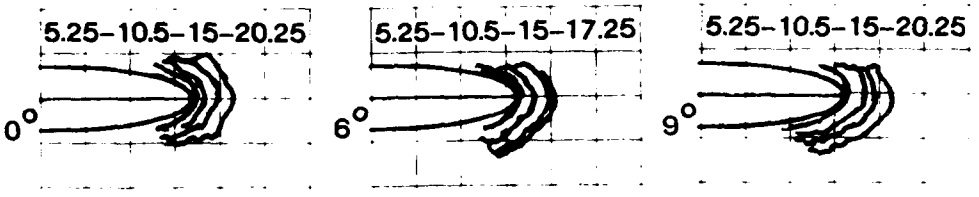

Average Flight Conditions:			
Static temp (°C)	-7.2	-7.2	-7.2
Airspeed (KTAS)	120	120	120
Press. Alt. (ft)	7520	7520	7500

NACA 0012 Airfoil with 21 inch chord

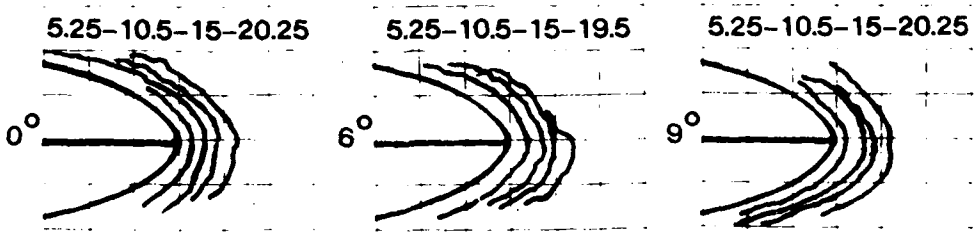

FIGURE E-22

AIRFOIL SECTION ICE SHAPE PROFILES

Notes: 1. Artificial icing condition, HISS set at 13 gpm flow rate for nominal LWC of 0.5 gm/m^3
2. Both airfoil sections of 18-inch span mounted above left wing of JU-21A
3. Successive profiles show ice accretion near outboard edge for indicated minutes duration
4. Grid scale = 0.5 inch squares
5. Flight No. 16

SC1094 R8 Airfoil with 21 inch chord

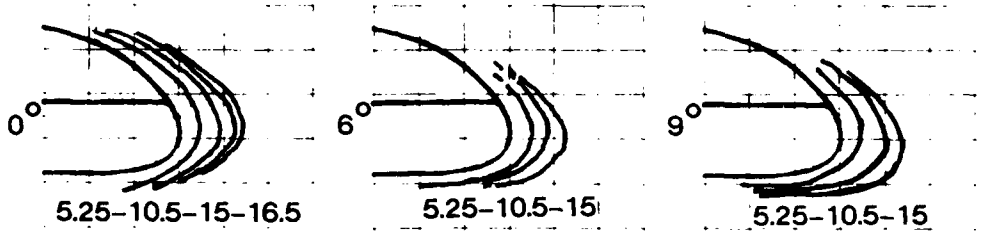

Average Flight Conditions:			
Static temp (°C)	-11.0	-11.0	-11.0
Airspeed (KTAS)	119	119	119
Press. Alt. (ft)	9600	10200	10400

NACA 0012 Airfoil with 21 inch chord

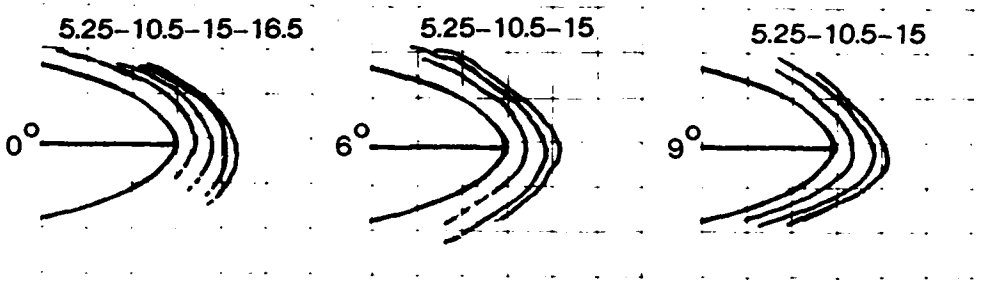

FIGURE E-23

AIRFOIL SECTION ICE SHAPE PROFILES

Notes: 1. Artificial icing condition, HISS set at 13 gpm flow rate for nominal LWC of 0.5 gm/m^3
2. Both airfoil sections of 18-inch span mounted above left wing of JU-21A
3. Successive profiles show ice accretion near outboard edge for indicated minutes duration
4. Grid scale = 0.5 inch squares
5. Flight No. 6

SC1094 R8 Airfoil with 6 inch chord

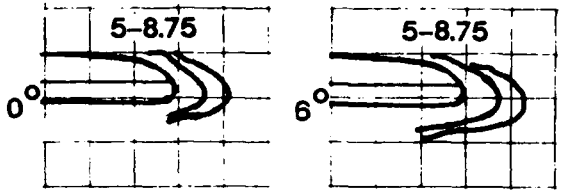

Average Flight Conditions:		
Static temp (°C)	-13.7	-13.7
Airspeed (KTAS)	121	120
Press. Alt. (ft)	8320	8020

NACA 0012 Airfoil with 6 inch chord

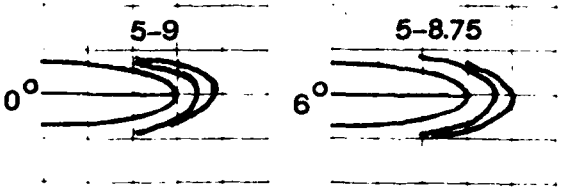

FIGURE E-24

AIRFOIL SECTION ICE SHAPE PROFILES

Notes: 1. Artificial icing condition, HISS set at 13 gpm flow rate for nominal LWC of 0.5 gm/m^3
2. Both airfoil sections of 18-inch span mounted above left wing of JU-21A
3. Successive profiles show ice accretion near outboard edge for indicated minutes duration
4. Grid scale = 0.5 inch squares
5. Flight No. 12

NACA 0012 Airfoil with 6 inch chord

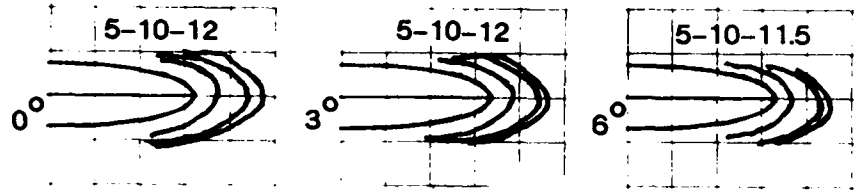

Average Flight Conditions:				
Static temp (°C)	-16.5	-16.2	-16.3	-16.5
Airspeed (KTAS)	122	123	122	121
Press. Alt. (ft)	5940	6100	6060	5800

NACA 0012 Airfoil with 21 inch chord

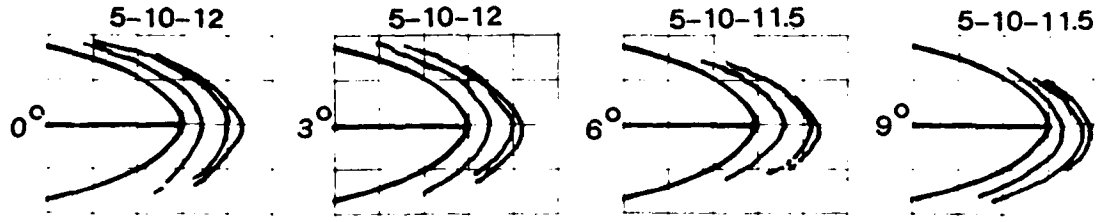

FIGURE E-25

AIRFOIL SECTION ICE SHAPE PROFILES

Notes: 1. Artificial icing condition, HISS set at 13 gpm flow rate for nominal LWC of 0.5 gm/m^3
2. Both airfoil sections of 18-inch span mounted above left wing of JU-21A
3. Successive profiles show ice accretion near outboard edge for indicated minutes duration
4. Grid scale = 0.5 inch squares
5. Flight No. 8

NACA 0012 Airfoil with 6 inch chord

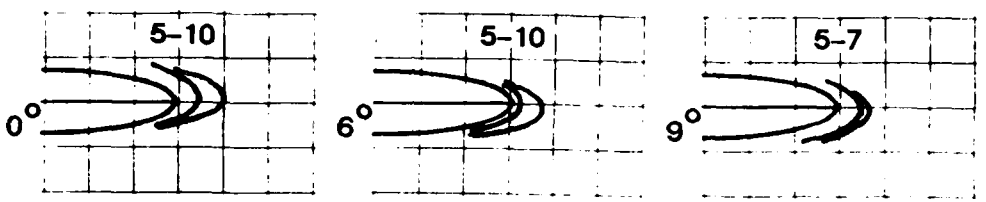

Average Flight Conditions:			
Static temp (°C)	-19.6	-19.6	-19.3
Airspeed (KTAS)	121	120	121
Press. Alt. (ft)	6700	6700	6740

NACA 0012 Airfoil with 15.75 inch chord

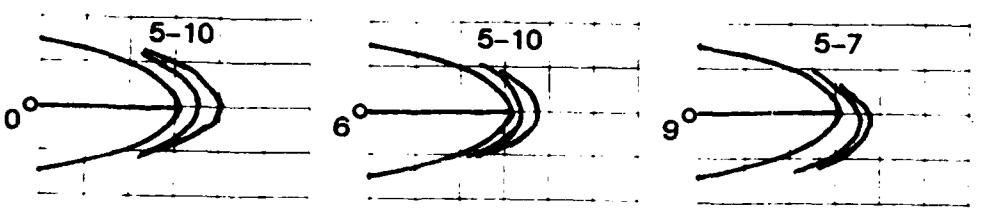

FIGURE E-26

UH-1H SCALING PARAMETERS

NOTES: 1. VALUES CALCULATED USING SIMICE COMPUTER ROUTINE (REF 24)
2. CONDITIONS SHOWN FOR MID-SPAN LOCATION AT HOVER, 5000 FT PRESSURE ALTITUDE, 15 MINUTE IMMERSION TIME

LWC (gm/m^3) 0.2 — — — —
0.5 ————

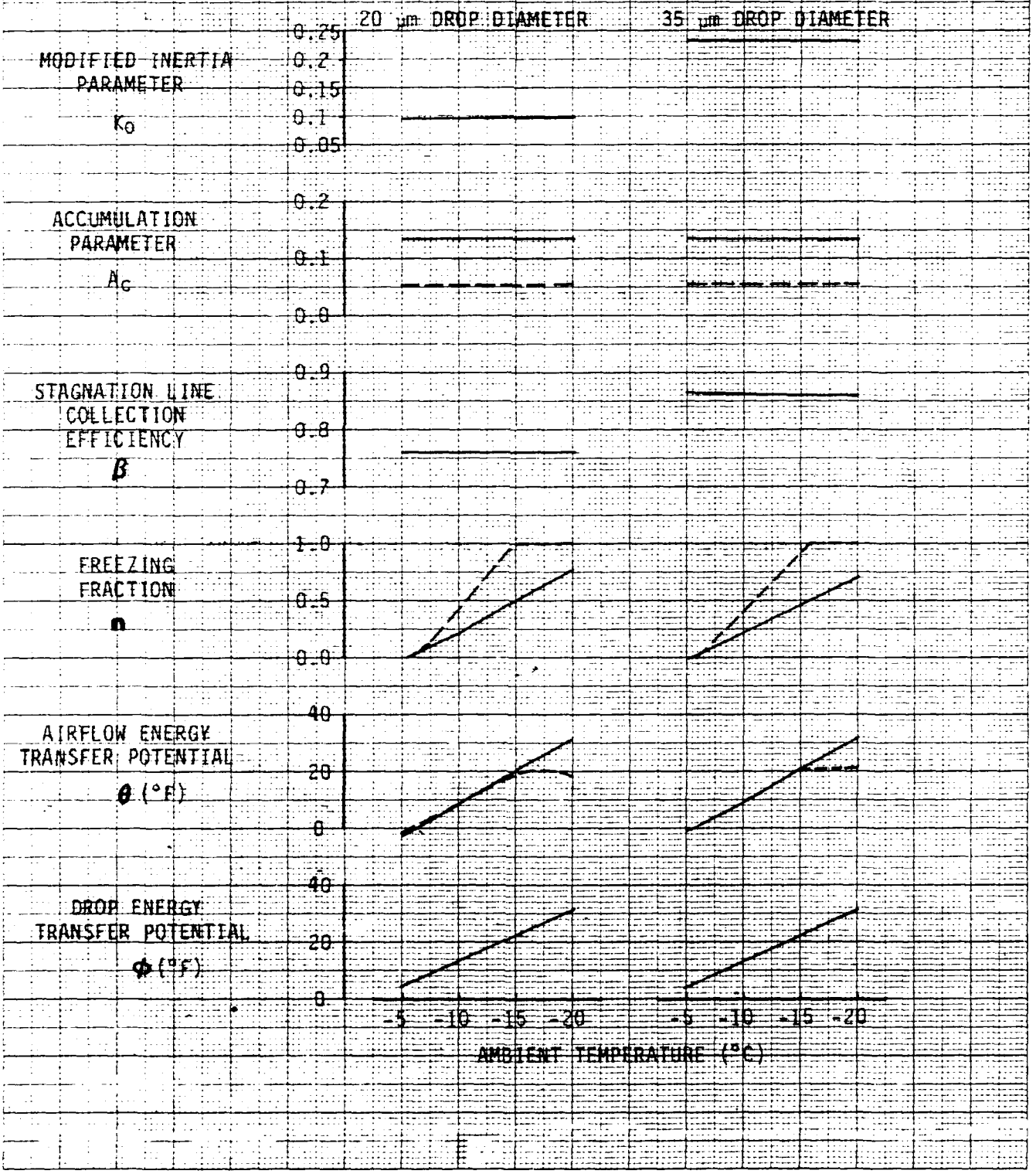

FIGURE E-27

UH-60A SCALING PARAMETERS

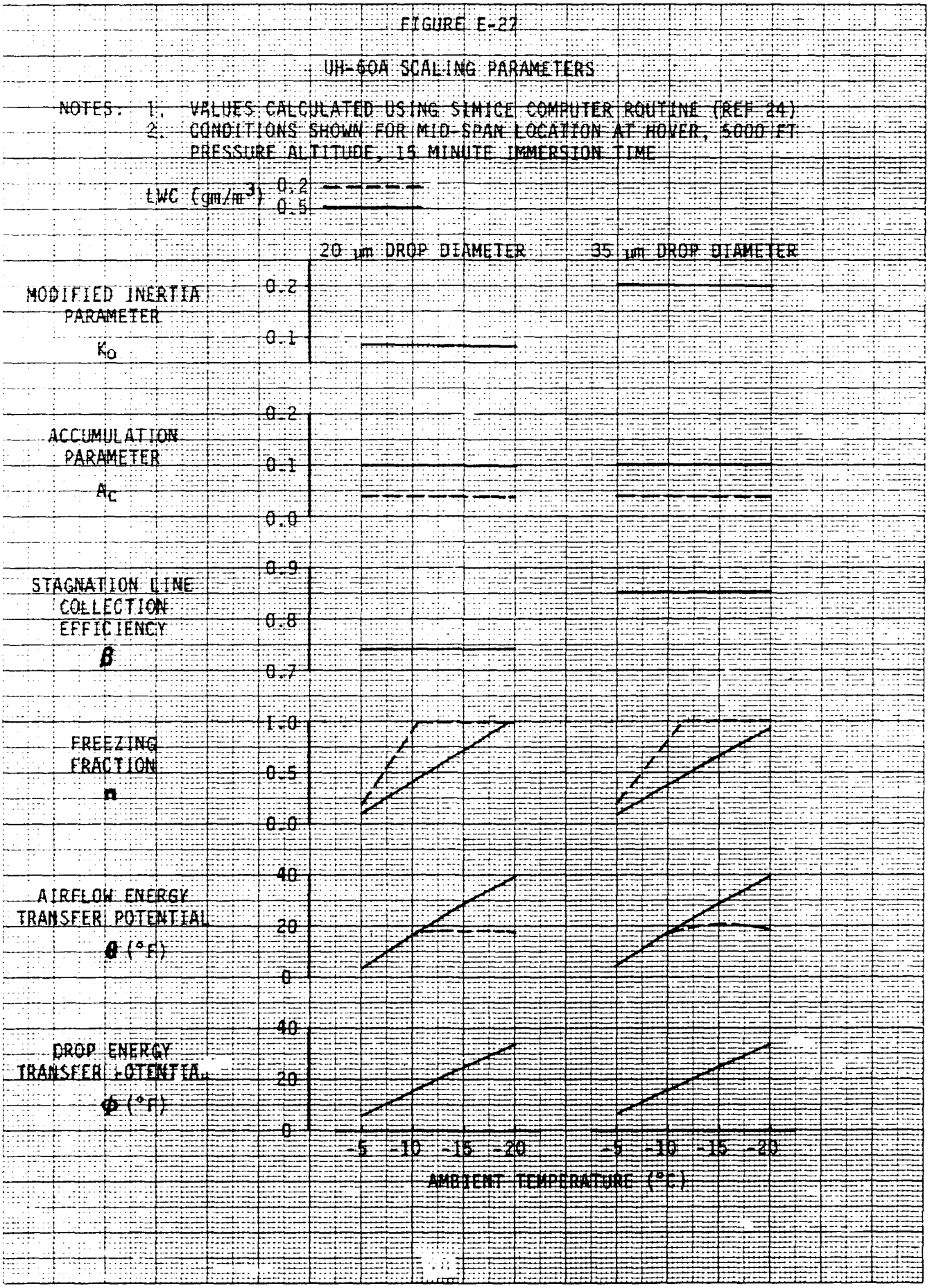

Table E-1. ASA Airfoil and Icing Conditions Cross Reference

Airfoil Section		Icing Conditions			
		Natural[1]		Artificial[2]	
Type	Chord[3] Length	Figure Number[4]	Average[5] Temperature (°C)	Figure Number	Average Temperature (°C)
NACA 0012 (UH-1H)	6 inch	(10) top (7) top	-7	(21) top (19) top	-7
		(13) top	-9	(23) bottom	-14
		(14) top	-12	(24) top	-16
		(16) bottom	-21	(25) top	-19
	15.75 inch (3/4 scale)	(13) bottom (12) top	-9	(25) bottom	-19
		(15) top	-12		
	21 inch (full scale)	(10) bottom (9) top (8) top (8) top	-7	(18) bottom	-6
				(21) bottom (19) bottom	-7
				(22) bottom	-11
				(24) bottom	-16
SC1094 R8 (UH-60A)	6 inch	(11) top (7) bottom	-7	(20) top	-6
		(14) bottom	-12	(23) top	-14
		(16) top	-21		
		(17) top	-24		
	15.75 inch (3/4 scale)	(12) bottom	-9	None	
		(15) bottom	-12		
		(17) bottom	-24		
	21 inch (full scale)	(11) bottom (9) bottom (8) bottom	-7	(18) top (20) bottom	-6
				(22) top	-11

NOTES:

[1]Natural icing airspeeds generally ranged from 150 to 155 KTAS.
[2]Artificial icing immersions flown at 120 KTAS in HISS spray cloud set for 0.5 gm/m^3 LWC.
[3]All airfoil sections had an 18 inch span.
[4]Figure numbers shown refer to ice shape tracings in appendix E.
"Top" or "Bottom" indicates airfoil mounting location on ASA framework.
[5]Static temperatures represent an average over the ranges covered by each data set rounded to nearest degree.

Table E-2. Icing Similitude Parameters
Natural Icing of NACA 0012 Airfoil

Chord Size = 6 inches

Test Conditions							Scaling Parameters							Equivalent Conditions for 21 inch chord at 120 KTAS				
Flt. No.	Fig. No.	Inc. Angle (deg)	H_p (ft)	Air-speed (KTAS)	T_s (°C)	Icing Time (min.)	K_o	β	n	θ	ϕ	A_c	b	T_s (°C)	H_p (ft)	LWC (gm/m^3)	MVD (μm)	Icing Time (min)
13	10	0	5060	154	-7.1	15	.238	.868	1.0	9.94	11.43	.103	.075	-6.81	-3700	0.14	52.5	95.0
		6	5000	155	-7.1	17	.239	.869	1.0	9.97	11.41	.117	.075	-6.80	-4070	0.14	52.9	107.4
		9	5060	154	-6.6	16	.238	.868	1.0	9.99	10.53	.109	.074	-6.31	-3377	0.14	52.4	101.9
23	7	0	3400	154	-7.4	11	.283	.868	1.0	9.59	11.97	.075	.072	-7.11	-6418	0.14	53.2	68.5
		6	3460	156	-5.8	14	.235	.867	1.0	9.81	9.04	.097	.072	-5.48	-5658	0.14	53.07	88.74
		9	3700	153	-7.2	11	.233	.866	1.0	9.63	11.63	.075	.072	-6.92	-5529	0.14	52.73	68.97
9	13	0	4240	151	-8.6	9	.232	.866	1.0	9.54	14.19	.060	.073	-8.34	-5158	0.14	52.6	55.9
		3	5000	153	-9.0	9	.237	.868	1.0	9.73	14.88	.061	.075	-8.72	-4963	0.14	53.1	55.6
		6	4120	149	-9.1	8	.230	.865	1.0	9.40	15.13	.053	.072	-8.86	-5077	0.14	52.2	49.5
		9	4880	151	-10.5	10	.235	.867	1.0	9.50	17.63	.067	.075	-10.24	-5817	0.15	53.3	60.7
7	14	0	3960	146	-11.6	25	.227	.863	1.0	9.05	19.70	.162	.072	-11.39	-6370	0.14	58.4	150.3
		6	4040	148	-12.2	18	.229	.864	1.0	9.08	20.75	.118	.073	-11.96	-8429	0.15	54.1	105.6
7A	16	0	8800	159	-21.0	11	.2556	.873	1.0	9.44	36.46	.078	.088	-20.68	-31947	.24	76.0	41.9

Chord Size = 15.75 inches

Test Conditions							Scaling Parameters							Equivalent Conditions for 6 inch chord at 120 KTAS				
Flt. No.	Fig. No.	Inc. Angle (deg)	H_p (ft)	Air-speed (KTAS)	T_s (°C)	Icing Time (min.)	K_o	β	n	θ	ϕ	A_c	b	T_s (°C)	H_p (ft)	LWC (gm/m^3)	MVD (μm)	Icing Time (min)
9	13	0	4240	151	-8.6	9	.089	.753	1.0	13.35	14.20	.023	.103	-8.34	-2459	.41	12.79	2.1
		3	5000	153	-9.0	9	.090	.755	1.0	13.62	14.88	.023	.106	-8.72	-2071	.42	12.90	2.1
		6	4120	149	-9.1	8	.088	.752	1.0	13.15	15.13	.020	.102	-8.86	-2407	.41	12.71	1.86
		9	4880	151	-10.5	10	.089	.754	1.0	13.29	17.63	.026	.105	-10.24	-2599	.42	12.87	2.31
24	12	0	4460	157	-8.7	20	.091	.756	1.0	13.71	14.27	.053	.106	-8.38	-3547	.43	13.11	4.66
		6	4460	156	-9.1	19	.091	.756	1.0	13.65	15.01	.050	.106	-8.79	-3342	.43	13.07	4.41
		9	4140	153	-9.2	14	.089	.754	1.0	13.35	15.25	.036	.104	-8.92	-3376	.42	12.93	3.25
10A	15	0	11340	154	-12.1	13	.099	.766	1.0	15.17	20.47	.034	.123	-11.82	4886	.41	12.96	3.1
		6	11540	153	-11.9	13	.099	.766	1.0	15.94	20.47	.034	.130	-11.82	5214	.41	12.93	3.1
		9	11160	163	-12.1	22	.103	.770	1.0	15.61	20.31	.061	.127	-11.73	2859	.44	13.43	5.2

Chord Size = 21 inches

Test Conditions							Scaling Parameters							Equivalent Conditions for 6 inch chord at 120 KTAS				
Flt. No.	Fig. No.	Inc. Angle (deg)	H_p (ft)	Air-speed (KTAS)	T_s (°C)	Icing Time (min.)	K_o	β	n	θ	ϕ	A_c	b	T_s (°C)	H_p (ft)	LWC (gm/m^3)	MVD (μm)	Icing Time (min)
13	10	0	5060	154	-7.1	15	.068	.710	1.0	15.09	11.43	.029	.114	-6.81	-808	.47	10.78	2.33
		6	5000	155	-7.1	17	.068	.711	.996	15.04	11.42	.033	.114	-6.80	-1590	.48	10.86	2.62
		9	5060	154	-6.6	16	.068	.710	.914	13.77	10.53	.031	.114	-6.3	-1679	.48	10.85	2.45
20	9	0	3220	154	-6.9	9	.066	.706	.972	14.08	11.07	.018	.109	-6.61	-3513	.48	10.85	1.37
		6	3040	154	-7.2	17	.066	.075	1.0	14.43	11.61	.033	.109	-6.91	-3513	.48	10.80	2.61
		9	2980	153	-6.8	13	.066	.705	.964	13.82	10.91	.025	.108	-6.52	-4036	.48	10.81	1.98
21	3	6	3960	154	-7.0	15	.067	.708	.987	14.55	11.25	.029	.111	-6.71	-2808	.48	10.83	2.29
22		0	4000	153	-6.9	20	.067	.707	.980	14.37	11.09	.039	.111	-6.62	-2582	.48	10.79	3.06

Table E-3. Icing Similitude Parameters
Natural Icing of SC1094 R8 Airfoil

Chord Size = 6 inches

Flt. No.	Fig. No.	Test Conditions: Inc. Angle (deg)	H_p (ft)	Air-speed (KTAS)	T_a (°C)	Icing Time (min.)	Scaling Parameters: K_o	β	n	θ	ϕ	A_c	b	Equivalent Conditions for 21 inch chord at 120 KTAS: T_a (°C)	H_p (ft)	LWC (gm/m³)	MVD (μm)	Icing Time (min)
		6	3300	144	-7.9	15	.228	.864	1.0	9.35	2.97	.099	.071	-7.66	-5384	0.14	51.93	93.72
19	11	0	3080	147	-6.6	12	.225	.862	1.0	9.35	10.65	.078	.070	-6.37	-4253	0.13	50.93	76.24
		0	3400	154	-7.4	11	.233	.866	1.0	10.09	11.98	.075	.076	-7.11	-5945	0.14	52.97	69.06
23	7	6	3460	156	-7.4	14	.235	.867	1.0	10.32	9.05	.097	.076	-5.48	-5239	0.14	52.84	89.38
		9	3700	153	-7.2	11	.233	.866	1.0	10.13	11.63	.075	.076	-6.92	-5093	0.14	52.49	69.49
		0	3960	146	-11.6	25	.227	.863	1.0	9.52	19.70	.162	.076	-11.39	-5817	0.14	52.11	151.77
7	14	6	4040	148	-12.2	18	.229	.864	1.0	9.55	20.75	.118	.077	-11.96	-7725	0.15	53.72	106.87
7A	16	0	8800	159	-21.0	11	.256	.873	1.0	9.92	36.46	.078	.097	-20.68	-27489	0.23	72.17	11.88
		0	13220	158	-23.8	18	.271	.877	1.0	10.46	41.54	.126	.102	-23.49	-22603	0.23	71.23	72.3
11	17	3	13040	159	-23.5	19	.272	.878	1.0	10.50	40.98	.134	.102	-23.18	-22978	0.23	71.59	76.4
		6	13160	158	-23.8	24	.271	.873	1.0	10.45	41.54	.168	.102	-23.49	-22928	0.23	71.45	95.99
		9	13620	160	-24.7	25	.275	.876	1.0	10.50	43.13	.178	.104	-24.88	-32100	0.27	80.54	86.73

Chord Size = 15.75 inches

Flt. No.	Fig. No.	Test Conditions: Inc. Angle (deg)	H_p (ft)	Air-speed (KTAS)	T_a (°C)	Icing Time (min.)	Scaling Parameters: K_o	β	n	θ	ϕ	A_c	b	Equivalent Conditions for 6 inch chord at 120 KTAS: T_a (°C)	H_p (ft)	LWC (gm/m³)	MVD (μm)	Icing Time (min)
		0	4460	157	-8.7	20	.091	.756	1.0	14.41	14.27	.053	.111	-8.38	-3137	0.43	13.07	4.69
24	12	6	4600	156	-9.1	19	.091	.756	1.0	14.35	15.01	.050	.112	-8.79	-2930	0.42	13.03	4.44
		9	4140	153	-9.2	14	.089	.754	1.0	14.03	15.25	.036	.109	-8.92	-2999	0.42	12.89	3.27
		0	11340	154	-12.1	13	.099	.766	1.0	15.17	20.47	.034	.123	-11.82	4886	0.41	12.96	3.07
10A	15	6	11540	153	-11.9	15	.099	.766	1.0	15.99	20.12	.039	.130	-11.62	5747	0.41	12.86	3.57
		9	11160	163	-12.1	22	.103	.770	1.0	16.41	20.31	.061	.133	-11.73	3292	0.44	13.38	5.20
		0	13220	158	-23.8	18	.103	.771	1.0	14.71	41.54	.048	.145	-23.49	-5040	0.52	14.36	3.47
11	17	3	13040	159	-23.5	19	.104	.771	1.0	14.77	40.98	.051	.145	-23.18	-5384	0.52	14.42	3.66
		6	13160	158	-23.8	24	.103	.771	1.0	14.69	41.54	.064	.145	-23.49	-5384	0.52	14.37	4.62
		9	13620	160	-24.7	25	.105	.773	1.0	14.77	43.13	.068	.148	-24.38	-7544	0.55	14.78	4.60

Chord Size = 21 inches

Flt. No.	Fig. No.	Test Conditions: Inc. Angle (deg)	H_p (ft)	Air-speed (KTAS)	T_a (°C)	Icing Time (min.)	Scaling Parameters: K_o	β	n	θ	ϕ	A_c	b	Equivalent Conditions for 6 inch chord at 120 KTAS: T_a (°C)	H_p (ft)	LWC (gm/m³)	MVD (μm)	Icing Time (min)
		6	3300	149	-7.9	15	.065	.073	1.0	14.12	12.97	.028	.018	-7.66	-2477	0.46	10.61	2.3
19	11	0	3090	147	-6.6	12	.064	.701	.980	13.78	10.65	.022	.106	-6.37	-2424	0.46	10.54	1.84
		0	3220	154	-6.9	9	.066	.706	.928	14.08	11.07	.018	.115	-6.61	-3902	0.48	10.85	1.37
20	9	6	3040	154	-7.2	17	.066	.705	.981	14.83	11.61	.033	.115	-6.91	-3885	0.48	10.83	2.6
		9	2980	153	-6.8	13	.066	.705	.919	13.82	10.91	.025	.114	-6.52	-4036	0.48	10.81	1.98
21	8	6	3960	154	-7.0	15	.067	.708	.944	14.55	11.25	.029	.117	-6.71	-2898	0.48	10.83	2.29
22		9	4000	153	-6.9	20	.067	.707	.935	14.37	11.09	.039	.117	-6.62	-2582	0.48	10.79	3.06

Table E-4. Icing Similitude Parameters
Artificial Icing of NACA 0012 Airfoil

Chord Size = 6 inches

Flt. No.	Fig. No.	Test Conditions: Inc. Angle (deg)	H_p (ft)	Air-speed (KTAS)	T_a (°C)	Icing Time (min.)	Scaling Parameters: K_o	β	n	θ	ϕ	A_c	b	Equivalent Conditions for 21 inch chord at 120 KTAS: T_a (°C)	H_p (ft)	LWC (gm/m³)	MVD (μm)	Icing Time (min)
		0	7520	120	-7.2	20	.522	.922	.796	18.9	12.14	.266	.183	-7.50	11909	.22	67.24	125.47
14	21	6	7520	120	-7.2	17	.522	.922	.796	18.69	12.14	.226	.183	-7.50	11909	.22	67.24	106.65
		9	7500	120	-7.2	20	.522	.922	.796	18.68	12.14	.266	.183	-7.50	11909	.22	67.24	125.48
		0	7300	120	-6.5	14	.521	.922	.712	16.63	10.88	.186	.182	-6.81	12017	.21	67.00	88.30
15	19	6	7320	118	-6.5	15	.515	.922	.722	16.76	10.91	.196	.180	-6.82	12236	.21	66.42	94.27
		9	7060	118	-7.3	15.5	.513	.921	.820	18.93	12.35	.203	.180	-7.62	11693	.21	66.67	96.86
		0	8320	121	-13.7	9	.531	.923	1.0	22.80	23.86	.121	.193	-13.98	12760	.22	67.44	56.73
6	23	6	8020	120	-13.7	9	.525	.923	1.0	22.57	23.87	.120	.191	-13.99	12649	.21	67.10	56.81
		0	5940	122	-16.5	12	.514	.921	1.0	21.18	28.90	.162	.187	-16.77	11639	.21	66.98	77.90
		3	6100	123	-16.2	12	.518	.922	1.0	21.41	28.34	.164	.189	-16.47	11505	.21	67.41	77.75
12	24	6	6060	122	-16.3	11.5	.515	.923	1.0	21.28	28.53	.156	.188	-16.57	11666	.21	67.04	74.51
		9	5800	121	-16.5	11.5	.510	.921	1.0	21.04	28.91	.154	.186	-16.78	11720	.21	66.62	74.65
		0	6700	121	-19.6	12	.516	.922	1.0	20.65	34.51	.161	.192	-19.88	13606	.21	65.81	79.53
8	25	6	6700	120	-19.6	10	.514	.921	1.0	20.58	34.51	.133	.192	-19.88	13865	.20	65.46	66.24
		9	6740	121	-19.3	7	.517	.922	1.0	20.74	33.96	.094	.192	-19.58	13521	.21	65.91	46.26

Chord Size = 15.75 inches

Flt. No.	Fig. No.	Test Conditions: Inc. Angle (deg)	H_p (ft)	Air-speed (KTAS)	T_a (°C)	Icing Time (min.)	Scaling Parameters: K_o	β	n	θ	ϕ	A_c	b	Equivalent Conditions for 6 inch chord at 120 KTAS: T_a (°C)	H_p (ft)	LWC (gm/m³)	MVD (μm)	Icing Time (min)
		0	6700	121	-19.6	12	.1967	.850	1.0	30.12	34.50	.061	.287	-19.88	11319	.65	16.82	2.73
8	25	6	6700	120	-19.6	10	.196	.850	1.0	30.03	34.51	.051	.286	-19.88	11505	.65	16.75	2.27
		9	6740	121	-19.3	7	.197	.850	1.0	30.26	33.96	.036	.287	-19.58	11265	.66	16.83	1.59

Chord Size = 21 inches

Flt. No.	Fig. No.	Test Conditions: Inc. Angle (deg)	H_p (ft)	Air-speed (KTAS)	T_a (°C)	Icing Time (min.)	Scaling Parameters: K_o	β	n	θ	ϕ	A_c	b	Equivalent Conditions for 6 inch chord at 120 KTAS: T_a (°C)	H_p (ft)	LWC (gm/m³)	MVD (μm)	Icing Time (min)
		0	8800	119	-5.6	15	.151	.820	.390	14.53	9.27	.057	.308	-5.91	13779	.74	14.07	2.21
17	18	6	8860	120	-5.5	15	.152	.821	.379	14.19	9.08	.057	.310	-5.81	13779	.75	14.12	2.22
		9	8900	120	-5.7	15	.152	.821	.395	14.80	9.44	.057	.310	-6.01	13692	.75	14.14	2.21
		0	7520	120	-7.2	20	.149	.818	.513	18.69	12.14	.076	.304	-7.5	11909	.76	14.16	2.93
14	21	6	7520	120	-7.2	17	.149	.818	.513	18.69	12.14	.065	.304	-7.5	11909	.76	14.16	2.49
		9	7500	120	-7.2	20	.149	.818	.513	18.68	12.14	.076	.304	-7.5	11909	.76	14.16	2.93
		0	7300	120	-6.5	14	.149	.818	.459	16.63	10.88	.053	.301	-6.81	12017	.75	14.12	2.06
15	19	6	7320	118	-6.5	15	.148	.817	.466	16.76	10.91	.056	.298	-6.82	12236	.74	14.01	2.20
		9	7060	118	-7.3	15.5	.147	.816	.529	18.93	12.35	.058	.298	-7.62	11693	.75	14.04	2.26
		0	9600	119	-11.0	16.5	.153	.821	.796	29.97	19.01	.062	.322	-11.31	12872	.77	14.26	2.35
16	22	6	10200	119	-11.0	15.0	.155	.823	.795	30.29	19.01	.057	.326	-11.31	13378	.77	14.26	2.14
		9	10400	119	-11.0	15	.155	.823	.794	30.40	19.01	.057	.328	-11.31	13549	.77	14.25	2.14
		0	5940	122	-16.5	12	.147	.816	1.0	34.12	28.90	.046	.311	-16.77	9410	.78	14.36	1.74
		3	6100	123	-16.2	12	.148	.817	1.0	34.51	28.34	.047	.313	-16.47	9385	.78	14.36	1.74
12	24	6	6060	122	-16.3	12	.147	.816	1.0	34.29	28.53	.045	.311	-16.57	9485	.78	14.31	1.66
		9	5800	121	-16.5	11.5	.146	.816	1.0	33.86	28.91	.044	.308	-16.78	9410	.77	14.24	1.66

Table E-5. Icing Similitude Parameters
Artificial Icing of SC1094 R8 Airfoil

Chord Size = 6 inches

Flt. No.	Fig. No.	Test Conditions: Inc. Angle (deg)	H_p (ft)	Airspeed (KTAS)	T_a (°C)	Icing Time (min.)	K_o	β	n	θ	ϕ	A_c	b	Equivalent Conditions for 21 inch chord at 120 KTAS: T_a (°C)	H_p (ft)	LWC (gm/m³)	MVD (μm)	Icing Time (min)
18	20	0	3040	121	-5.7	11	.529	.923	.580	14.74	9.42	.148	.194	-5.99	12899	.21	67.03	70.0
		6	8440	122	-6.7	10.5	.535	.924	.692	17.45	11.21	.142	.197	-6.99	12649	.22	67.70	66.22
		9	8460	121	-6.6	8	.535	.923	.686	17.24	11.05	.107	.197	-6.89	12816	.22	67.38	50.38
6	23	0	8320	121	-13.9	9	.531	.923	1.0	23.94	23.86	.121	.203	-13.98	12566	.22	67.59	55.60
		6	8020	120	-13.7	9	.525	.923	1.0	23.70	23.87	.120	.201	-13.99	12455	.22	67.27	56.56

Chord Size = 21 inches

Flt. No.	Fig. No.	Test Conditions: Inc. Angle (deg)	H_p (ft)	Airspeed (KTAS)	T_a (°C)	Icing Time (min.)	K_o	β	n	θ	ϕ	A_c	b	Equivalent Conditions for 6 inch chord at 120 KTAS: T_a (°C)	H_p (ft)	LWC (gm/m³)	MVD (μm)	Icing Time (min)
17	18	0	8800	119	-5.6	15	.151	.820	.374	14.53	9.27	.057	.324	-5.91	13779	.74	14.07	2.21
		6	8860	120	-5.5	15	.152	.821	.363	14.19	9.08	.057	.326	-5.81	13779	.75	14.12	2.22
		9	8900	120	-5.7	15	.152	.821	.378	14.80	9.44	.057	.327	-6.01	13692	.75	14.14	2.21
18	20	0	8040	121	-5.7	11	.151	.820	.376	14.47	9.42	.042	.322	-5.99	12899	.75	14.16	1.63
		6	8440	122	-6.7	10.5	.153	.821	.447	17.45	11.21	.041	.328	-6.99	12649	.76	14.28	1.54
		9	8460	121	-6.6	8	.152	.821	.443	17.23	11.05	.031	.327	-6.89	12816	.76	14.22	1.17
16	22	0	9600	119	-11.0	16.5	.153	.821	.763	29.97	19.01	.062	.339	-11.31	12872	.77	14.26	2.35
		6	10200	119	-11.0	15	.155	.822	.762	30.29	19.01	.057	.344	-11.31	13378	.77	14.28	2.14
		9	10400	119	-11.0	15	.155	.823	.761	30.40	19.01	.057	.345	-11.31	13549	.77	14.29	2.14

APPENDIX F. PHOTOGRAPHS

INDEX

Figure F-1.

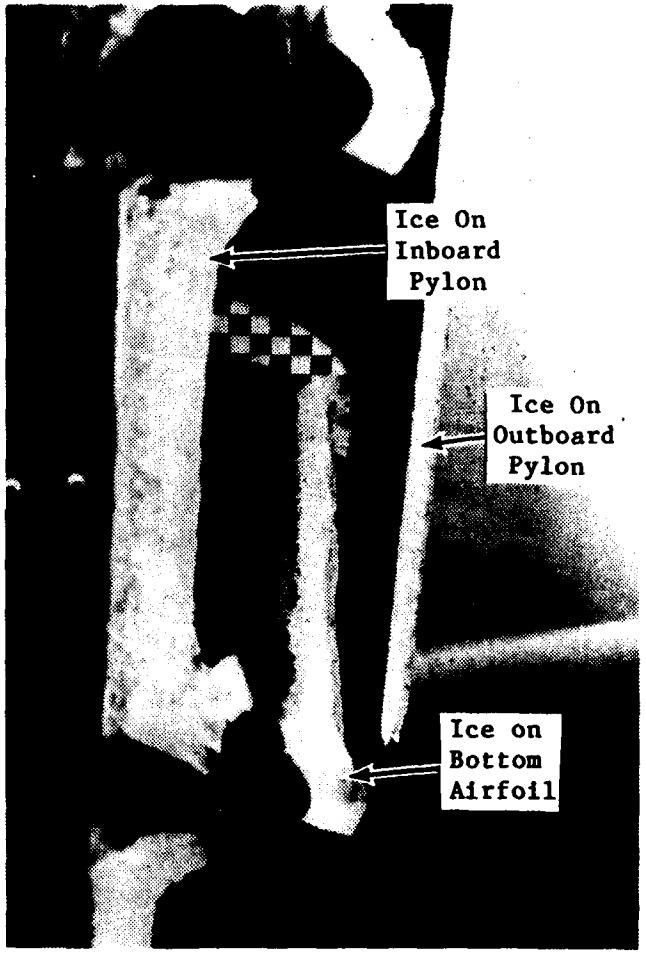

Figure F-2.

Ice Shape Variation Along Span of Test Airfoil

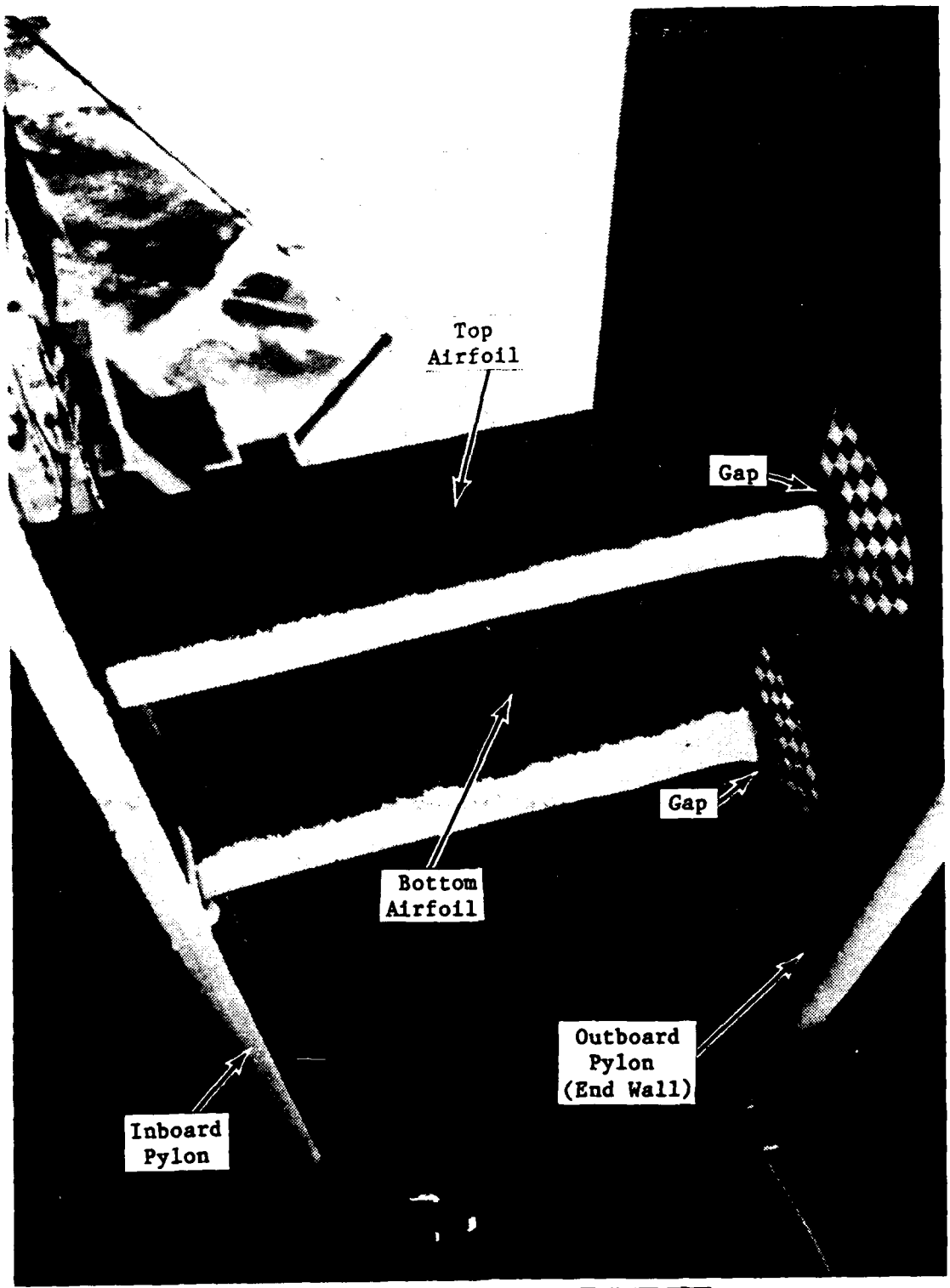

Figure F-3. Ice-Free Gap from End-Wall
Boundary Layer Adjacaent to Grid

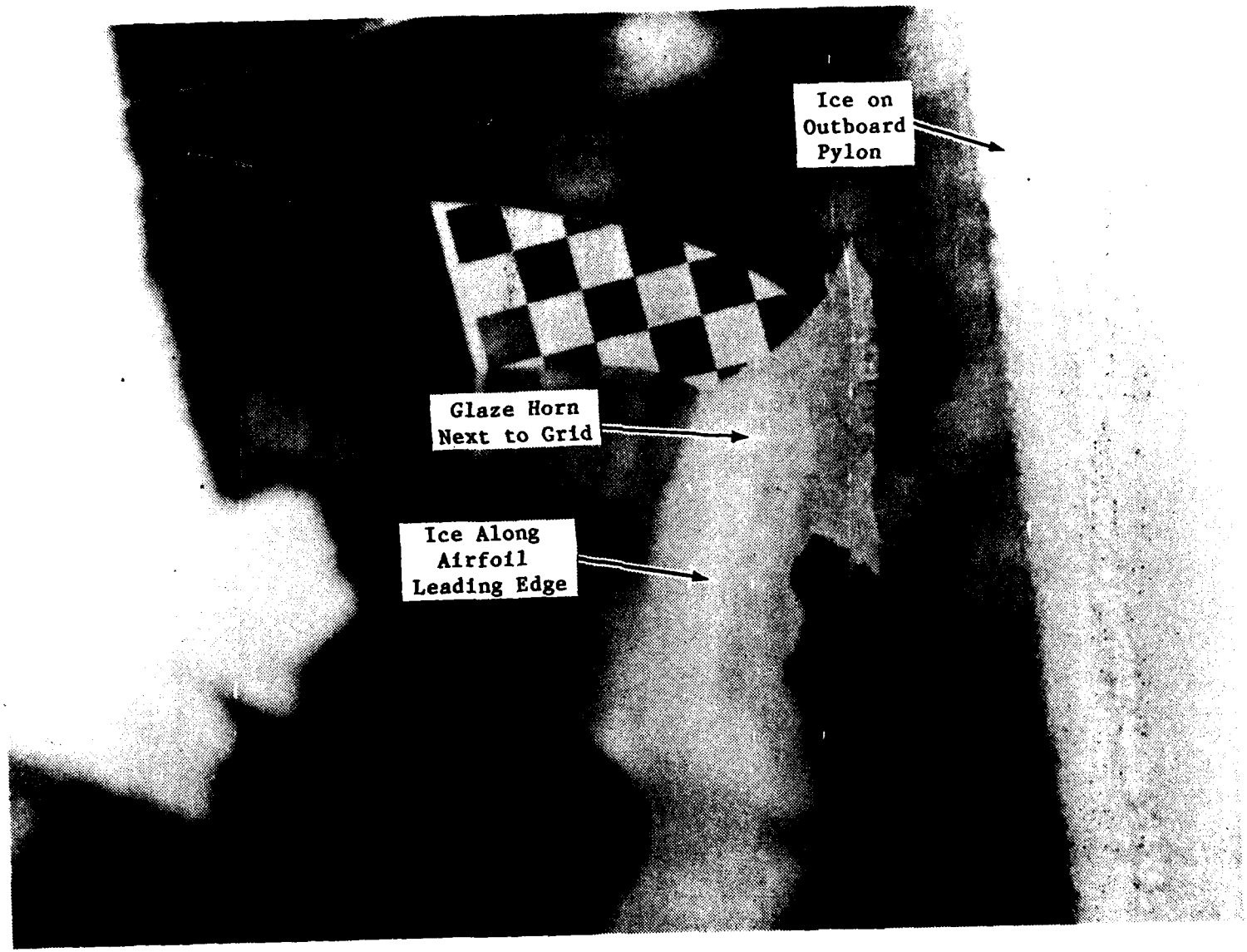

Figure F-4. Exaggerated Glaze Horns
Adjacent to Grid

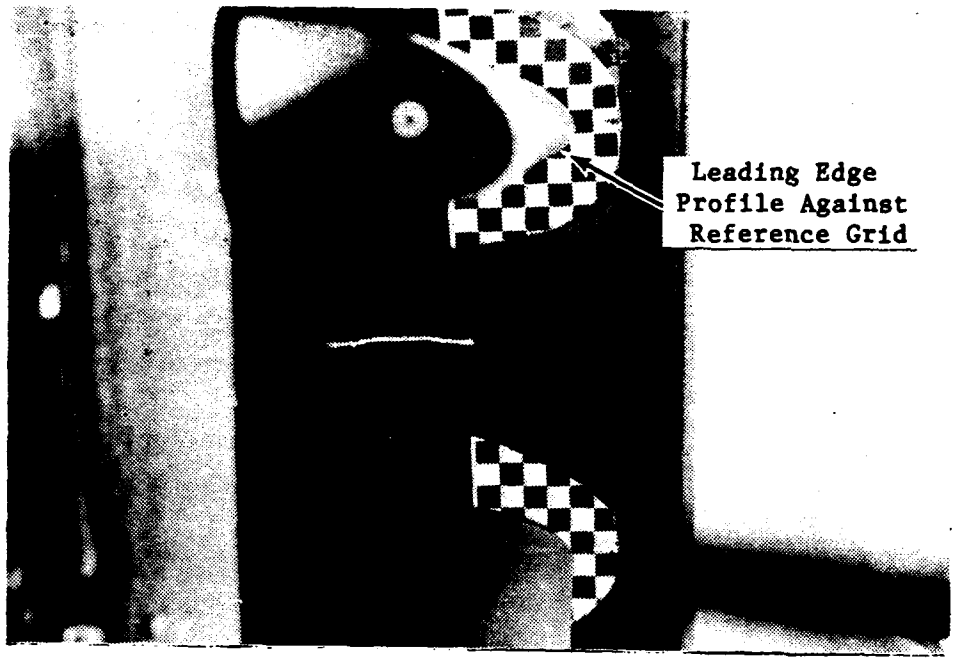

Figure F-5. Top Airfoil Sequence Exposure

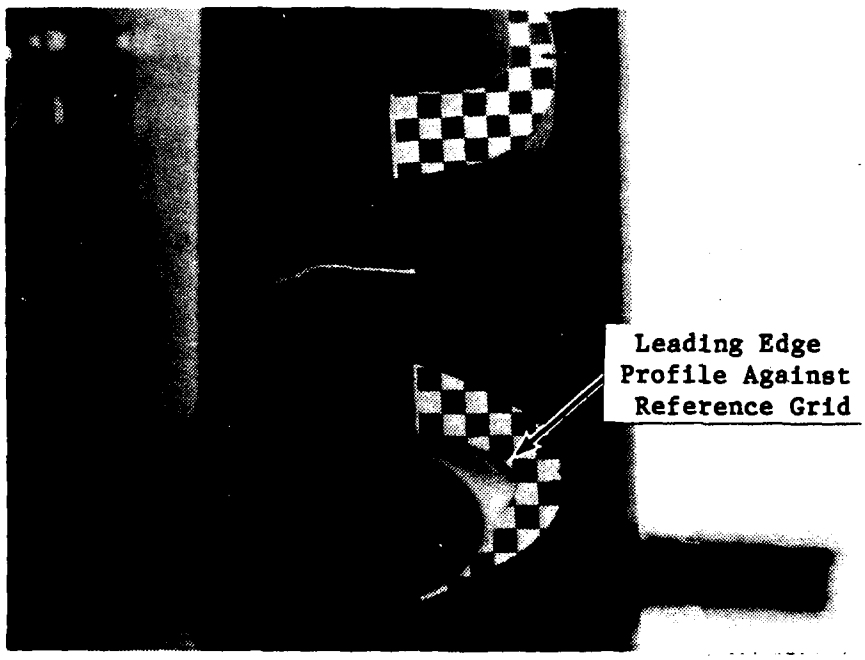

Figure F-6. Bottom Airfoil Sequence Exposure

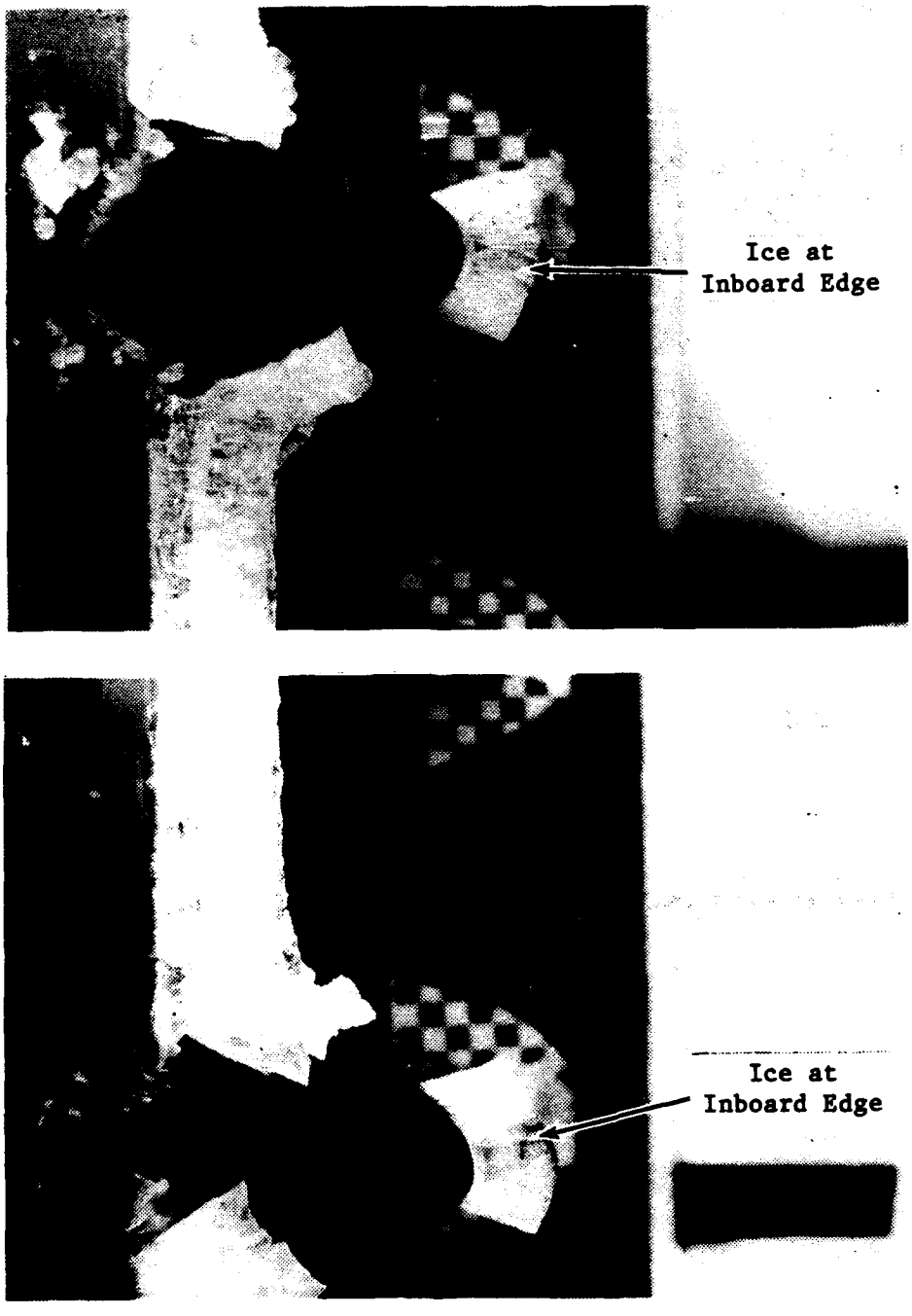

Figure F-7. Inboard Edge View of 21-Inch Chord Airfoils, NACA 0012 Top, and SC1094 R8 Bottom (Natural Icing, -7°C for 20 Minutes at 0° Incidence Angle, Flight No. 22)

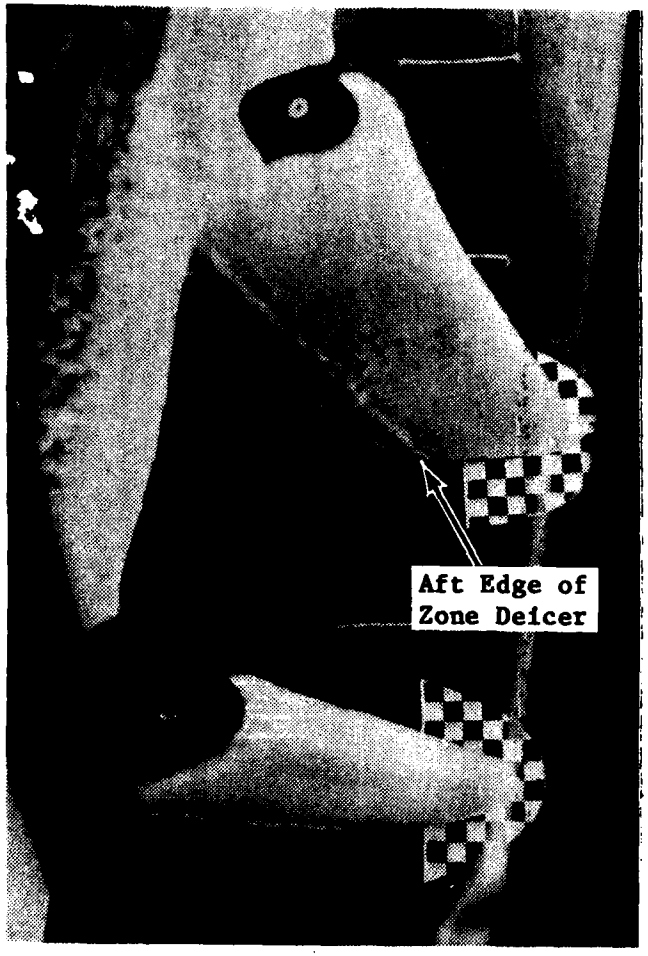

Figure F-8.

Figure F-9.

Ice Formations Along Aft Edge of Heated Zone (Top Airfoil)

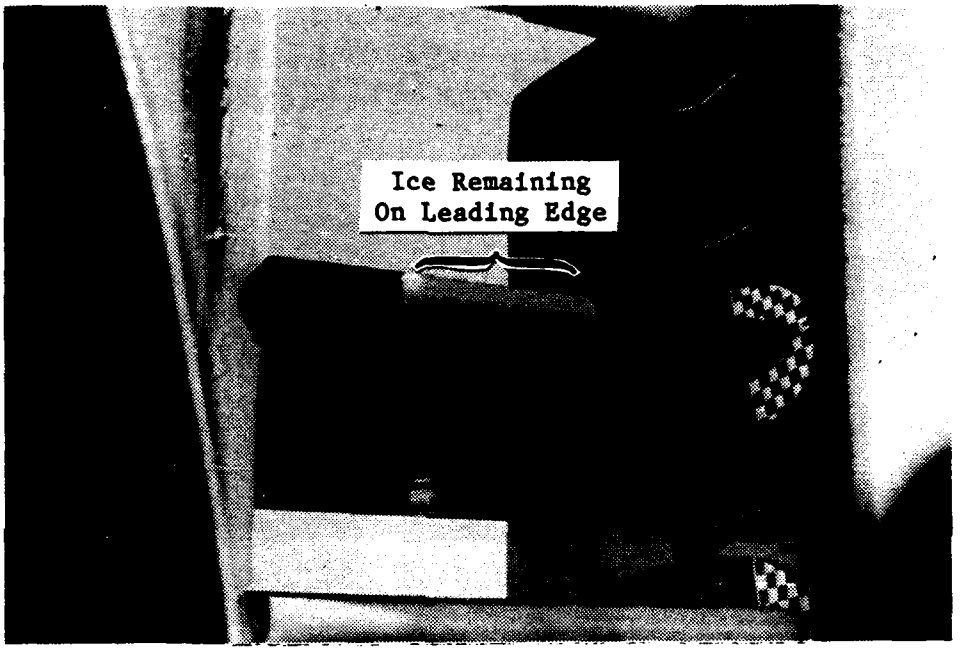

Figure F-10. Ice Retained Over Cold Region
of Heater Mat on Test Airfoil

Figure F-11. Ice-Free Region on ASA Outboard Pylon

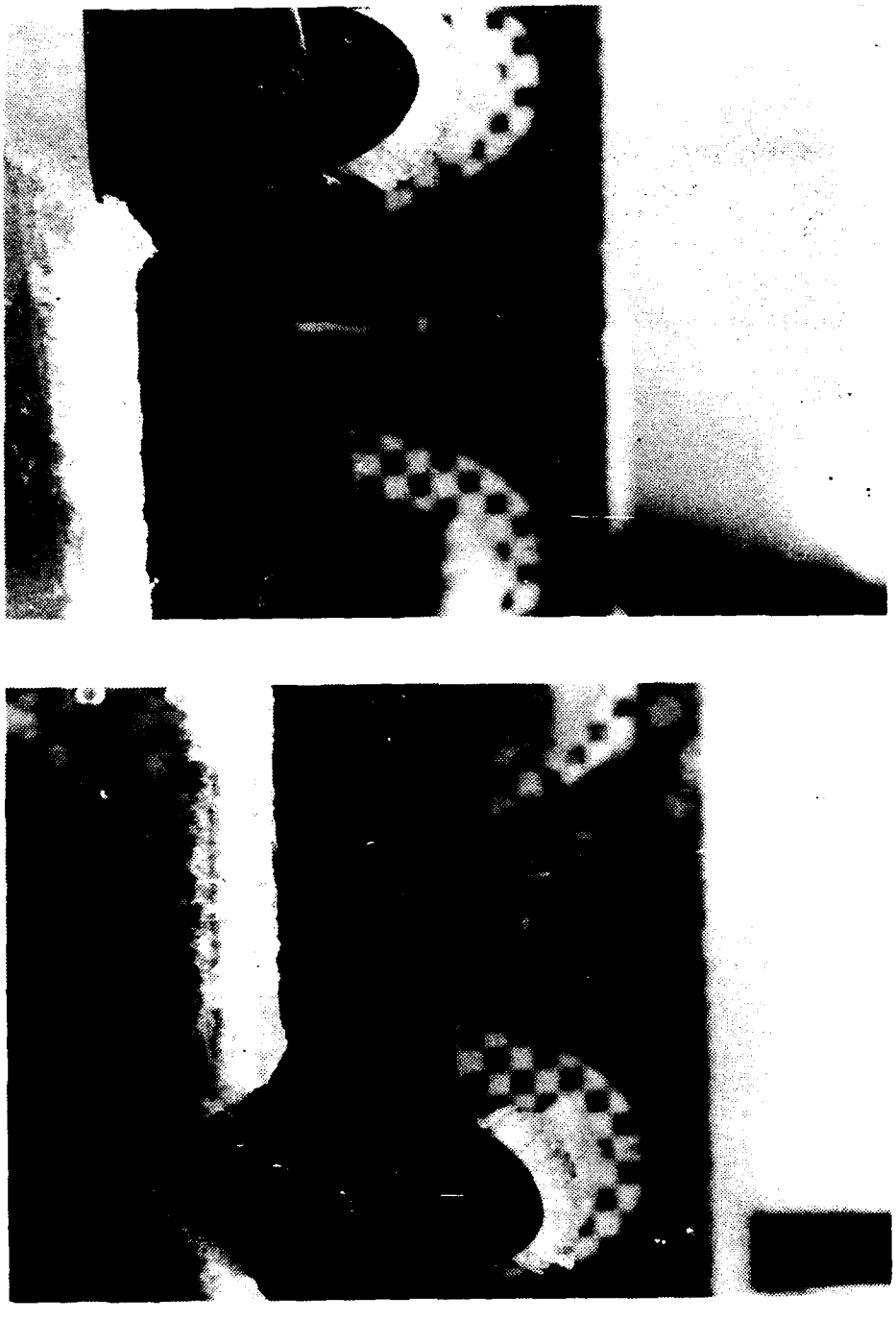

Figure F-12. Inboard Edge View of 21-Inch Chord Airfoils, NACA 0012 Top and SC1094 R8 Bottom (Natural Icing, -7°C for 5 Minutes at 0° Incidence Angle, Flight No. 20)

Figure F-13. Inboard Edge View of 21-Inch Chord Airfoils, NACA 0012 Top and SC1094 R8 Bottom (Natural Icing, -7°C for 6.5 Minutes at 9° Incidence Angle, Flight No. 20)

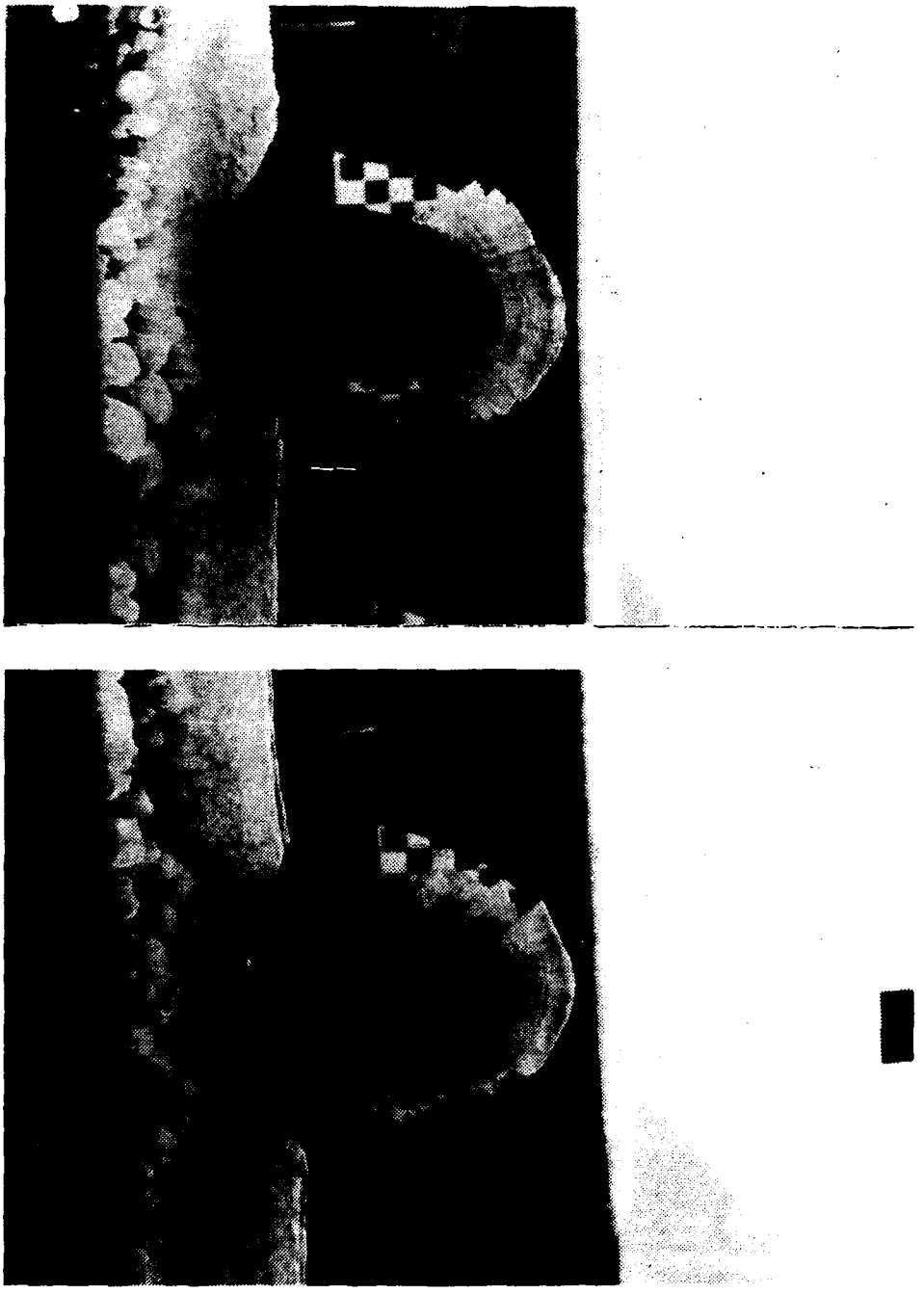

Figure F-14. Inboard Edge View of 21-Inch Chord Airfoils, SC1094 R8 Top and NACA 0012 Bottom (Artificial Icing, -5.5°C for 15 Minutes at 0° Incidence Angle, Flight No. 17)

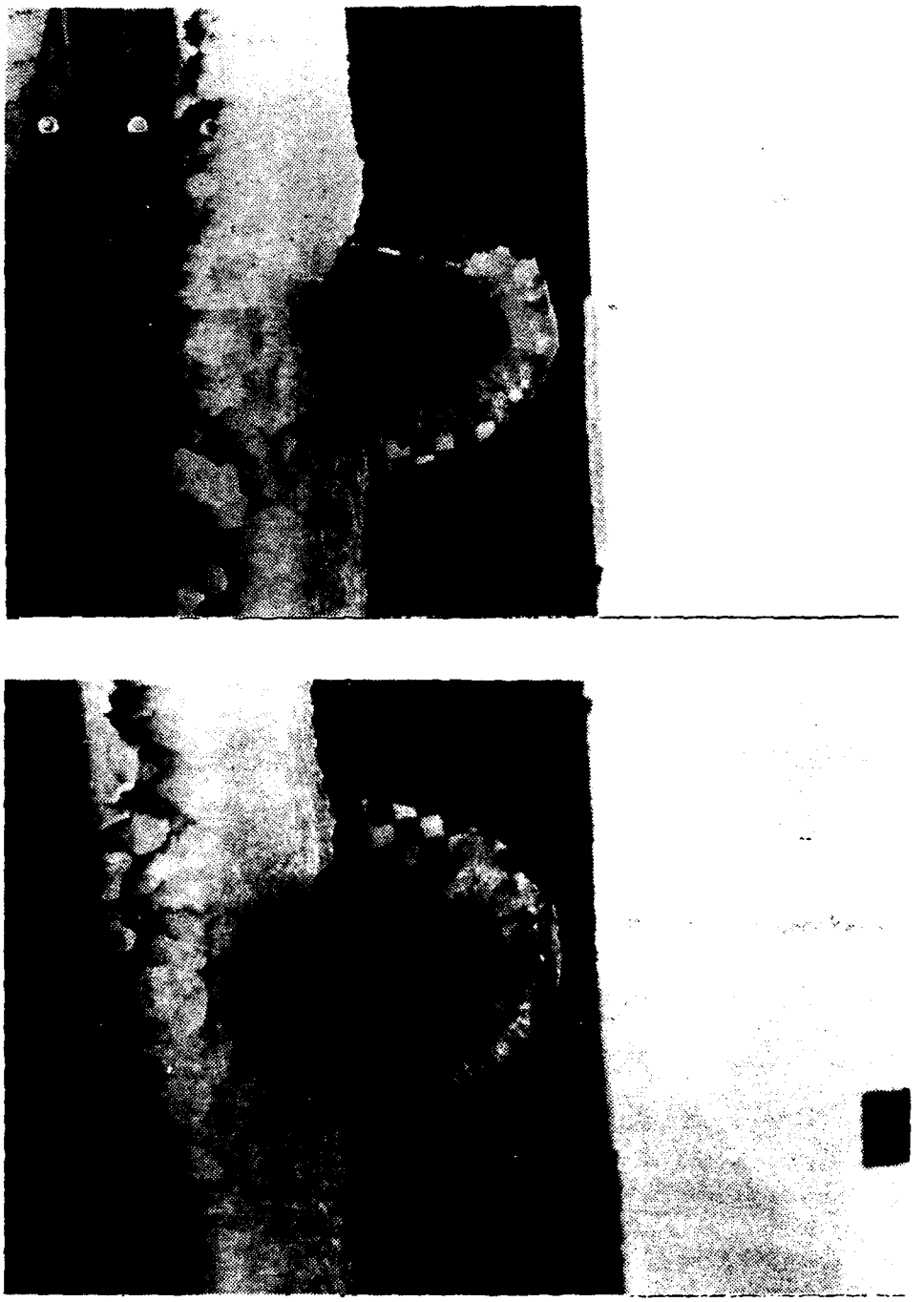

Figure F-15. Inboard Edge View of 21-Inch Cnord Airfoils, SC1094 R8 Top and NACA 0012 Bottom (Artifi al Icing, -5.5°C for 15 Minutes at 6° Incidence Angle, Flight No. 17)

Figure F-16. Inboard Edge View of 21-Inch Chord Airfoils, SC1094 R8 Top and NACA 0012 Bottom (Artificial Icing, -5.5°C for 15 Minutes at 9° Incidence Angle, Flight No. 17)

Figure F-17. Artificial Icing Rime Feathers on Inboard Pylon

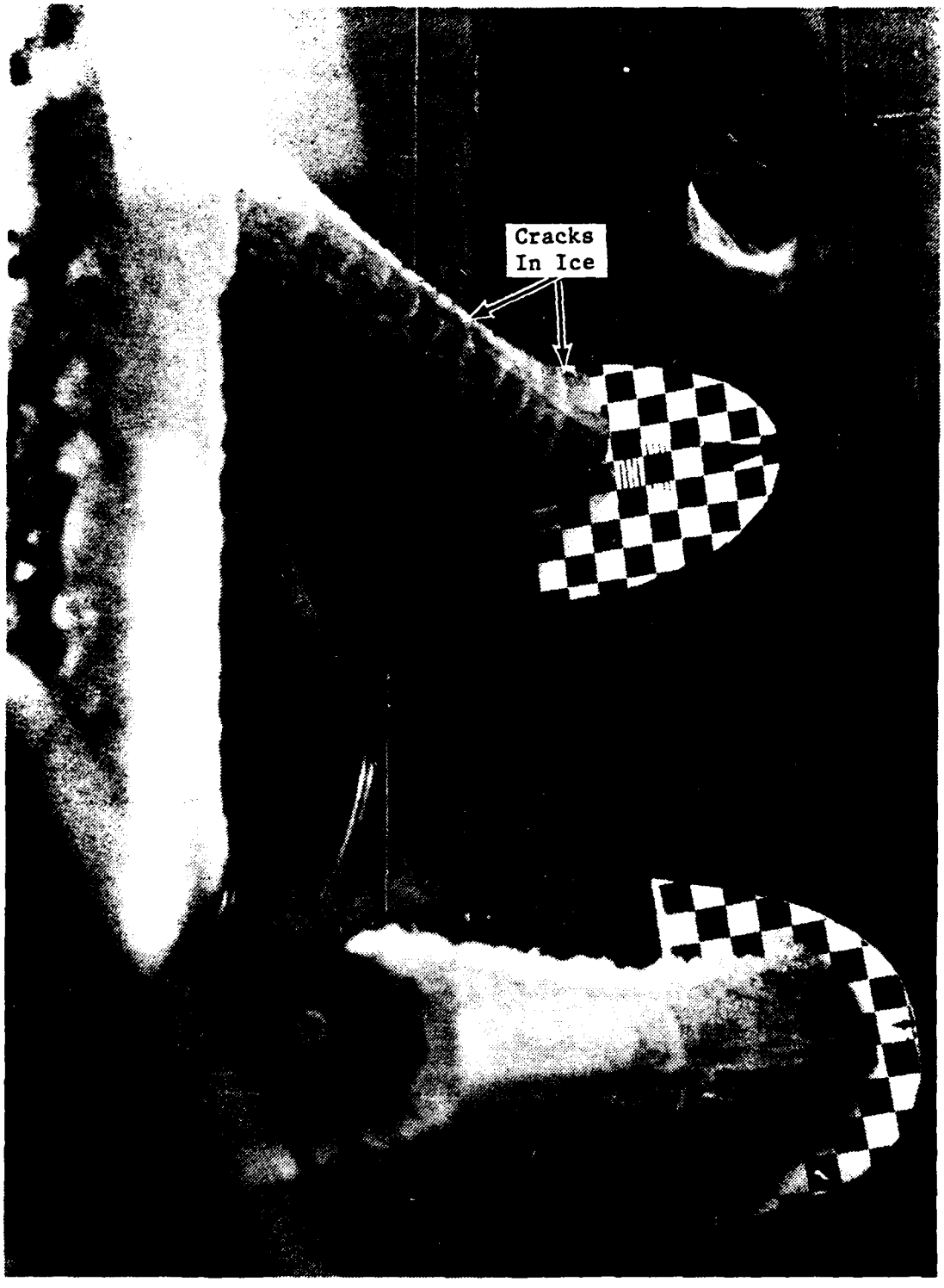

Figure F-18. Vertical Cracks in Ice Accretion Along Span of 6-Inch Chord Airfoil (Top Airfoil)

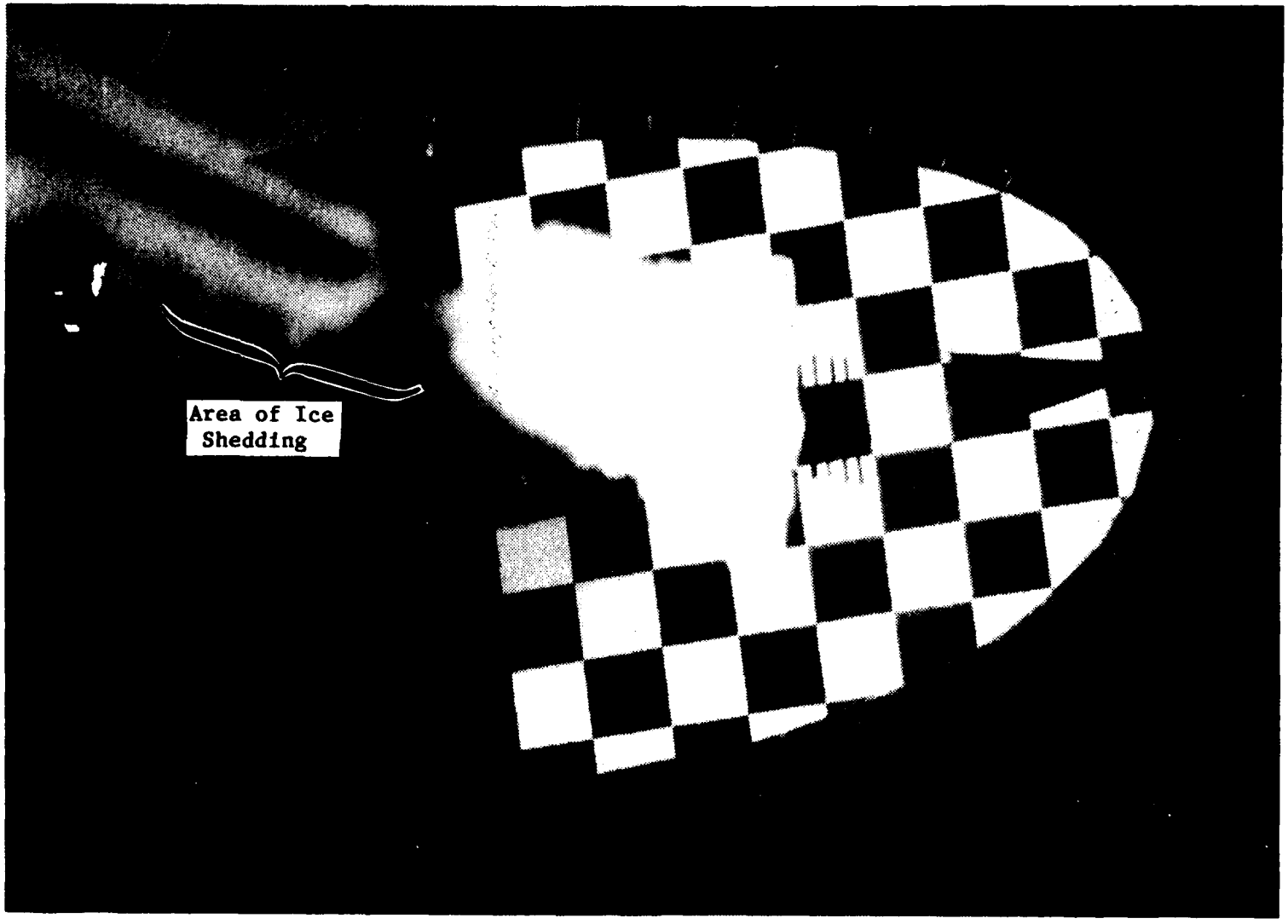

Figure F-19. Ice Section Shed from Small Airfoil During Immersion

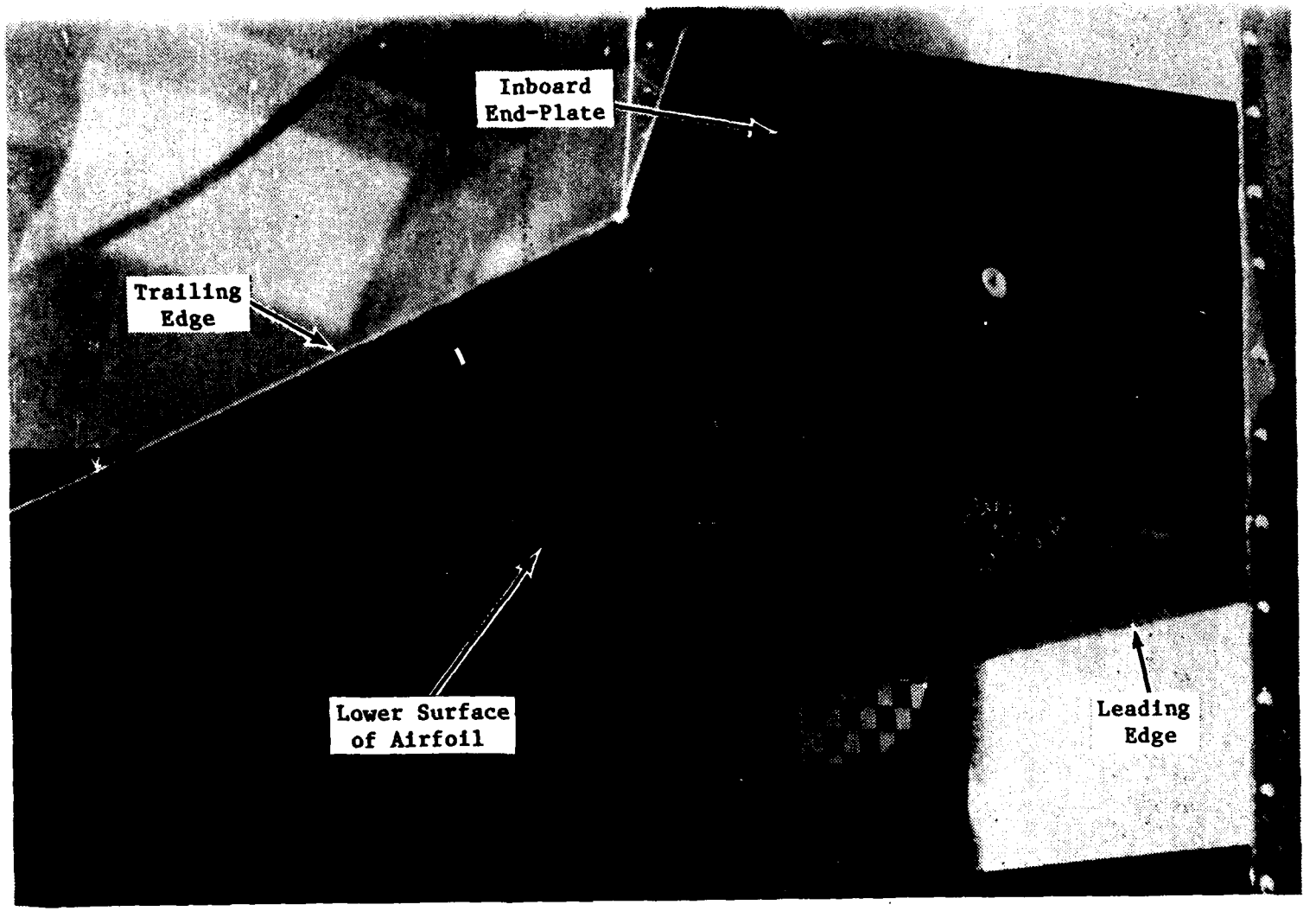

Figure F-20. Ice Spicules on Airfoil Lower Surface Reach Trailing Edge at 6° Incidence Angle (Artificial)

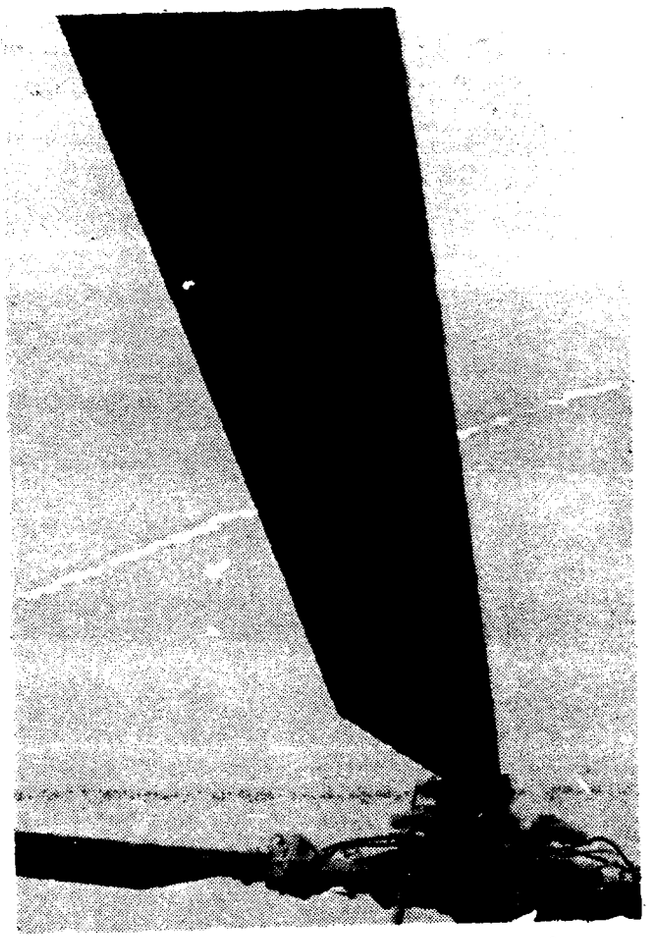

Figure F-21. Artificial Ice Formations on Lower Surface of SH-60B Main Rotor

DISTRIBUTION

HQDA (DALO-AV)	1
HQDA (DALO-FDQ)	1
HQDA (DAMO-HRS)	1
HQDA (SARD-PPM-T)	1
HQDA (SARD-RA)	1
HQDA (SARD-WSA)	1
US Army Material Command (AMCDE-SA, AMCDE-P, AMCQA-SA, AMCQA-ST)	4
US Training and Doctrine Command (ATCD-T, ATCD-B)	2
US Army Aviation Systems Command (AMSAV-8, AMSAV-Q, AMSAV-MC, AMSAV-ME, AMSAV-L, AMSAV-N, AMSAV-GTD)	8
US Army Test and Evaluation Command (AMSTE-TE-V, AMSTE-TE-O)	2
US Army Logistics Evaluation Agency (DALO-LEI)	1
US Army Materiel Systems Analysis Agency (AMXSY-RV, AMXSY-MP)	8
US Army Operational Test and Evaluation Agency (CSTE-AVSD-E)	2
US Army Armor School (ATSB-CD-TE)	1
US Army Aviation Center (ATZQ-D-T, ATZQ-CDC-C, ATZQ-TSM-A, ATZQ-TSM-S, ATZQ-TSM-LH)	5
US Army Combined Arms Center (ATZL-TIE)	1
US Army Safety Center (PESC-SPA, PESC-SE)	2
US Army Cost and Economic Analysis Center (CACC-AM)	1
US Army Aviation Research and Technology Activity (AVSCOM)	3
NASA/Ames Research Center (SAVRT-R, SAVRT-M (Library)	

US Army Aviation Research and Technology Activity (AVSCOM)	2
Aviation Applied Technology Directorate (SAVRT-TY-DRD, SAVRT-TY-TSC (Tech Library)	
US Army Aviation Research and Technology Activity (AVSCOM)	1
Aeroflightdynamics Directorate (SAVRT-AF-D)	
US Army Aviation Research and Technology Activity (AVSCOM	1
Propulsion Directorate (SAVRT-PN-D)	
Defense Technical Information Center (FDAC)	2
US Military Academy, Department of Mechanics (Aero Group Director)	1
ASD/AFXT, ASD/ENF	2
US Army Aviation Development Test Activity (STEBG-CT)	2
Assistant Technical Director for Projects, Code: CT-24 (Mr. Joseph Dunn)	2
6520 Test Group (ENML)	1
Commander, Naval Air Systems Command (AIR 5115B, AIR 5301)	3
Defense Intelligence Agency (DIA-DT-2D)	1
School of Aerospace Engineering (Dr. Daniel P. Schrage)	1
Headquarters United States Army Aviation Center and Fort Rucker	1
(ATZQ-ESO-L)	
US Army Aviation Systems Command (AMSAV-EA)	1
US Army Aviation Systems Command (AMSAV-EC)	1
US Army Aviation Systems Command (AMSAV-ED)	4
NASA-Lewis Research Center, Mail Stop 77-10 (Mr. John Reinmann)	1
NASA-Lewis Research Center, Mail Stop 86-7 (Dr. Joe Shaw)	1

Federal Aviation Administration, National Resource Specialist, AWS-104 (Mr. Richard Adams)	1
Federal Avaition Administration, Flight Research Branch (ACT 340), Program Manager (Mr. Charles Masters)	1
Federal Aviation Administration, AWS-110 (Mr. Wayne Barbini)	1
GE Aircraft Engines (Mr. Richard Keller)	1
Pratt & Whitney (Mr. Paul Matheny)	1
Allison Gas Turbine Division GMC (Mr. Francis McDonald)	1
Hartzell Propeller Company (Mr. Arthur Bowser)	1
Wichita State University, Aerospace Engineering Department (Mr. Glen Sumwalt)	1
Texas A&M University, Department of Aeronautical Engineering (Mr. Kenneth Korkan)	1
Massachusetts Institute of Technology, Department of Aeronautics (Dr. John Hansman)	1
University of Dayton Research Institute (Mr. James K. Lvers)	1
Cal Poly, Mechanical Engineering Department (Mr. Bill Patterson)	1
University of Michigan, Department of Aerospace (Mr. Gary Ruff)	1
Univesity of Toledo, Department of Mechanical Engineering (Mr. K.C. Masuilaniec)	1
Wichita State University, Aeronautical Engineering Box 44 (Mr. Robert Friedberg)	1
The Ohio State University, Aero/Astro Research Lab (Mr. Michael Bragg)	1
US Air Force Aeronautical Systems Division (ASD-WE, Mr. Steve Johnson)	1
National Center for Atmospheric Research (Mr. Wayne Sand)	1
Flight Safety Foundation (Mr. John Enders)	1

Naval Air Test Center, Flight Systems Department (Mr. Brion Picard)	1
Naval Research Laboratory, Code 4113 (Mr. Richard Jeck)	1
US Army, CRREL (Mr. K. Itagaki)	1
Sikorsky Technologies Corporation, United Technologies Corporation, Aeromechanics MS S317A (Mr. Robert Flemming, Jr.)	1
Boeing Helicoptes (Mr. Andy Peterson, MS 32-16)	1
McDonnel Douglas Helicopter, Co. (Mr. David Balch)	1
Bell Helicopter Textron (Mr. Herb Coffman)	1
B.F. Goodrich (Mr. Jim Hindel)	1
Cessna Aircraft Company, Aircraft Division (Mr. Bruce Barrett)	1
Cessna Aircraft, Dept. 178/MS14 (Mr. David Ellis)	1
Beech Aircraft Corporation, Mail Stop E-9 (Mr. Don M. St. Peter)	1
Fluidyne Engineering Corp. (Mr. Julian Idzorek)	1
JTD Environmental Services, Inc., Icing Testing–Instrumentation (Mr. Lawrence J. Jahnsen)	1
Aerometrics, Inc. (Mr. William D. Bachalo)	1
Son Enterprises, Inc. (Mr. Earle Binckey)	1
Task Research, Inc. (Mr. Jim Kern)	
Particle Measuring Systems, Incl (Mr. John D. Knollenberg)	1
Northrop Corporation (Mr. Chris Daughters)	1
Rockwell International, North American Aircraft Division (Mr. Al Bockstahler)	1
Lockheed Aircraft Corporation, Commercial-Tech Operation (63-38), Lochkeed-CALAC (Mr. Frank Brown)	1
General Dynamics (Mr. Steve Dunkelberg)	1

McDonnel Aircraft Company, McDonnel Douglas Corporation, Mail Stop 212-10

(Mr. Frank Lynch) 1

McDonnel Aircraft Company (Mr. Stephen Miesner) 1

Boeing Commerical Airplane Company (Mr. Dennis Newton) 1